UCSF
UC San Francisco Electronic Theses and Dissertations

Title

Structural and Enzymatic Characterization of the Yeast mRNA Decapping Enzyme, Dcp2

Permalink

https://escholarship.org/uc/item/6gd105jk

Author

Jones, Brittnee Noelle

Publication Date

2010

Peer reviewed|Thesis/dissertation

Structural and Enzymatic characterization of the
yeast mRNA decapping enzyme, Dcp2

by

Brittnee Jones

DISSERTATION

Submitted in partial satisfaction of the requirements for the degree of

DOCTOR OF PHILOSOPHY

in

Chemistry and Chemical Biology

in the

GRADUATE DIVISION

of the

UNIVERSITY OF CALIFORNIA, SAN FRANCISCO

ACKNOWLEDGEMENTS

I cannot begin to thank everyone that has helped with this thesis. I will begin by thanking everyone that had a direct role in its creation scientifically but even then, I'm certain I will leave some people out.

My advisor, Dr. John Gross, has been supportive and understanding throughout my career. He helped me at the bench in the beginning, let me find my own path when I needed to develop and make mistakes, and gave me the freedom to grow in the end. He has truly helped me grow as a person and as a scientist. I have and will never meet anyone more dedicated to science and the pursuit of knowledge. In this way, he continues to be a motivation and inspiration.

He is also one of the best collaborators I have ever worked with. As such, this project truly took a village to create. I have had the privilege of working in and with many labs during my graduate career. Those are predominantly the labs of my thesis committee members, Christine Guthrie, Geeta Narlikar, and Alan Frankel, without whom I am certain I would not have graduated. Their support and insight, and even lab space and reagents, has been instrumental in my scientific growth. I cannot thank them enough.

The people in these labs are also scientists of the highest quality and integrity and have provided valuable insight and even help with protocols and techniques. Some of them must be named individually for their roles: Matt Daugherty who helped me at every step along the way; Tommaso Villa, Tracy Kress, and others in the Guthrie Lab for teaching me to work with yeast and answering my million questions; Rebecca Howard for teaching me CD and giving me her time and reagents; and both Carolyn Decker in

Structural and Enzymatic Characterization of the

Yeast mRNA Decapping Enzyme, Dcp2

By

Brittnee Jones

_____

John D. Gross, PhD

Thesis advisor and thesis committee chair

mRNA turnover represents a fundamental point of post-transcriptional control of gene expression in eukaryotes. Decapping is a highly regulated, irreversible step in mRNA decay and is involved in many different decay pathways. The yeast mRNA decapping enzyme is comprised of the catalytic subunit, Dcp2, in complex with Dcp1, an obligate *in vivo* activator.   The goal of this study is to characterize the mechanism of mRNA decapping by Dcp2 and the role of activators.

We embarked on this study by establishing an *in vitro* model system for decapping. Reconstituting this system required purifying the decapping holoenzyme and the catalytic subunit, preparing radiolabeled RNA substrate and determining optimal assay conditions.   This assay allowed us to investigate how Dcp2 binds and recognizes its mRNA substrate, as well as the role of Dcp1 as an activator of decapping, by

examining the various kinetic and thermodynamic parameters of this process. We discovered that Dcp2 contains an extensive, highly charged RNA binding surface extending from the active site through a channel to the dorsal side of the protein. This surface is bipartite in function: the dorsal surface binds the RNA body and provides the majority of the binding energy, whereas the cap proximal nucleotides are involved in the catalytic mechanism.

We also determined that Dcp1 stimulates decapping during the catalytic step, wherein Dcp2 undergoes an open-to-closed transition into a catalytically active conformation. This is supported by our result that the cap is recognized during the transition state, suggesting closure promotes cap recognition and enzyme activity. This represents a possible fundamental point of control of this process as activators could shift the balance by promoting the closed, active form of the enzyme. We began studies on one such activator of decapping, Edc3, and discovered that it directly interacts with Dcp2 to activate decapping, though further studies are necessary for determine which step in the catalytic cycle is affected.

This study is the first to mechanistically examine the decapping enzyme, Dcp2, using a multidisciplinary approach involving enzymology, biochemistry, biophysics, and genetics. Our goals were to investigate the structural and biochemical basis for RNA recognition and the mechanism of activation. These studies provide the first insights into control of decapping at the molecular level.

TABLE OF

CONTENTS

UCSF Library Release Form:

CHAPTER 1:

Introduction

mRNA degradation is a highly regulated, key step in the posttranslational control of gene expression. The balance between mRNAs undergoing translation and decay provides for the basal level of gene expression. Half-lives of individual mRNAs in eukaryotic cells vary greatly from minutes to hours and can be altered in rapid response to hormones, cell cycle progression, and as a viral response (Muhlrad et al., 1994; Muhlrad et al., 1995; Cao and Parker, 2001; Waterhouse et al., 2001). mRNA decay plays a key role in early animal development, cell growth and differentiation, adaptation to stress and the quality control of gene expression (Chen and Shyu, 1995; Maquat, 2004a; Amrani et al., 2006; Hilgers et al., 2006; Schier, 2007).

Eukaryotic mRNAs possess both a 5' N-7 methyl guanosine (m^7G) cap structure as well as a 3' poly adenylate (polyA) tail. These features serve to protect the mRNA from aberrant decay and also act to promote translation (Sachs, 1990; Ross, 1995). The cap structure is added cotranscriptionally and necessary for cap dependant translation initiation (Maniatis and Reed, 2002; Neugebauer, 2002; Zorio and Bentley, 2004). The eukaryotic translation initiation factor eIF4E, a part of the cytoplasmic cap binding complex collectively known as eIF4F, binds the cap in a deep pocket and promotes translation of most eukaryotic mRNAs (Hodel et al., 1997; Marcotrigiano et al., 1997; Gross et al., 2003). Such an interaction between the cap and cap-binding complex is promoted by interaction with the poly(A) binding proteins (PABs) in eukaryotes (Wells et al., 1998; Amrani et al., 2008). This is thought to circularize the mRNA and promote recycling of the ribosomes for multiple rounds of translation and thus inhibit decapping (Caponigro and Parker, 1995; Coller et al., 1998; Wilusz et al., 2001; Khanna and

Kiledjian, 2004). It is therefore necessary to displace these complexes, thereby

repressing translation initiation, for the message to be sentenced to decay (Coller and

Parker, 2005; Parker and Sheth, 2007). Translational repression is the first in a series of

events necessary for decay of the mRNA transcript (Schwartz and Parker, 1999 2000)

It is well appreciated that these two mutually exclusive processes, translation and

decay, are directly coupled for a given transcript. Given the importance of the cap

binding complexes within these paths, it is conceivable that modulation of cap occupancy

influences the differential stabilities of various mRNAs (Parker and Sheth, 2007).   This

model is supported by evidence of the inhibition of decapping by the cap binding

complex (Schwartz and Parker, 1999; Schwartz and Parker, 2000) (Tharun and Parker,

2001). Also, the stability of the interaction between eIF4F and the mRNA cap directly

influences the efficiency of the decapping complex (Schwartz and Parker, 1999;

Schwartz and Parker, 2000; Vilela et al., 2000; Ramirez et al., 2002). Despite the

importance of this transition in the life of an mRNA, control of this process from a

molecular standpoint is poorly understood.

Once an mRNA is sentenced to degradation, it enters into one of several mRNA

decay pathways. In yeast, bulk mRNA decay is initiated by the shortening of the poly(A)

tail (Muhlrad and Parker, 1992; Decker and Parker, 1993; Meyer et al., 2004; Parker and

Song, 2004a).   Removal of the poly(A) tail is thought to displace the PABs and thereby

expose the 3' end of the mRNA. In 3' to 5' decay, this is followed by 3' to 5'

degradation by an assembly of proteins and exonucleases known as the exosome

(Anderson and Parker, 1998). The resulting cap structure from exosomal decay is further

processed by the scavenger decapping enzyme DcpS to produce m^7GMP (Wang and

Kiledjian, 2001; Liu et al., 2002; van Dijk et al., 2003).

In 5' to 3' decay, deadenylation promotes removal of the cap binding complex

(Cheng et al., 2007). This exposes the cap for binding by the yeast mRNA decapping

complex, comprised of decapping factors 1 and 2, Dcp1 and Dcp2 (Beelman et al., 1996;

Dunckley and Parker, 1999; Steiger et al., 2003). mRNA decapping is the penultimate

step in this and several other pathways that regulate mRNA stability including AU–rich

element (ARE) mediated decay, nonsense mediated decay, deadenylation independent

decapping and decay, and microRNA mediated decay (Coller and Parker, 2004; Maquat,

2004b; Parker and Song, 2004b; Fenger-Gron et al., 2005; Rehwinkel et al., 2005;

Weischenfeldt et al., 2005; Parker and Sheth, 2007).

mRNAs no longer undergoing active translation accumulate in punctate

cyctoplasmic foci termed mRNA processing bodies (P bodies) (Sheth and Parker, 2003;

Brengues et al., 2005; Anderson and Kedersha, 2006; Eulalio et al., 2007a). P bodies

contain mRNA substrates and proteins known to activate mRNA decay (Sheth and

Parker, 2003; Andrei et al., 2005; Ferraiuolo et al., 2005; Barbee et al., 2006). It has also

recently been shown that mRNAs are sequestered to P bodies as points of storage and

later shuttled back to actively translating pools of mRNA (Sheth and Parker, 2003;

Brengues et al., 2005; Anderson and Kedersha, 2006; Eulalio et al., 2007a). Depletion of

P bodies by inhibiting efficient translational termination and thereby blocking translating

4

messages from entering the decay pool has been shown to diminish P body size and abundance (Sheth and Parker, 2003; Teixeira et al., 2005). P body size is used as an indirect measure of the nontranslating pool of mRNA (Sheth and Parker, 2003; Cougot et al., 2004; Coller and Parker, 2005; Teixeira et al., 2005). The deletion of proteins and enzymes known to catalyze decay causes an increase in size and abundance of P bodies as determined by monitoring common P body markers (Lykke-Andersen, 2002; van Dijk et al., 2002; Sheth and Parker, 2003). For example, deletion of the decapping enzyme Dcp2 increases the size of P bodies as visualized by GFP-tagged Dcp1 (Hatfield et al., 1996; Teixeira et al., 2005). Recently, however, it has been shown that P bodies are not a necessary prerequisite for mRNA decay; mRNAs can be decayed on polysomes (Hu et al., 2009). Further study is needed to further characterize the role P bodies is decay.

Deadenylation is thought to be the rate-limiting step in degradation. However, it can occur as mRNAs actively undergo translation. Decapping is irreversible and thereby commits the mRNA to immediate decay as it liberates a 5' monophosphate RNA, the canonical substrate for the 5' exonuclease XRN1 (Stevens and Maupin, 1987). The catalytic subunit of the decapping complex, Dcp2, catalyzes the removal of the cap to produce an m^7GDP cap structure and the mRNA body (Beelman et al., 1996; Lykke-Andersen, 2002; van Dijk et al., 2002; Wang et al., 2002; Steiger et al., 2003). Dcp2 is known to only efficiently act on long RNA substrates *in vitro*. (van Dijk et al., 2002a; Piccirillo et al., 2003; Steiger et al., 2003; Cohen et al., 2005). Neither m^7GpppG cap analogue nor short capped RNAs are efficiently hydrolyzed, and neither moiety can be

cross-linked to Dcp2 (Piccirillo et al., 2003). This requirement for the presence of a substantial RNA body for decapping by Dcp2 is not understood.

The structure of Dcp2 reveals a bilobal protein comprised of a C-terminal Nudix domain and an N-terminal domain known to interact with Dcp1, an obligate *in vivo* activator of decapping (She et al., 2006). The Nudix domain of Dcp2 contains a highly conserved nudix helix and fold and is part of the nudix hydrolase super family of proteins. Nudix hydrolases are metal binding proteins that catalyze the hydrolysis of nucleoside diphosphates linked to some x moity (Bessman et al., 1996; Mildvan et al., 2005). These proteins bind differing numbers of metal cations with two or more conserved glutamates and have a general base that acts to deprotonate a highly conserved water molecule coordinated in the active site. Dcp2 is known to use magnesium to catalyze the removal of the m^7GDP cap structure leaving a 5' monophosphate body (Lykke-Andersen, 2002; Piccirillo et al., 2003; Steiger et al., 2003). Structural studies have identified two highly conserved tandem glutamates located on the same face of the nudix helix that are essential for catalysis (van Dijk et al., 2002; Mildvan et al., 2005; She et al., 2006; Wang et al., 2002; Dunckley and Parker, 1999). The number of magnesiums and the identity of the general base, however, have yet to be determined. In addition to the nudix motif, the C terminal domain of Dcp2 also posses a conserved basic patch known as Box B, though its function is unknown (Wang et al., 2002; Piccirillo et al., 2003).

The N terminal lobe of Dcp2 is known to interact with Dcp1 to form the decapping holoenzyme (Beelman et al., 1996; Dunckley and Parker, 1999; Steiger et al., 2003). Dcp1 binds Dcp2 via a conserved patch of hydrophobic residues. The residues are critical for Dcp1 to stimulate decapping by Dcp2 both *in vitro* and *in vivo* (She et al., 2006). Dcp1 contains an Evh1 fold, which is know to mediate protein interactions by recognizing proline rich sequences on protein binding partners (She et al., 2004). It has been hypothesized that Dcp1 mediates other protein interactions.

The structure of the decapping holoenzyme has recently been solved and reveals two conformations, dependant on domain orientation rearrangements around flexible linker between the two domains of Dcp2 (She et al., 2006). The more compact, closed structure is proposed to be the catalytically active form of the enzyme. The transition between these two conformations represents a possible point of regulation, as inhibition of closure blocks decapping. This represents a step in the catalytic cycle where activator proteins could function to facilitate or stabilize the closure of the Dcp1/Dcp2 complex. This will be a critical area of research going forward.

Due to its critical nature in the decay of both stable and unstable mRNAs, it is expected that decapping is highly regulated and modulated by both activator and inhibitor proteins (Parker and Song, 2004a). Also, both general and transcript specific activators of decapping have been identified and highlight the complex nature of the control of decapping at the molecular level. Several evolutionarily conserved proteins identified as general enhancers of decapping are the DEAD-box helicase RCK/p54/Me31b/Dhh1,

the Lsm1-7 complex, Pat1, and another Lsm family of proteins including Edc3 and Edc4/Tral/Scd6 (Decker and Parker, 2006; Decourty et al., 2008; Franks and Lykke-Andersen, 2008). Several of these factors, including Dhh1 and Pat1, act early in the decay process by promoting translational repression (Coller and Parker, 2005). Others factors presumably have a direct role in catalyzing the mechanism of decapping. The LSM1-7 complex binds substrate mRNA after the formation of the decapping mRNP and activates decapping of bulk mRNA by an unknown mechanism (Teixeira and Parker, 2007)). While many activators act generally, others act in a transcript specific way, such as Edc1 and Edc2 proteins (Dunckley et al., 2001; Schwartz et al., 2003; Steiger et al., 2003).

One such activator of decapping thought to act both generally as well as specifically is Edc3. Edc3 was identified genetically as an activator of decapping when the activity of the Dcp1 and Dcp2 complex was compromised. Though Edc3 is dispensable for the decay of certain reporter mRNAs, it is crucial for specific mRNAs *in vivo* (Badis et al., 2004; Dong et al., 2007). Edc3 is also important for the degradation of some miRNAs in Drosophila S2 cells (Eulalio et al., 2007b). *In vitro*, Edc3 is found to directly interact with other components of the decapping mRNP and has recently been shown to directly interact with Dcp2 to stimulate decapping (Decker et al., 2007; Tritschler et al., 2007). These results indicate that Edc3 is a key component of the decapping machinery. However, little is understood of the mechanism by which Edc3 stimulates decapping nor has the interaction with Dcp2 been characterized.

REFERENCES

Amrani, N., Ghosh, S., Mangus, D. A., Jacobson, A., 2008. Translation factors promote the formation of two states of the closed-loop mRNP. Nature. 453**,** 1276-80.

Amrani, N., Sachs, M. S., Jacobson, A., 2006. Early nonsense: mRNA decay solves a translational problem. Nat Rev Mol Cell Biol. 7**,** 415-25.

Anderson, J. S., Parker, R. P., 1998. The 3' to 5' degradation of yeast mRNAs is a general mechanism for mRNA turnover that requires the SKI2 DEVH box protein and 3' to 5' exonucleases of the exosome complex. Embo J. 17**,** 1497-506.

Anderson, P., Kedersha, N., 2006. RNA granules. J Cell Biol. 172**,** 803-8.

Andrei, M. A., Ingelfinger, D., Heintzmann, R., Achsel, T., Rivera-Pomar, R., Luhrmann, R., 2005. A role for eIF4E and eIF4E-transporter in targeting mRNPs to mammalian processing bodies. Rna. 11**,** 717-27.

Badis, G., Saveanu, C., Fromont-Racine, M., Jacquier, A., 2004. Targeted mRNA degradation by deadenylation-independent decapping. Mol Cell. 15**,** 5-15.

Barbee, S. A., et al., 2006. Staufen- and FMRP-containing neuronal RNPs are structurally and functionally related to somatic P bodies. Neuron. 52**,** 997-1009.

Beelman, C. A., Stevens, A., Caponigro, G., LaGrandeur, T. E., Hatfield, L., Fortner, D. M., Parker, R., 1996. An essential component of the decapping enzyme required for normal rates of mRNA turnover. Nature. 382**,** 642-6.

Bessman, M. J., Frick, D. N., O'Handley, S. F., 1996. The MutT proteins or "Nudix" hydrolases, a family of versatile, widely distributed, "housecleaning" enzymes. J Biol Chem. 271**,** 25059-62.

Brengues, M., Teixeira, D., Parker, R., 2005. Movement of eukaryotic mRNAs between polysomes and cytoplasmic processing bodies. Science. 310**,** 486-9.

Cao, D., Parker, R., 2001. Computational modeling of eukaryotic mRNA turnover. Rna. 7**,** 1192-212.

Caponigro, G., Parker, R., 1995. Multiple functions for the poly(A)-binding protein in mRNA decapping and deadenylation in yeast. Genes Dev. 9**,** 2421-32.

Chen, C. Y., Shyu, A. B., 1995. AU-rich elements: characterization and importance in mRNA degradation. Trends Biochem Sci. 20**,** 465-70.

Cheng, Z., Muhlrad, D., Lim, M. K., Parker, R., Song, H., 2007. Structural and functional insights into the human Upf1 helicase core. EMBO J. 26**,** 253-64.

Coller, J., Parker, R., 2004. Eukaryotic mRNA decapping. Annu Rev Biochem. 73**,** 861-90.

Coller, J., Parker, R., 2005. General translational repression by activators of mRNA decapping. Cell. 122**,** 875-86.

Coller, J. M., Gray, N. K., Wickens, M. P., 1998. mRNA stabilization by poly(A) binding protein is independent of poly(A) and requires translation. Genes Dev. 12**,** 3226-35.

Cougot, N., Babajko, S., Seraphin, B., 2004. Cytoplasmic foci are sites of mRNA decay in human cells. J Cell Biol. 165**,** 31-40.

Decker, C. J., Parker, R., 1993. A turnover pathway for both stable and unstable mRNAs in yeast: evidence for a requirement for deadenylation. Genes Dev. 7**,** 1632-43.

Decker, C. J., Parker, R., 2006. CAR-1 and trailer hitch: driving mRNP granule function at the ER? J Cell Biol. 173**,** 159-63.

Decker, C. J., Teixeira, D., Parker, R., 2007. Edc3p and a glutamine/asparagine-rich domain of Lsm4p function in processing body assembly in Saccharomyces cerevisiae. J Cell Biol. 179**,** 437-49.

Decourty, L., Saveanu, C., Zemam, K., Hantraye, F., Frachon, E., Rousselle, J. C., Fromont-Racine, M., Jacquier, A., 2008. Linking functionally related genes by sensitive and quantitative characterization of genetic interaction profiles. Proc Natl Acad Sci U S A. 105**,** 5821-6.

Dong, S., Li, C., Zenklusen, D., Singer, R. H., Jacobson, A., He, F., 2007. YRA1 autoregulation requires nuclear export and cytoplasmic Edc3p-mediated degradation of its pre-mRNA. Mol Cell. 25**,** 559-73.

Dunckley, T., Parker, R., 1999. The DCP2 protein is required for mRNA decapping in Saccharomyces cerevisiae and contains a functional MutT motif. Embo J. 18**,** 5411-22.

Dunckley, T., Tucker, M., Parker, R., 2001. Two related proteins, Edc1p and Edc2p, stimulate mRNA decapping in Saccharomyces cerevisiae. Genetics. 157**,** 27-37.

Eulalio, A., Behm-Ansmant, I., Izaurralde, E., 2007a. P bodies: at the crossroads of post-transcriptional pathways. Nat Rev Mol Cell Biol. 8**,** 9-22.

Eulalio, A., Rehwinkel, J., Stricker, M., Huntzinger, E., Yang, S. F., Doerks, T., Dorner, S., Bork, P., Boutros, M., Izaurralde, E., 2007b. Target-specific requirements for enhancers of decapping in miRNA-mediated gene silencing. Genes Dev. 21**,** 2558-70.

Fenger-Gron, M., Fillman, C., Norrild, B., Lykke-Andersen, J., 2005. Multiple processing body factors and the ARE binding protein TTP activate mRNA decapping. Mol Cell. 20**,** 905-15.

Ferraiuolo, M. A., Basak, S., Dostie, J., Murray, E. L., Schoenberg, D. R., Sonenberg, N., 2005. A role for the eIF4E-binding protein 4E-T in P-body formation and mRNA decay. J Cell Biol. 170**,** 913-24.

Franks, T. M., Lykke-Andersen, J., 2008. The control of mRNA decapping and P-body formation. Mol Cell. 32**,** 605-15.

Gross, J. D., Moerke, N. J., von der Haar, T., Lugovskoy, A. A., Sachs, A. B., McCarthy, J. E., Wagner, G., 2003. Ribosome loading onto the mRNA cap is driven by conformational coupling between eIF4G and eIF4E. Cell. 115**,** 739-50.

Hatfield, L., Beelman, C. A., Stevens, A., Parker, R., 1996. Mutations in trans-acting factors affecting mRNA decapping in Saccharomyces cerevisiae. Mol Cell Biol. 16**,** 5830-8.

Hilgers, V., Teixeira, D., Parker, R., 2006. Translation-independent inhibition of mRNA deadenylation during stress in Saccharomyces cerevisiae. Rna. 12**,** 1835-45.

Hodel, A. E., Gershon, P. D., Shi, X., Wang, S. M., Quiocho, F. A., 1997. Specific protein recognition of an mRNA cap through its alkylated base. Nat Struct Biol. 4, 350-4.

Hu, W., Sweet, T. J., Chamnongpol, S., Baker, K. E., Coller, J., 2009. Co-translational mRNA decay in Saccharomyces cerevisiae. Nature. 461, 225-9.

Khanna, R., Kiledjian, M., 2004. Poly(A)-binding-protein-mediated regulation of hDcp2 decapping in vitro. Embo J. 23, 1968-76.

Liu, H., Rodgers, N. D., Jiao, X., Kiledjian, M., 2002. The scavenger mRNA decapping enzyme DcpS is a member of the HIT family of pyrophosphatases. EMBO J. 21, 4699-708.

Lykke-Andersen, J., 2002. Identification of a human decapping complex associated with hUpf proteins in nonsense-mediated decay. Mol Cell Biol. 22, 8114-21.

Maniatis, T., Reed, R., 2002. An extensive network of coupling among gene expression machines. Nature. 416, 499-506.

Maquat, L. E., 2004a. Nonsense-mediated mRNA decay: splicing, translation and mRNP dynamics. Nat Rev Mol Cell Biol. 5, 89-99.

Maquat, L. E., 2004b. Nonsense-mediated mRNA decay: splicing, translation and mRNP dynamics. . Nat Rev Mol Cell Biol 5, ,89-99.

Marcotrigiano, J., Gingras, A. C., Sonenberg, N., Burley, S. K., 1997. Cocrystal structure of the messenger RNA 5' cap-binding protein (eIF4E) bound to 7-methyl-GDP. Cell. 89, 951-61.

Meyer, S., Temme, C., Wahle, E., 2004. Messenger RNA turnover in eukaryotes: pathways and enzymes. Crit Rev Biochem Mol Biol. 39, 197-216.

Mildvan, A. S., Xia, Z., Azurmendi, H. F., Saraswat, V., Legler, P. M., Massiah, M. A., Gabelli, S. B., Bianchet, M. A., Kang, L. W., Amzel, L. M., 2005. Structures and mechanisms of Nudix hydrolases. Arch Biochem Biophys. 433, 129-43.

Muhlrad, D., Decker, C. J., Parker, R., 1994. Deadenylation of the unstable mRNA encoded by the yeast MFA2 gene leads to decapping followed by 5'-->3' digestion of the transcript. Genes Dev. 8, 855-66

Muhlrad, D., Decker, C. J., Parker, R., 1995. Turnover mechanisms of the stable yeast PGK1 mRNA. Mol Cell Biol. 15, 2145-56.

Muhlrad, D., Parker, R., 1992. Mutations affecting stability and deadenylation of the yeast MFA2 transcript. Genes Dev. 6, 2100-11.

Neugebauer, K. M., 2002. On the importance of being co-transcriptional. J Cell Sci. 115, 3865-71.

Parker, R., Sheth, U., 2007. P bodies and the control of mRNA translation and degradation. Mol Cell. 25, 635-46.

Parker, R., Song, H., 2004a. The enzymes and control of eukaryotic mRNA turnover. Nat Struct Mol Biol. 11, 121-7.

Parker, R., Song, H., 2004b. The enzymes and control of eukaryotic mRNA turnover. . Nat Struct Mol Biol. 11, 121-7

Piccirillo, C., Khanna, R., Kiledjian, M., 2003. Functional characterization of the mammalian mRNA decapping enzyme hDcp2. RNA. 9, 1138-47.

Ramirez, C. V., Vilela, C., Berthelot, K., McCarthy, J. E., 2002. Modulation of eukaryotic mRNA stability via the cap-binding translation complex eIF4F. J Mol Biol. 318, 951-62.

Rehwinkel, J., Behm-Ansmant, I., Gatfield, D., Izaurralde, E., 2005. A crucial role for GW182 and the DCP1:DCP2 decapping complex in miRNA-mediated gene silencing. . RNA. 11 1640-1647.

Ross, J., 1995. mRNA stability in mammalian cells. Microbiol Rev. 59, 423-50.

Sachs, A., 1990. The role of poly(A) in the translation and stability of mRNA. Curr Opin Cell Biol. 2, 1092-8.

Schier, A. F., 2007. The maternal-zygotic transition: death and birth of RNAs. Science. 316, 406-7.

Schwartz, D., Decker, C. J., Parker, R., 2003. The enhancer of decapping proteins, Edc1p and Edc2p, bind RNA and stimulate the activity of the decapping enzyme. Rna. 9, 239-51.

Schwartz, D. C., Parker, R., 1999. Mutations in translation initiation factors lead to increased rates of deadenylation and decapping of mRNAs in Saccharomyces cerevisiae. Mol Cell Biol. 19, 5247-56.

Schwartz, D. C., Parker, R., 2000. mRNA decapping in yeast requires dissociation of the cap binding protein, eukaryotic translation initiation factor 4E. Mol Cell Biol. 20, 7933-42.

She, M., Decker, C. J., Chen, N., Tumati, S., Parker, R., Song, H., 2006. Crystal structure and functional analysis of Dcp2p from Schizosaccharomyces pombe. Nat Struct Mol Biol. 13, 63-70.

She, M., Decker, C. J., Sundramurthy, K., Liu, Y., Chen, N., Parker, R., Song, H., 2004. Crystal structure of Dcp1p and its functional implications in mRNA decapping. Nat Struct Mol Biol. 11, 249-56.

Sheth, U., Parker, R., 2003. Decapping and decay of messenger RNA occur in cytoplasmic processing bodies. Science. 300, 805-8.

Steiger, M., Carr-Schmid, A., Schwartz, D. C., Kiledjian, M., Parker, R., 2003. Analysis of recombinant yeast decapping enzyme. Rna. 9, 231-8.

Stevens, A., Maupin, M. K., 1987. A 5'----3' exoribonuclease of Saccharomyces cerevisiae: size and novel substrate specificity. Arch Biochem Biophys. 252, 339-47.

Teixeira, D., Parker, R., 2007. Analysis of P-body assembly in Saccharomyces cerevisiae. Mol Biol Cell. 18, 2274-87.

Teixeira, D., Sheth, U., Valencia-Sanchez, M. A., Brengues, M., Parker, R., 2005. Processing bodies require RNA for assembly and contain nontranslating mRNAs. RNA. 11, 371-82.

Tharun, S., Parker, R., 2001. Targeting an mRNA for decapping: displacement of translation factors and association of the Lsm1p-7p complex on deadenylated yeast mRNAs. Mol Cell. 8**,** 1075-83.

Tritschler, F., Eulalio, A., Truffault, V., Hartmann, M. D., Helms, S., Schmidt, S., Coles, M., Izaurralde, E., Weichenrieder, O., 2007. A divergent Sm fold in EDC3 proteins mediates DCP1 binding and P-body targeting. Mol Cell Biol. 27**,** 8600-11.

van Dijk, E., Cougot, N., Meyer, S., Babajko, S., Wahle, E., Seraphin, B., 2002. Human Dcp2: a catalytically active mRNA decapping enzyme located in specific cytoplasmic structures. EMBO J 21**,** 6915-6924.

van Dijk, E., Le Hir, H., Seraphin, B., 2003. DcpS can act in the 5'-3' mRNA decay pathway in addition to the 3'-5' pathway. Proc Natl Acad Sci U S A. 100**,** 12081-6.

Vilela, C., Velasco, C., Ptushkina, M., McCarthy, J. E., 2000. The eukaryotic mRNA decapping protein Dcp1 interacts physically and functionally with the eIF4F translation initiation complex. Embo J. 19**,** 4372-82.

Wang, Z., Jiao, X., Carr-Schmid, A., Kiledjian, M., 2002. The hDcp2 protein is a mammalian mRNA decapping enzyme. Proc Natl Acad Sci U S A. 99**,** 12663-8.

Wang, Z., Kiledjian, M., 2001. Functional link between the mammalian exosome and mRNA decapping. Cell. 107**,** 751-62.

Waterhouse, P. M., Wang, M. B., Lough, T., 2001. Gene silencing as an adaptive defence against viruses. Nature. 411**,** 834-42.

Weischenfeldt, J., Lykke-Andersen, J., Porse, B., 2005. Messenger RNA surveillance: neutralizing natural nonsense. Curr Biol. 15**,** R559-62.

Wells, S. E., Hillner, P. E., Vale, R. D., Sachs, A. B., 1998. Circularization of mRNA by eukaryotic translation initiation factors. Mol Cell. 2**,** 135-40.

Wilusz, C. J., Gao, M., Jones, C. L., Wilusz, J., Peltz, S. W., 2001. Poly(A)-binding proteins regulate both mRNA deadenylation and decapping in yeast cytoplasmic extracts. Rna. 7**,** 1416-24.

Zorio, D. A., Bentley, D. L., 2004. The link between mRNA processing and transcription: communication works both ways. Exp Cell Res. 296**,** 91-7.

CHAPTER 2:

A Kinetic Assay to Monitor RNA Decapping

Under Single Turnover Conditions

A Kinetic Assay to Monitor RNA Decapping Under Single Turnover Conditions

Brittnee N. Jones[1], Duc-Uy Quang-Dang[2], Yuko Oku, John D. Gross[2,3]

[1]Program in Chemistry and Chemical Biology,

[2]Department of Pharmaceutical Chemistry, University of California, San Francisco, CA

94158

[3]Corresponding Author: John Gross

Address: UCSF Mission Bay-Genentech Hall Box 2280,

San Francisco, CA 94158

Tel: (415) 514-4402

Fax (415) 502-8298

Email: jdgross@picasso.ucsf.edu

Running Title: Monitoring RNA decapping kinetics

ABSTRACT

The stability of all RNA Polymerase II transcripts depends on the 5' terminal cap structure. Removal of the cap is a prerequisite for 5'-3' decay and is catalyzed by distinct cellular and viral decapping activities. Over the last decade, several decapping enzymes have been characterized through functional and structural studies. An emerging theme is that function is regulated by protein interactions, however *in vitro* assays to dissect the effects on enzyme activity are unavailable. Here we present a kinetic assay to monitor decapping by the heterodimeric yeast Dcp1/Dcp2 complex. Kinetic constants related to RNA binding and the rate of the catalytic step can be determined with recombinant enzyme and cap radiolabeled RNA substrate, allowing substrate specificity and the role of activating factors to be firmly established.

INTRODUCTION

All RNA polymerase II transcripts contain an m^{7}GpppN (N any nucleotide) cap structure (Shatkin, 1976). Cap recognition drives nearly every stage of mRNA metabolism while hypermethylation of the cap, m^{2,2,7}GpppN, promotes nuclear localization of snoRNA and snRNAs (Cougot et al., 2004; Moore, 2005; Reddy et al., 1992). Removal of the cap by decapping enzymes triggers degradation by conserved 5' to 3' exonucleases (Rat 1, Xrn1) that recognize a 5' monophosphate substrate (Johnson, 1997; Muhlrad et al., 1994; Stevens and Maupin, 1987).

Several decapping enzymes have been identified that act in different RNA decay pathways. The mRNA decapping enzyme, Dcp2, is part of a large mRNP responsible for deadenylation dependent 5'-3' decay, AU rich element (ARE) mediated decay, nonsense mediated decay (NMD), deadenylation independent decapping, and decay of some miRNA targets (Coller and Parker, 2004; Fenger-Gron et al., 2005; Maquat, 2004; Parker and Sheth, 2007; Parker and Song, 2004; Rehwinkel et al., 2005; Weischenfeldt et al., 2005). The scavenger decapping enzyme, DcpS, functions with the exosome in 3' to 5' decay possibly to remove residual cap structures that may inhibit cap-binding proteins (Liu et al., 2002; van Dijk et al., 2003; Wang and Kiledjian, 2001). The nuclear decapping enzyme X29 functions in the turnover of U8 snoRNA, which is essential for vertebrate ribosome biogenesis (Ghosh et al., 2004; Peculis and Steitz, 1993; Tomasevic and Peculis, 1999). The Pox virus family decapping enzymes, D9 and D10, downregulate both host and viral m^{7}GpppN capped RNA, thereby aiding with

progression through the viral life cycle (Parrish and Moss, 2007; Parrish et al., 2007; Shors et al., 1999).

Structural and functional studies of decapping enzymes indicate that substrate binding and activity are regulated by protein interactions. Crystallographic analysis of *S. pombe* Dcp2 reveals a dumbbell shaped structure composed of an alpha-helical domain, which binds the essential activator Dcp1, followed by a C-terminal catalytic domain containing a classic Nudix fold (Beelman, 1996; She et al., 2006). Dcp1 enhances the activity of Dcp2 *in vitro* and is required for function in yeast, however, the Nudix domain is necessary and sufficient for substrate binding and pyrophosphate chemistry (Deshmukh et al., 2008; Dunckley and Parker, 1999; Piccirillo et al., 2003; Steiger et al., 2003). X29 also contains a Nudix fold with additional insertions that mediate an extensive dimer interface (Scarsdale et al., 2006). Residues from one protomer contact cap-dinucleotide and a loop containing the putative catalytic base in the other, suggesting that dimerization is linked to activation. The crystal structure of DcpS in complex with cap-dinucleotide reveals a homodimer containing a beta-strand swapped regulatory domain followed by a catalytic domain related to the HIT protein family (Chen et al., 2005; Gu et al., 2004; Han et al., 2005). A structure-based model of catalysis by DcpS posits that decapping by one protomer is coupled to product release in the other through binding of cap-dinucleotide (Gu et al., 2004). The HIT and Nudix folds each define separate superfamilies, where members can function as single domain enzymes (Bessman et al., 1996; Lima et al., 1997; Mildvan et al., 2005; Seraphin, 1992). Therefore, an emerging principle for

21

decapping enzymes is that protein interactions provide a mechanism for modulating activity through insertions and domains that extend beyond a defined catalytic core.

The substrate preferences of decapping enzymes are dictated by geometry and sequence specific contacts. Dcp2 has strong preferences for long mRNA substrates, unlike DcpS, which has no activity on long mRNAs but efficiently processes capped oligonucleotides (Liu et al., 2004; van Dijk et al., 2002). Similarly, the Pox Virus Nudix enzymes D9 and D10 preferentially decap long and short RNAs, respectively (Parrish and Moss, 2007; Parrish et al., 2007). Structural and biochemical studies indicate that Dcp2 and DcpS form specific contacts with m^7G whereas X29 does not (Deshmukh et al., 2008; Gu et al., 2004; Scarsdale et al., 2006). Instead, X29 forms specific contacts with the RNA body that restrict decapping to the U8 snoRNA in a metal dependent manner (Ghosh et al., 2004; Peculis et al., 2007; Tomasevic and Peculis, 1999). The length requirements of mRNA decapping enzymes may safeguard translating messages from precocious decapping. The differences in specificity amongst decapping enzymes are consistent with their biological role to act on either an exclusive or broad set of substrates.

Regulation of decapping activity almost certainly extends beyond the binary protein interactions surveyed here. For example, X29 forms part of a large U8 snoRNP, DcpS interacts with the multisubunit exosome and Dcp2 function is controlled by a dense network of protein interactions in different mRNA decay pathways (Eulalio et al., 2007; Ghosh et al., 2004; Krogan et al., 2006; Parker and Sheth, 2007). To better understand

how protein interactions regulate decapping activity and substrate specificity, we have developed a simple *in vitro* kinetic assay to measure substrate binding and the rate of the catalytic step of decapping by the yeast Dcp1/2 complex.

KINETIC EQUATIONS

Single-turnover kinetics allow the evaluation of rate constants for formation of reaction intermediates (Johnson, 1992). When the concentration of enzyme [E] is in excess of substrate [S], the rate of the catalytic step is measured directly. This approach has been used extensively by researchers studying the mechanism of ribozymes (Herschlag and Cech, 1990a; Herschlag and Cech, 1990b; McConnell et al., 1993).

The distinction between single and multiple turnover kinetics is best illustrated by considering the mechanism:

$$E + S \underset{k_{off}}{\overset{k_{on}}{\longleftrightarrow}} E \cdot S \xrightarrow{k_{max}} E \cdot P \xrightarrow{k_{rel}} E + P$$
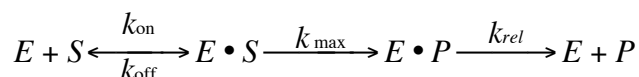
Scheme (I)

where k_{max} is the rate of the catalytic step, k_{rel} is the rate of product release, and k_{on} and k_{off} are the rate for enzyme substrate association and dissociation, respectively.

Under multiple turnover conditions, k_{cat} is obtained from the maximal velocity of the reaction under conditions of saturating substrate (Fersht, 1999). For scheme **(I)** above,

$$k_{cat} = \frac{k_{max} * k_{rel}}{k_{max} + k_{rel}},$$ **Equation (1)**

therefore k_{cat} is not merely the rate of the catalytic step (k_{max}) as it also depends on the rate of product release. In this case the interpretation of k_{cat} relies heavily on knowledge of whether the catalytic step or product release is rate limiting.

In single turnover kinetics, the observed rates do not depend on product release and the maximal velocity of the reaction corresponds to the rate of the catalytic step, k_{max}. The rate equations for single-turnover kinetics follow from the condition of excess enzyme over substrate ([E]>[S]). This ensures a nearly constant enzyme concentration throughout the course of the reaction, so that the concentration of enzyme at any time is approximately equal to the total enzyme concentration (E_T). Rate equations for substrate and product follow from a steady-state assumption on [E]:

$$\frac{\partial}{\partial t}[S] = -k_{obs}[S]$$
Equation (2)

where the observed first order rate constant, k_{obs}, describes the rate of conversion of substrate to product. The amount of substrate present in the system is given by the equation

$$[S] = [S]_0 e^{-k_{obs}t}$$
Equation (3)

Similarly, the amount of product produced at that time is also proportional to the observed rate of the reaction and can be found:

$$[P] = [S]_0 \left[1 - e^{-k_{obs}t}\right]$$
Equation (4)

By monitoring product formation as a function of time, the observed first order rate constant k_{obs} can be obtained by curve fitting. The kinetic constants K'_m and k_{max} can be obtained by measuring k_{obs} at several enzyme concentrations through the relation:

$$k_{obs} = \frac{k_{max} * E_T}{E_T + K'_m}$$
Equation (5)

with k_{max} the rate of the chemical step, E_T the total enzyme concentration and

$$K'_{\text{m}} = \frac{k_{\text{off}} + k_{\text{max}}}{k_{\text{on}}}$$
Equation (6)

The prime symbol is used to distinguish the K_m measured under single turnover conditions from that obtained under multiple turnover conditions since both depend on k_{max} whereas the latter also depends on k_{rel}. In the limit where $k_{\text{max}} \ll k_{\text{off}}$, or when the catalytic step is slow compared to the rate at which the enzyme substrate complex dissociates, K'_m is K_d. This point can be tested by comparing K'_m with K_d measured by direct binding of non-hydrolyzable substrate. If non-hydrolyzable substrate is not available, a chase experiment can be performed to determine whether k_{off} is fast relative to the catalytic step (Dixon, 1953). Hereafter the prime symbol for K_m will be omitted for simplicity.

It should be noted that the rate of the catalytic step reports on all substeps that occur after substrate binding and prior to the formation of product, including the rate of the chemical step. This would include a scenario in which an enzyme undergoes a conformational change from an open, inactive state to a closed, catalytically active form.

While single-turnover experiments are valuable for directly measuring the rate of the catalytic step, they do not address if this step is rate limiting in the biological context of multiple-turnovers. The rate of product release relative to the catalytic step may be ascertained in one of three ways. First, if k_{cat} measured under multiple turnover conditions is equal to the k_{max} measured in the single-turnover experiment, then product release is not rate limiting. Second, if K_m measured under multiple turnovers conditions is K_d for non-hydrolysable substrate, then product release is not rate limiting. Third, the rate

of product release may be measured directly and if $k_{rel} > k_{max}$, product release is not rate limiting.

MATERIALS

2.1 In vitro transcription

Short RNAs (10-40nt) are transcribed *in vitro* using, 1 μM oligonucleotide template DNA, 10 μL 10xT7 buffer, 5 mM each NTP, 2 mM DTT, and 2 μL recombinant T7 RNA polymerase (20U/μL) in the presence of 0.1U RNasin in a total reaction volume of 100 μL (Milligan et al., 1987) (see **Appendix A** for buffer recipes). The reaction is incubated at 37°C for 3 hrs or until a considerable amount of magnesium pyrophosphate precipitate is visible. The product is purified by denaturing PAGE, visualized by UV shadowing, and subsequently excised, diced, and eluted overnight in gel extraction buffer (**Appendix A**). Eluted RNA undergoes phenol:chloroform extraction and ethanol precipitation, with the resulting pellet dissolved in water and quantified using UV spectrophotometry. The 5'triphosphate RNA is stored at -20°C in 5μL aliquots at a concentration of 20 μM.

2.2 Cap Labeled RNA preparation:

Capping is carried out using 10μL α-^{32}P GTP (MP Biomedicals, 6000 Ci/mmol), 4μL recombinant Vaccinia virus guanylyltransferase (Ambion 5 U/μL) in the presence of 1mM S-adenosyl methionine (SAM, NEB) at a final volume of 20μL as described (Haley et al., 2003). Quickspin columns (G25, Roche) are used to separate unincorporated α-^{32}P GTP. The capped RNA is separated from minor degradation products by denaturing PAGE. Cap radiolabeled RNA is radioimaged (Kodak Biomax XAR) and subsequently excised, diced, and eluted overnight in gel extraction buffer (**Appendix A**). The aqueous

product is phenol:chloroform extracted and ethanol precipitated. The precipitate is washed with 70% ethanol and resuspended in water, quantified by scintillation counting and stored at 4°C.

The aforementioned procedure can be adapted to prepare capped, radiolabeled RNA lacking the N^7-methyl modification (GpppG RNA) as described except 1 mM S-adenosyl homocysteine (SAH, Sigma) is used in the capping reaction instead of SAM. The integrity of the capped RNA is analyzed using denaturing PAGE against standards (Ambion).

Three measures were taken to ensure consistent, highly efficient preparation of cap radiolabeled RNA. First, since SAM degrades rapidly once thawed, we use a fresh aliquot for each capping reaction. Second, we use commercial 10X capping reaction buffer (Ambion) to ensure RNase free assay conditions. Third, a fresh aliquot of 5' triphosphate RNA is used for each capping reaction to prevent multiple freeze thaw cycles, which compromise the integrity of the 5' triphosphate.

2.3 Substrate Characterization

Before proceeding with kinetic assays, we evaluate the extent of N^7-methylation using Nuclease P1. Typically, cap radiolabeled RNA (50,000 cpm) is added to 10 μL Nuclease P1 in buffer (Ambion) for a total volume of 20 μL, and incubated at 37°C for 1 hr as described (Wang and Kiledjian, 2001). Four microliters of the reaction are spotted onto a PEI-F TLC plate (Baker) and TLC analysis is performed as described below.

Migration of cap structures is visualized by phosphorimaging and compared to cold m7GpppG and GpppG standards, loaded in separate lanes and visualized by UV shadowing (NEB).

Nuclease P1 treatment of a 29nt cap radiolabeled RNA results in two species, which co-migrate with m^7GpppG and GpppG **(Figure 1)**. The fraction m^7GpppG RNA and GpppG RNA, calculated as cap species divided by that for the total radiolabeled RNA (m^7GpppG, GpppG, and origin), are 60% and 40% respectively. This information is used for later analysis of decapping data as an endpoint for fitting.

The rates extracted through single turnover kinetics do not depend on substrate concentration in contrast to multiple-turnover experiments, which have explicit substrate dependence (**Eq. (4)**). The presence of unmethylated GpppG RNA does not affect the observed kinetic constants given that, as with m^7GpppG RNA, it is present in trace amounts relative to the enzyme.

2.4 Protein Expression and purification:

Budding yeast Dcp2 is poorly behaved on its own, so we have developed a co-expression system for Dcp1/Dcp2 (Deshmukh et al.). The solubility of the Dcp1/Dcp2 complex is enhanced by fusing Dcp1 to the C-terminus of the B1 domain of streptococcal protein G. His-tagged GB1- Dcp1/Dcp2 (1-245) was expressed and purified by immobilized metal affinity chromatography using Talon resin. Enzyme eluted with varying concentration of imidazole in 10ml fractions were pooled, concentrated and

purified by size-exclusion chromatography using a 10/30 GL Superdex 200 column (GE Healthcare) (**Appendix A**).

The benefit of the size exclusion analysis is threefold. First, it ensures a monodisperse species. Second, a singular peak for the Dcp1/2 complex is indicative of a 1:1 molar ratio of complex components. This step is critical as single turnover kinetics relies heavily on accurate determinations of the enzyme concentration and an excess of one subunit over the other will skew subsequent concentration measurements. Third, gel filtration into storage buffer ensures the removal of any inhibitors or contaminants in solution, ensuring maximally active enzyme. For example, we have observed that sulfate and phosphate ions, high salt, or polyamines, such as spermine, inhibit decapping. In addition, since we quantify the enzyme by UV spectrophotometry, we avoid detergents and other compounds that absorb at 280 nm. If these are necessary for storage, it is worthy to consider desalting columns (PD-10 Sephadex G-25M, Amersham) for removing these contaminants before quantification.

KINETIC ASSAY

3.1 Overview

The general workflow of the assay is presented in **Figure 2.** To extract k_{max} and K_m from **Eq. (5)**, we measure k_{obs} for m^7GDP formation at a series of enzyme concentrations.

For each enzyme concentration, a typical decapping reaction is initiated by adding 40 μL of enzyme mix to 80 μL of RNA substrate mix at 4°C using an ultrathin-walled low retention PCR tube (Island Scientific). Kinetics is followed by manual pipetting with 6 μL of the decapping reaction withdrawn at variable times and rapidly quenched by addition to tubes containing 1 μL 0.5M EDTA on ice. Four microliters of each quenched reaction is blotted onto TLC plates, developed, exposed, and analyzed. Reactions obeyed first-order kinetics and were typically followed for times out to $3/k_{obs}$. This ensures adequate data for fitting **Eq. (4)**.

Kinetic constants are measured in the course of a single day using a single enzyme aliquot to ensure consistency and minimize reductions in enzyme activity due to aggregation.

3.2 Enzyme quantification and dilution

It is useful to measure rates (k_{obs}) at a range of enzyme concentrations above and below the K_m so that kinetic constants may be determined accurately through **Eq. (5)**.

For the yeast Dcp1/Dcp2 complex, with a K_m of 4 µM, we typically measure rates at enzyme concentrations of 1, 2, 3, 4, 5, 7, and 9 µM. Enzyme is prepared at three times the desired final concentration in 1X Dcp Reaction buffer using low retention microcentrifuge tubes (Fisher) (**Appendix A**). Serial protein dilution is required to reduce variation between decapping time courses, reducing scatter in plots of **Eq. (5)** and increasing accuracy of k_{max} and K_m.

3.3 Substrate mix

Two general considerations must be made when preparing the substrate mix. To ensure single turnover conditions, all assays are carried out with enzyme in excess of substrate. In our assay this condition is strongly obeyed as our lowest enzyme concentration is 1 µM while cap radiolabeled RNA was calculated to roughly 0.1-10 nM. In practice, a 10-fold excess of enzyme is adequate. Secondly, to achieve sufficient signal to noise during TLC analysis, the decapping reaction must contain at least 160 cpm/µL radiolabeled substrate.

We typically measure k_{obs} at 7 different enzyme concentrations to obtain kinetic constants through **Eq. (5)**. To ensure consistency in reagents, we prepare the substrate mix as a single batch and then aliquot it into separate reaction tubes for each enzyme concentration. Substrate mix is prepared in low retention microcentrifuge tubes (Fisher) by adding cap radiolabeled RNA (150,000 cpm) , 8 µL RNasin (Promega, 40 U/µL), 96 µL RNase free BSA (Promega, 1 mg/ml), 320 µL 2X Dcp reaction buffer and water for a final volume of 640 µL (**Appendix A**)

The inclusion of BSA and use of low retention tubes decrease variability in rates from enzyme adherence to the tube surface. This effect is especially pronounced at low concentrations, and causes a lower effective enzyme concentration that skews calculated results. For the yeast Dcp1/Dcp2 complex, omission of BSA or use of standard microcentrifuge tubes gives rise to a sigmoidal plot of k_{obs} versus E instead of the hyperbolic behavior predicted from **Eq. (5)**. However, a sigmoidal plot can also result from cooperative activation of enzyme through multimerization. This result may be corroborated by an assay to monitor multimerization, such as light-scattering or analytical ultracentrifugation.

3.4 TLC Analysis

Liberation of m^7GDP product is visualized by spotting onto PEI-F cellulose TLC plates (J.T. Baker). TLC plates are prerun the entire length in ddH_2O. The plates are allowed to dry and pencil marks are made every 1.5 cm, allowing 1 cm from the sides and bottom of the plate. Aliquots of each quenched reaction are spotted onto the marked TLC plate, which is subsequently dried and developed in 0.75M LiCl until solvent spans three-fourths the height of the plate. Dry plates are exposed to phosphorimaging screens (Amersham) overnight and scanned using a phosphorimager (Typhoon, GE Healthscience systems).

The spacing between TLC spots is important to ensure reaction products do not overlap during development. TLC plates may be prerun in advance and stored at 4°C in a

34

dry area or plastic bag. Migration of m⁷GDP and GDP products are verified by UV

shadowing with cold standards or treatment of products with NDPK as described (Wang

and Kiledjian, 2001).

3.5 Curve fitting

Exposed plates are scanned and processed using Imagequant (Molecular

Dynamics) to calculate the fraction of m^7GDP released as cpm m^7GDP divided by that

for total radiolabeled RNA (m^7GDP, GDP and Origin).

The data are transferred to SigmaPlot (Systat Software), and the fraction m^7GDP

(F) released is plotted versus time (minutes) (**Figure 3**).   The time courses are fit by non-

linear regression using the following equation (exponential rise to the max, 3 parameter,

where $a=F_{ep}$ and $b=k_{obs}$):

$$F(t) = F_{ep}\left[1 - e^{-k_{obs}t}\right]$$
<div align="right">**Equation (7)**</div>

with the end-point (F_{ep}) and first-order rate constant for product formation (k_{obs}) as fit-

parameters.

For very slow reactions that are linear throughout the time course **(Figure 4)**, the

observed rate constant is obtained from the initial rate, using the equation (standard

curves, 2 parameter):

$$F(t) = y_0 + a*t \text{ where } k_{obs} = \frac{a}{F_{ep}}$$
<div align="right">**Equation (8)**</div>

35

using the endpoint (F_{ep}) obtained by Nuclease P1 treatment. We obtain good first-order fits with end-points between 0.5-0.6.

Rates determined are then plotted at different enzyme concentrations and fit to **Eq. (5)** (Hyperbola, 3 parameter, where $a=k_{max}$ and $b=K_m$) with k_{max} the apparent rate of the catalytic step and K_m corresponding to $\dfrac{k_{off} + k_{max}}{k_{on}}$. **(Figure 5)**

3.6 Metal activation

Assays involving the Dcp1/2 complex are performed using 5 mM Mg^{2+}. This is an important variable in the reaction as the concentration, as well as type, of metal, varies depending on enzyme. Optimum metal concentration is determined using the assay described with minor modifications: a single enzyme concentration is chosen and the amount of metal is varied. Rates (k_{obs}) are plotted as a function of metal concentration and the optimum metal concentration is determined.

In addition, the metal occupancy is determined by fitting the metal activation data to the following equation (Sigmoidal, Hill 3 parameter):

$$F(x) = \frac{ax^b}{(c^b + x^b)}$$ **Equation (9)**

where, a is F_{ep}, c corresponds to the concentration of metal that gives half-maximal activation and b is the Hill coefficient, or minimum number of metals bound by enzyme (**Figure 7**).

SUMMARY

Removal of the 5' cap sentences an RNA to destruction and is a highly regulated step in 5'-3' RNA decay. We have developed a simple *in vitro* assay for monitoring substrate binding and the catalytic step of decapping using recombinant yeast decapping enzyme complex (Dcp1/Dcp2) and cap radiolabeled RNA. We anticipate that this procedure will be useful for dissecting the role of protein interactions at the level of regulating RNA specificity and enzyme activity. A powerful application of this assay will entail examining how decapping enzymes are regulated be additional components of the decapping RNP, added as either recombinant purified proteins or purified from cell extracts. The combination of kinetic assays and structural studies will allow the molecular mechanisms of RNA decapping to be clearly defined.

ACKNOWLEDGEMENTS

APPENDIX A: Buffers

10X T7 Transcription Buffer
380 mM $MgCl_2$
400 mM Tris-HCl (pH 8.0)
25 mM Spermidine
0.1% Triton-X

Gel Extraction Buffer, pH 8.3
200 mM Tris-Cl
25 mM EDTA
300 mM NaCl
2% w/v SDS

Dcp1/2 Lysis Buffer, pH 7.5
50 mM NaPhos (38.7mM Na_2HPO_4,
11.3 mM NaH_2PO_4)
300 mM NaCl
5 mM 2-mercaptoethanol (βMe)
5% glycerol
Complete EDTA free protease inhibitors
(Roche)

Dcp1/2 Wash Buffer, pH 7.5
50 mM NaPhos (38.7 mM Na_2HPO_4,
11.3 mM NaH_2PO_4)
300 mM NaCl
5 mM 2-mercaptoethanol (βMe)
5% glycerol
20 mM Imidazole

Dcp1/2 Elution buffer, pH 7.5
50 mM NaPhos (38.7 mM Na_2HPO_4,
11.3 mM NaH_2PO_4)
300 mM NaCl
4 mM 2-mercaptoethanol (βMe)
5% glycerol
50, 100, 150, 200, 250 mM Imidazole
Fractions

Gel Filtration Buffer, pH 7.5
50 mM HEPES
100 mM NaCl
5 % glycerol
5 mM DTT

Storage Buffer, pH 7.5
50 mM HEPES
100 mM NaCl
20 % glycerol
5 mM DTT

Substrate Mix
0.1-10 nM Cap Radiolabeled RNA
8 U RNasin
0.15 mg/mL BSA
1X Dcp Reaction Buffer

Dcp Reaction Buffer (1X)
50 mM Tris-Cl (pH 8 at RT)
50 mM NH_4Cl
0.01% NP-40
1 mM DTT
5 mM $MgCl_2$

REFERENCES

Beelman, C. A., Stevens, A., Caponigro, G., LaGrandeur, T.E., Hatfield, L., Fortner, D.M., and Parker, R., 1996. An essential component of the decapping enzyme required for normal rates of mRNA turnover. Nature 382**,** 642-646.

Bessman, M. J., Frick, D. N., O'Handley, S. F., 1996. The MutT proteins or "Nudix" hydrolases, a family of versatile, widely distributed, "housecleaning" enzymes. J Biol Chem. 271**,** 25059-62.

Chen, N., Walsh, M. A., Liu, Y., Parker, R., Song, H., 2005. Crystal structures of human DcpS in ligand-free and m7GDP-bound forms suggest a dynamic mechanism for scavenger mRNA decapping. J Mol Biol. 347**,** 707-18.

Coller, J., Parker, R., 2004. Eukaryotic mRNA decapping. Annu Rev Biochem. 73**,** 861-90.

Cougot, N., van Dijk, E., Babajko, S., Seraphin, B., 2004. 'Cap-tabolism'. Trends Biochem Sci. 29**,** 436-44.

Deshmukh, M. V., Jones, B. N., Quang-Dang, D.-U., Flinders, J., Floor S. N., Kim, C., Jemielity, J., Kalek, M., Darzynkiewicz, E., Gross, J. D., 2008. mRNA decapping is promoted by an RNA binding channel in Dcp2. Mol Cell 29**,** 324-36.

Dixon, M., 1953. The determination of enzyme inhibitor constants. Biochem J. 55**,** 170-1.

Dunckley, T., Parker, R., 1999. The DCP2 protein is required for mRNA decapping in Saccharomyces cerevisiae and contains a functional MutT motif. EMBO J. 18**,** 5411-22.

Eulalio, A., Behm-Ansmant, I., Izaurralde, E., 2007. P bodies: at the crossroads of post-transcriptional pathways. Nat Rev Mol Cell Biol. 8**,** 9-22.

Fenger-Gron, M., Fillman, C., Norrild, B., Lykke-Andersen, J., 2005. Multiple processing body factors and the ARE binding protein TTP activate mRNA decapping. Mol Cell. 20**,** 905-15.

Fersht, A. R., 1999. Enzyme structure and mechanism. John Wiley & Sons, Chichester, UK (2nd ed.).

Ghosh, T., Peterson, B., Tomasevic, N., Peculis, B. A., 2004. Xenopus U8 snoRNA binding protein is a conserved nuclear decapping enzyme. Mol Cell. 13**,** 817-28.

Gu, M., Fabrega, C., Liu, S. W., Liu, H., Kiledjian, M., Lima, C. D., 2004. Insights into the structure, mechanism, and regulation of scavenger mRNA decapping activity. Mol Cell. 14**,** 67-80.

Han, G. W., et al., 2005. Crystal structure of an Apo mRNA decapping enzyme (DcpS) from Mouse at 1.83 A resolution. Proteins. 60**,** 797-802.

Herschlag, D., Cech, T. R., 1990a. Catalysis of RNA cleavage by the Tetrahymena thermophila ribozyme. 1. Kinetic description of the reaction of an RNA substrate complementary to the active site. Biochemistry. 29**,** 10159-71.

Herschlag, D., Cech, T. R., 1990b. DNA cleavage catalysed by the ribozyme from Tetrahymena. Nature. 344**,** 405-9.

Johnson, A. W., 1997. Rat1p and Xrn1p are functionally interchangeable exoribonucleases that are restricted to and required in the nucleus and cytoplasm, respectively. Mol Cell Biol. 17**,** 6122-30.

Johnson, K. A., 1992 Transient-state kinetic analysis of enzyme reaction pathways The Enzymes. XX 1–61.

Krogan, N. J., et al., 2006. Global landscape of protein complexes in the yeast Saccharomyces cerevisiae. Nature. 440**,** 637-43.

Lima, C. D., Klein, M. G., Hendrickson, W. A., 1997. Structure-based analysis of catalysis and substrate definition in the HIT protein family. Science. 278**,** 286-90.

Liu, H., Rodgers, N. D., Jiao, X., Kiledjian, M., 2002. The scavenger mRNA decapping enzyme DcpS is a member of the HIT family of pyrophosphatases. EMBO J. 21**,** 4699-708.

Liu, S. W., Jiao, X., Liu, H., Gu, M., Lima, C. D., Kiledjian, M., 2004. Functional analysis of mRNA scavenger decapping enzymes. RNA. 10**,** 1412-22.

Maquat, L. E., 2004. Nonsense-mediated mRNA decay: splicing, translation and mRNP dynamics. . Nat Rev Mol Cell Biol 5**,** ,89-99.

McConnell, T. S., Cech, T. R., Herschlag, D., 1993. Guanosine binding to the Tetrahymena ribozyme: thermodynamic coupling with oligonucleotide binding. Proc Natl Acad Sci U S A. 90**,** 8362-6.

Mildvan, A. S., Xia, Z., Azurmendi, H. F., Saraswat, V., Legler, P. M., Massiah, M. A., Gabelli, S. B., Bianchet, M. A., Kang, L. W., Amzel, L. M., 2005. Structures and mechanisms of Nudix hydrolases. Arch Biochem Biophys. 433**,** 129-43.

Moore, M. J., 2005. From birth to death: the complex lives of eukaryotic mRNAs. Science. 309**,** 1514-8.

Muhlrad, D., Decker, C. J., Parker, R., 1994. Deadenylation of the unstable mRNA encoded by the yeast MFA2 gene leads to decapping followed by 5'-->3' digestion of the transcript. Genes Dev. 8**,** 855-66

Parker, R., Sheth, U., 2007. P bodies and the control of mRNA translation and degradation. Mol Cell. 25**,** 635-46.

Parker, R., Song, H., 2004. The enzymes and control of eukaryotic mRNA turnover. . Nat Struct Mol Biol. 11**,** 121-7

Parrish, S., Moss, B., 2007. Characterization of a Second Vaccinia Virus mRNA-Decapping Enzyme Conserved in Poxviruses. J Virol. 81**,** 12973-8.

Parrish, S., Resch, W., Moss, B., 2007. Vaccinia virus D10 protein has mRNA decapping activity, providing a mechanism for control of host and viral gene expression. Proc Natl Acad Sci U S A. 104**,** 2139-44.

Peculis, B. A., Reynolds, K., Cleland, M., 2007. Metal determines efficiency and substrate specificity of the nuclear NUDIX decapping proteins X29 and H29K (Nudt16). J Biol Chem. 282**,** 24792-805.

Peculis, B. A., Steitz, J. A., 1993. Disruption of U8 nucleolar snRNA inhibits 5.8S and 28S rRNA processing in the Xenopus oocyte. Cell. 73**,** 1233-45.

Piccirillo, C., Khanna, R., Kiledjian, M., 2003. Functional characterization of the mammalian mRNA decapping enzyme hDcp2. RNA. 9**,** 1138-47.

Reddy, R., Singh, R., Shimba, S., 1992. Methylated cap structures in eukaryotic RNAs: structure, synthesis and functions. Pharmacol Ther. 54**,** 249-67.

Rehwinkel, J., Behm-Ansmant, I., Gatfield, D., Izaurralde, E., 2005. A crucial role for GW182 and the DCP1:DCP2 decapping complex in miRNA-mediated gene silencing. . RNA. 11 1640-1647.

Scarsdale, J. N., Peculis, B. A., Wright, H. T., 2006. Crystal structures of U8 snoRNA decapping nudix hydrolase, X29, and its metal and cap complexes. Structure. 14**,** 331-43.

Seraphin, B., 1992. The HIT protein family: a new family of proteins present in prokaryotes, yeast and mammals. DNA Seq. 3**,** 177-9.

Shatkin, A. J., 1976. Capping of eucaryotic mRNAs. Cell. 9**,** 645-53.

She, M., Decker, C. J., Chen, N., Tumati, S., Parker, R., Song, H., 2006. Crystal structure and functional analysis of Dcp2p from Schizosaccharomyces pombe. Nat Struct Mol Biol. 13**,** 63-70.

Shors, T., Keck, J. G., Moss, B., 1999. Down regulation of gene expression by the vaccinia virus D10 protein. J Virol. 73**,** 791-6.

Steiger, M., Carr-Schmid, A., Schwartz, D. C., Kiledjian, M., Parker, R., 2003. Analysis of recombinant yeast decapping enzyme. RNA. 9**,** 231-8.

Stevens, A., Maupin, M. K., 1987. A 5'----3' exoribonuclease of Saccharomyces cerevisiae: size and novel substrate specificity. Arch Biochem Biophys. 252**,** 339-47.

Tomasevic, N., Peculis, B., 1999. Identification of a U8 snoRNA-specific binding protein. J Biol Chem. 274**,** 35914-20.

van Dijk, E., Cougot, N., Meyer, S., Babajko, S., Wahle, E., Seraphin, B., 2002. Human Dcp2: a catalytically active mRNA decapping enzyme located in specific cytoplasmic structures. EMBO J 21**,** 6915-6924.

van Dijk, E., Le Hir, H., Seraphin, B., 2003. DcpS can act in the 5'-3' mRNA decay pathway in addition to the 3'-5' pathway. Proc Natl Acad Sci U S A. 100**,** 12081-6.

Wang, Z., Kiledjian, M., 2001. Functional link between the mammalian exosome and mRNA decapping. Cell. 107**,** 751-62.

Weischenfeldt, J., Lykke-Andersen, J., Porse, B., 2005. Messenger RNA surveillance: neutralizing natural nonsense. Curr Biol. 15**,** R559-62.

FIGURE LEGENDS

Figure 1: A capped RNA preparation before and after nuclease P1 treatment, visualized by TLC analysis. Methylated and unmethylated GpppG cap run as indicated. Origin designates unreacted substrate.

Figure 2: The general workflow of the assay. For each enzyme concentration, we initiate the decapping reaction by adding enzyme to substrate. Kinetics are followed by removing aliquots from the decapping reaction at different times and rapidly quenched with EDTA.

Figure 3: Representative time course data as analyzed by TLC for 2μM enzyme. Methylated and unmethylated products run as indicated. Fraction m^7GDP product is calculated as m^7GDP product divided by total radiolabeled RNA (m^7GDP + GDP + Origin).

Figure 4: Time course data for wild-type Dcp1/2 complex at variable enzyme concentrations (1, 2, 3, 4, 5 7, 9 μM) as indicated. Time points were taken every 10 seconds and m^7GDP released was plotted as a function of time. Data were fit to **Eq. (7)**.

Figure 5: Linear time course data obtained by plotting m^{7}GDP released as a function of time for K135A Dcp1/2 complex at variable enzyme concentrations (1.5, 3, 4.5, 7.5, 10, and 12.5 μM) as indicated. Data were fit to **Eq. (8)**.

Figure 6: Graph of k_{obs}, versus enzyme concentration for wild type Dcp1/2 complex. Data were fit to **Eq. (5)** to obtain parameters of k_{max} and K_m. The error bars represent the standard error in k_{obs}.

Figure 7: Graph of k_{obs} at variable concentration of metal. A single enzyme concentration is used and data are fit to **Eq. (9)**. The error bars represent the standard error in k_{obs}. For the Dcp1/Dcp2 complex, the concentration of metal needed for maximal enzyme activity is 5 mM. The Hill coefficient is 2.4, indicating at least 2 metals bind the enzyme.
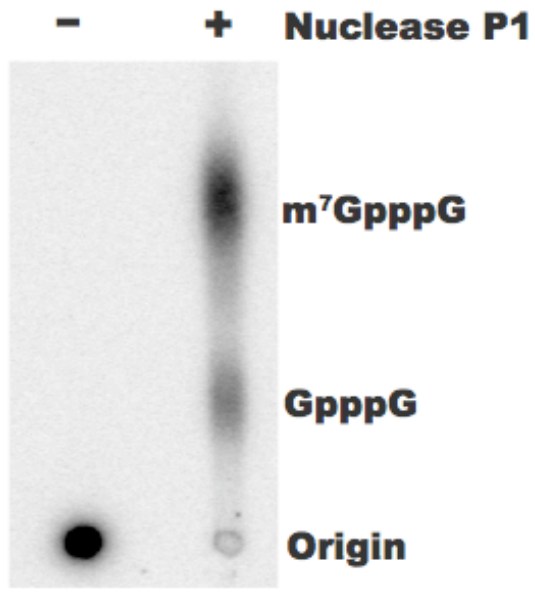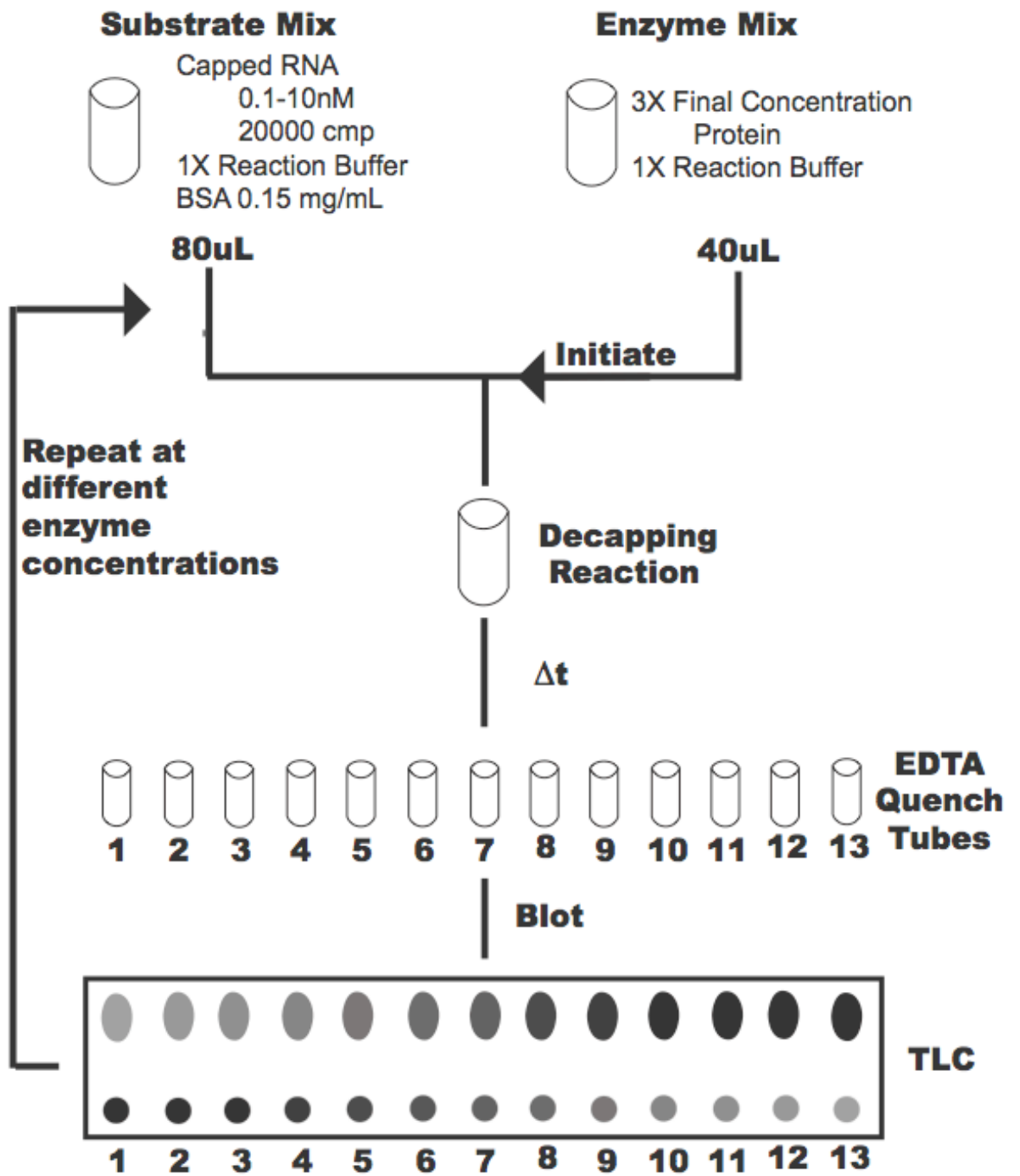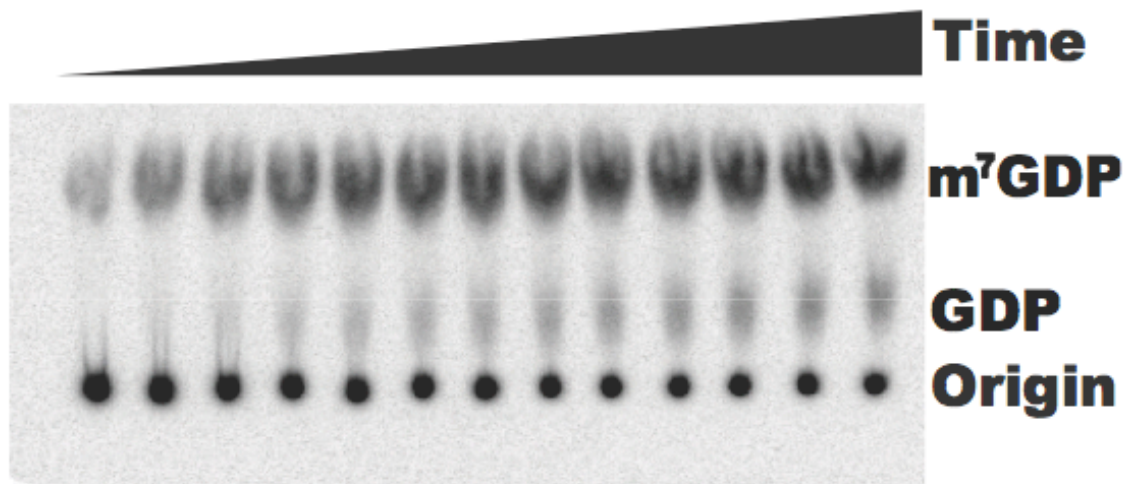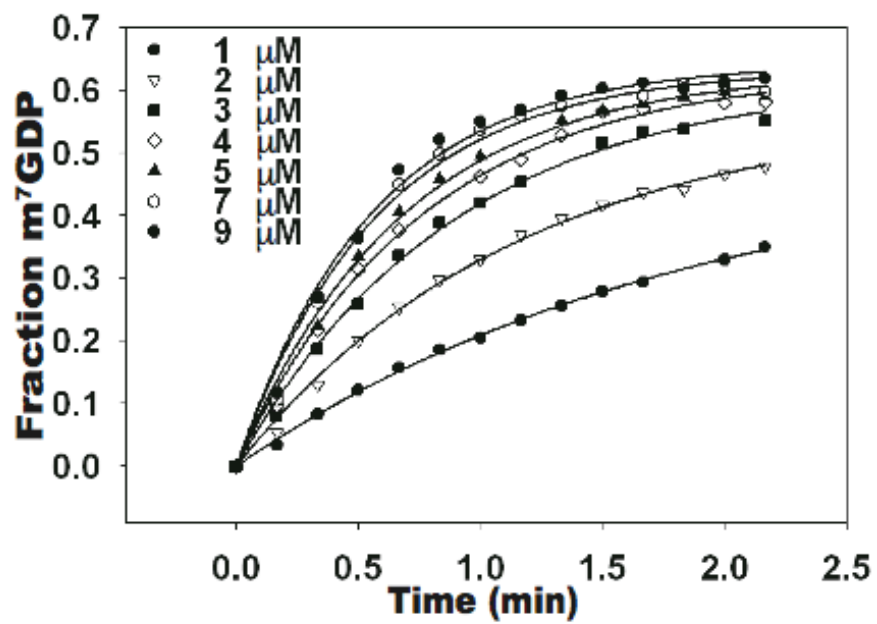
FIGURE 1

FIGURE 2

FIGURE 3
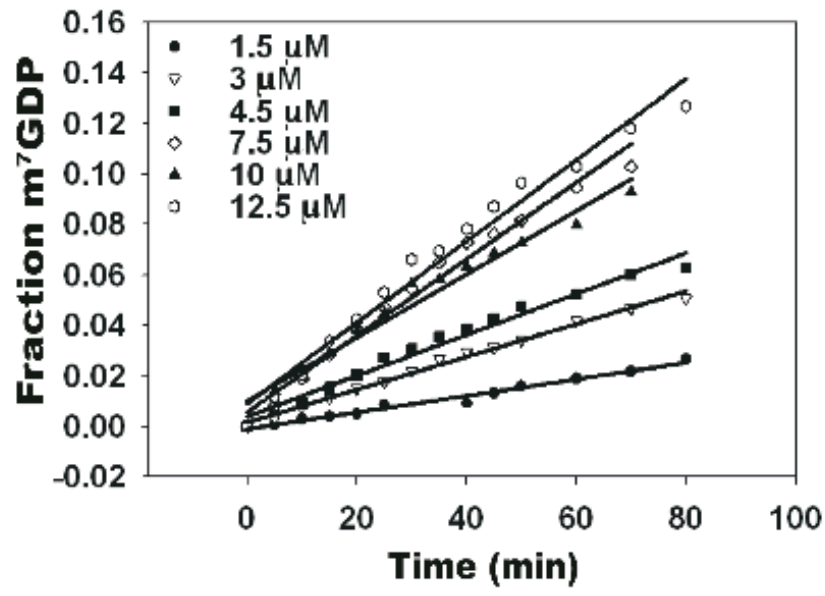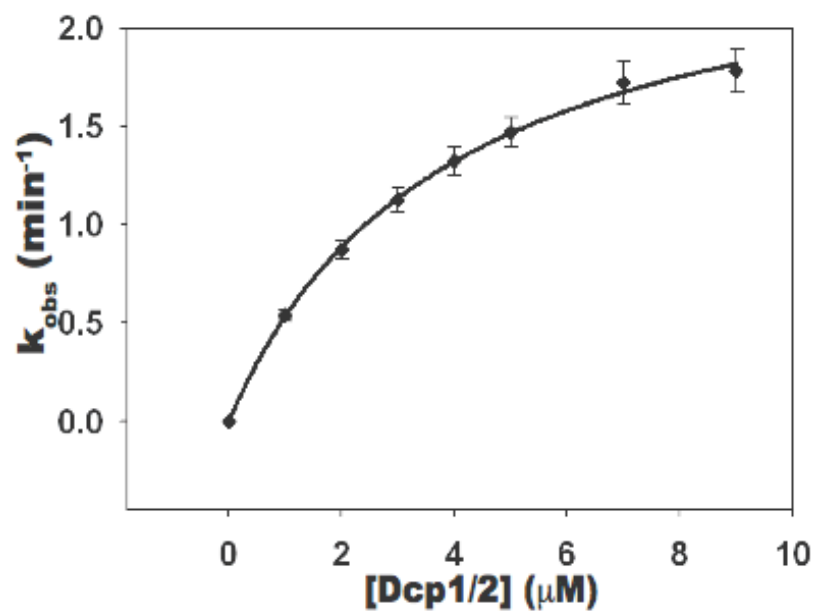
FIGURE 4
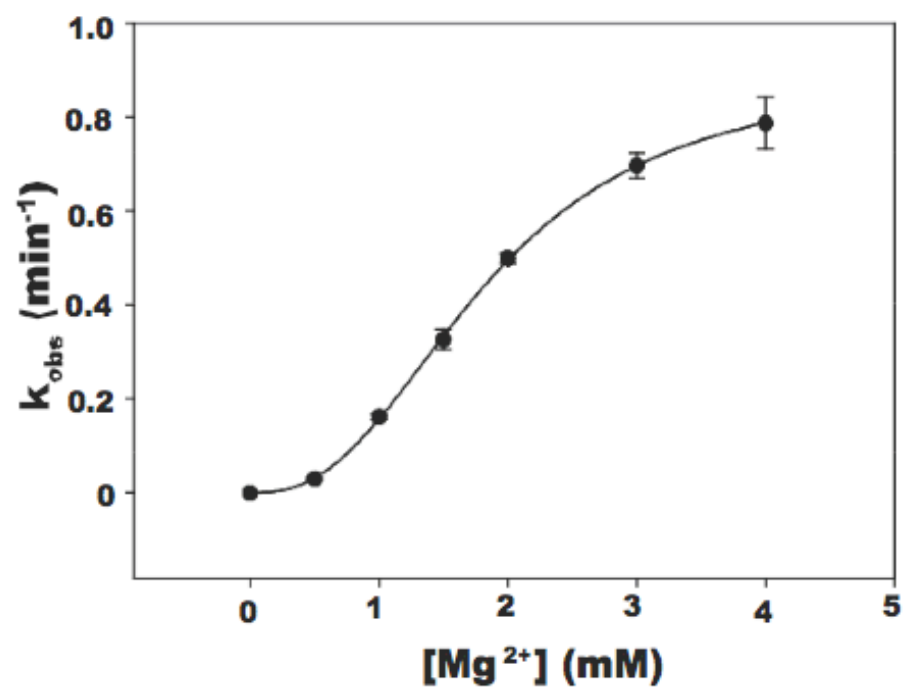
FIGURE 5

FIGURE 6

FIGURE 7

CHAPTER 3:

mRNA decapping is promoted by an RNA binding channel in Dcp2

mRNA decapping is promoted by an RNA binding channel in Dcp2

Mandar V. Deshmukh[1,6,7], Brittnee N. Jones[2,7], Duc-Uy Quang-Dang[1,7], Jeremy Flinders[1],

Stephen N. Floor[3], Candice Kim[1], Jacek Jemielity[4], Marcin Kalek[4],

Edward Darzynkiewicz[4] and John D. Gross[1,5]

[1]Department of Pharmaceutical Chemistry, [2]Program in Chemistry and Chemical Biology

and [3]Graduate Group in Biophysics, University of California, San Francisco, CA 94107

[4]Department of Biophysics, Institute for Experimental Physics

Warsaw University, 02-089 Warsaw, Poland

[5]Corresponding Author: John Gross, UCSF Mission Bay-Genentech Hall Box 2280

San Francisco, CA 94107

Tel: (415) 514-4402

Fax (415) 502-8298

Email: jdgross@picasso.ucsf.edu

[6]Present Address: Centre for Cellular and Molecular Biology, Uppal Road

Hyderabad-50007, AP, India

[7]These authors contributed equally.

Running Title: mRNA Recognition by Dcp2

SUMMARY

Cap hydrolysis by Dcp2 is a critical step in several eukaryotic mRNA decay pathways. Processing requires access to cap proximal nucleotides and the coordinated assembly of a decapping mRNP, but the mechanism of substrate recognition and regulation by protein interactions have remained elusive. Using NMR spectroscopy and kinetic analyses we show that yeast Dcp2 resolves interactions with the cap and RNA body using a bipartite surface, which forms a channel intersecting the catalytic and regulatory Dcp1 binding domains. The interaction with cap is weak but specific and requires binding of the RNA body to a dynamic interface. The catalytic step is stimulated by Dcp1 and its interaction domain, likely through a substrate induced conformational change. Thus, activation of the decapping mRNP is restricted by access to 5' proximal nucleotides, a feature that could act as a checkpoint in mRNA metabolism.

INTRODUCTION

 mRNA decay is highly regulated and plays a critical role in early animal development, cell growth and proliferation, adaptation to stress and the quality control of gene expression (Amrani et al., 2006; Chen and Shyu, 1995; Hilgers et al., 2006; Maquat, 2004; Schier, 2007). The mRNA decapping enzyme Dcp2 is the catalytic core of a multiprotein complex that assembles on the 5' end of a transcript to promote cap hydrolysis, liberating m7GDP and an RNA body containing a 5' monophosphate (Beelman et al., 1996; Lykke-Andersen, 2002; Steiger et al., 2003; van Dijk et al., 2002; Wang et al., 2002). The latter is efficiently recognized by the conserved exoribonuclease Xrn1 which degrades the RNA body in a 5'-3' fashion (Stevens and Maupin, 1987). As such, decapping precedes and permits 5'-3' decay and is the penultimate step in several pathways that regulate eukaryotic gene expression at the level of mRNA stability including the general 5'-3' decay pathway, AU rich element (ARE) mediated decay, non-sense mediated decay (NMD), deadenylation independent decapping and micro RNA coupled decapping pathways (Behm-Ansmant et al., 2006; Coller and Parker, 2004; Rehwinkel et al., 2005).

A unifying feature of pathways that culminate in decapping and 5'-3' decay is the requirement for translational repression which targets the transcript to processing bodies (P-bodies), sites of mRNA storage or decay (Anderson and Kedersha, 2006; Brengues et al., 2005; Eulalio et al., 2007; Sheth and Parker, 2003). P-bodies contain the decapping enzyme, activators of decapping and the exoribonuclease but lack ribosomes and nearly

all translation factors (Andrei et al., 2005; Barbee et al., 2006; Ferraiuolo et al., 2005; Sheth and Parker, 2003). These observations support the view that P-body formation is accompanied by a major reorganization of the mRNA from a state of occlusion by bound initiation factors and polyribosomes, to a state of availability, allowing assembly of either a repression or a decapping mRNP which is sufficient for function (Parker and Sheth, 2007). The molecular mechanisms of mRNA recognition by the repression or the decapping complex are thought to play a critical role in determining the overall fate of a transcript, though the structural details of these interactions are poorly understood.

Given its central role in mRNA metabolism, the molecular basis of mRNA decapping by Dcp2 has fallen under intense scrutiny. Crystallographic analysis of *S. pombe* Dcp2 indicates the conserved N-terminus of the enzyme forms an extended, bi-lobed structure containing an alpha-helical domain followed by a Nudix fold (She et al., 2006). The Nudix fold is found in a superfamily of metal dependent hydrolases that acts on substrates containing a nucleotide diphosphate linked to any moiety (x) (Bessman et al., 1996; Mildvan et al., 2005). The alpha-helical domain is unique to Dcp2, acts as a scaffold for interactions with Dcp1 and is required for decapping in yeast (She et al., 2006). Dcp1 is also essential for decapping in yeast and stimulates the activity of Dcp2 *in vitro*, suggesting that Dcp1 and Dcp2 work together as a holoenzyme (Beelman et al., 1996; Dunckley and Parker, 1999; Steiger et al., 2003). In addition, Dcp1 contains an Enabled-Vasp-Homology-1 (EVH1) fold, suggesting it may promote decapping by targeting Dcp2 to components of the larger decapping complex observed in cells (She et al., 2004). Although Dcp1 forms a direct interaction with Dcp2 in yeast, in higher

eukaryotes, Hedls/Ge-1/hEdc4 is also required to unite Dcp1 with Dcp2 (Fenger-Gron et al., 2005).

Despite extensive efforts, the mechanism of mRNA decapping by Dcp2 and how Dcp1 stimulates activity have remained elusive in part due to the lack of structural information with substrate. Several observations suggest Dcp2 recognizes the cap through an obligate interaction with the RNA body. First, cap analogue (m7GpppG) or short capped RNAs are not efficiently decapped in vitro whereas long mRNA substrates are efficiently hydrolyzed (Cohen et al., 2005; Piccirillo et al., 2003; Steiger et al., 2003; van Dijk et al., 2002). Second, Dcp2 can be cross-linked to capped RNA but not cap analogue (Piccirillo et al., 2003). Third, blocking access to cap proximal nucleotides by formation of DNA/RNA hybrids decreases processing by Dcp2 (Steiger et al., 2003). Fourth, Dcp2 efficiently processes N-7 methyl capped RNA but not the unmethylated counterparts (Piccirillo et al., 2003; van Dijk et al., 2002). Finally, Dcp2 interacts with ssDNA (Piccirillo et al., 2003) and was reported to process capped-DNA chimeras (Steiger et al., 2003), suggesting interactions with cap proximal nucleotides may not depend on sequence. These data indicate that the interaction of Dcp2 with cap is weak but specific, requiring access to an exposed stretch of cap proximal nucleotides for activity.

Structural studies of Dcp2 in complex with RNA are a challenge, given that Dcp2 acts on a variety of RNA substrates through an unfavorable combination of relatively weak specific and moderately strong non-specific interactions. High-resolution NMR is a

powerful tool to study transient complexes that may interact through multiple binding modes. Here we combine NMR with functional analyses to examine how the RNA body promotes decapping and how this activity is enhanced by Dcp1. We identify a conserved channel on the decapping enzyme that interacts with the cap and RNA body using a bipartite interaction surface that supports distinct steps in catalysis, through formation of specific interactions between the cap and non-specific interactions with the RNA body. The role of Dcp1 and its interaction domain are to promote the catalytic step, not RNA binding, possibly by stabilizing a substrate induced conformational transition into an active complex.   The architecture of the unusual channel within the core of the decapping complex may restrict processing to messages that have a freely available 5' end, a feature that could safeguard a message from precocious decapping and untimely destruction.

RESULTS

Capped RNA binds a narrow channel

To identify the substrate binding surface, we mapped the interaction between Dcp2 and RNA by NMR. The budding yeast enzyme containing the Nudix and Dcp1 binding domains were poorly behaved at NMR concentrations. Accordingly, we initially focused NMR studies on the Nudix domain since it contains a conserved region termed Box B which was implicated in substrate binding and is sufficient for decapping *in vitro* (Piccirillo et al., 2003). NMR experiments were performed using a solubility enhancement tag consisting of the B1 domain of protein G (GB1) fused to the yeast Dcp2, since the Nudix domain is only marginally soluble in the absence of RNA (Zhou et al., 2001). The tagged enzyme is active, its solution structure agrees well with the *S. pombe* Dcp2 crystal structure and GB1 does not interact with the enzyme in cis (**Figures 1a,b and S1**) (She et al., 2006).

We confirmed that potential RNA binding surfaces on budding yeast Dcp2 reside primarily on the Nudix domain by generating a homology model based on the fission yeast crystal structure (**Figure 1c**). The model reveals an extended channel that runs along a basic surface formed by the Nudix domain. The channel begins on the dorsal surface of the domain, continues into a cavity near the domain interface and terminates at a short beta strand (β_4) saddled above the Nudix box (α_1) (**Figure 1b-d**). The Nudix box is the catalytic center of the enzyme and defines the ventral surface of the domain. The cavity is delimited by loops between α_2-α_3, β_2-β_3, β_5-β_6, β_6-β_7 and the Nudix box while the dorsal surface is defined by α_2, α_3 and the intervening loop (**Figure 1b**). The cavity

corresponds to the nucleotide binding site observed in other Nudix enzymes (Mildvan et al., 2005) whereas the positively charged surface provided by the dorsum is unique to Dcp2. Unlike the nucleotide binding cavity, basic residues lining the dorsal surface are only moderately conserved at the level of primary sequence; however, this surface is highly enriched with positive charge in structures of both fission and budding yeast enzymes, suggesting a role in non-specific recognition of the phosphate backbone. (**Figures 1, S2 and S3**).

Since the basic surface of the channel resides primarily on the Nudix domain, it may serve as a binding site for substrate (**Figure 1c,d**). To test this idea, we performed chemical shift perturbation mapping with RNAs of different length and sequence. Both a 15nt MFA2 RNA and a random 29nt RNA sequence perturbed resonances of amino acids lining the dorsal surface and the nucleotide binding cavity (K135 and R133) (**Figure S4**). The same regions were perturbed by sulfate ions, which inhibit decapping *in vitro* (data not shown). These results indicate that the RNA body contacts the dorsal surface of the Nudix domain in addition to a subset of residues within the nucleotide binding cavity. Notably, partially conserved hydrophobic and aromatic residues within Box B (α_3 and the intervening loop with α_2) lie directly on the RNA binding surface, consistent with the proposal that this region binds substrate (**Figures 1 and S4**) (Piccirillo et al., 2003).

Given the specificity of Dcp2 for the N7-methyl moiety of mRNA substrates, we next asked if binding of capped and uncapped RNA were different. Binding of a 29 nt non-hydroylzable capped RNA caused resonance shifts in the same region as the

uncapped counterpart (**Figures 2a and S4**); however, additional shifts were observed on E153 and E198 which are conserved residues within the Nudix box and a remote loop which, by analogy to other Nudix enzymes, may act in metal coordination and as the general base (**Figure 2b-d**) (Gabelli et al., 2002). Residues within the flexible linker between GB1 and the Nudix domain were also shifted in the presence of capped but not uncapped RNA (**Figure S4**). In contrast, neither m7GDP nor cap analogue (m7GpppG) bound the Nudix domain at 1mM concentration under a variety of conditions (data not shown**).** These data suggest that recognition of the cap by the Nudix domain is weak but specific and is only observed when the cap is covalently linked to RNA. In contrast, binding of the RNA body occurs with relatively high affinity independent of sequence. We conclude that the cap and RNA body bind in separate regions of the Nudix domain that define the termini of the basic channel in Dcp2 (**Figure 2c**).

Mutation of channel residues disrupts activity

To determine the role of channel residues in decapping by the Nudix domain, we substituted surface exposed residues with alanine and assayed decapping activity *in vitro*. Mutation of conserved basic residues lining the nucleotide binding cavity (R133 and K135) reduced decapping relative to wild-type by at least 15-fold (**Figures 3a and S3**). Single or double mutation of residues (Y222, K212/R229, K216/R229, R170/R229) lining the dorsal RNA binding surface resulted in significant reductions in decapping (at least 5-fold) (**Figure 3a**). These data indicate that residues within the nucleotide binding cavity and the dorsal RNA binding site determined by NMR play an important role in decapping by the Nudix domain.

The contribution of channel residues to decapping by Dcp1/Dcp2 was also examined. Nearly all of the preceding residues found to be important for decapping by the Nudix domain in isolation were critical for decapping by the Dcp1/Dcp2 complex (**Figure 3b**). Notable differences (R133 and K175) may reflect compensation in RNA binding or decapping chemistry provided by Dcp1 or its interaction domain. Mutation of the conserved linker residue (K100) to alanine reduced decapping by 10-fold, consistent with a previous study (She et al., 2006).

Since Dcp1 and Dcp2 form the core of a larger decapping complex in cells, we next asked if channel residues were important for Dcp2 function in yeast. To this end, we assayed whether or not a plasmid born copy of mutant Dcp2 was able to complement the temperature sensitive lethal phenotype of the DCP2 gene disruption (**Figure 3c**). Mutation of residues near (K100) or within the nucleotide binding cleft (K135) resulted in a slow growth phenotype at 37 °C compared to wild-type (**Figure 3c**). Single mutations of residues lining the dorsal RNA binding surface did not affect growth in vivo in contrast to double mutations (R170/R229, K216/R229), which had a modest effect (**Figures 3c and S6**). These data support the interpretation that residues lining the channel derived from the NMR binding studies with non-hydrolyzable substrate RNA are important for decapping by Dcp2 *in vitro* and function in budding yeast.

The catalytic roles of Dcp1 and the RNA binding channel

To determine how the RNA binding channel promotes decapping by Dcp1/Dcp2, we first investigated the role of Dcp1 and its binding domain. One possibility is that Dcp1 enhances the interaction between Dcp2 and substrate RNA. Alternatively, Dcp1 could enhance the catalytic step of decapping. To distinguish between these possibilities, we developed an assay using excess enzyme over substrate to measure rates of decapping under single-turnover conditions. Accordingly, we measured the first order rate constant, k_{obs}, governing m7GDP formation at several enzyme concentrations and extracted K_m and k_{max} to provide measures of the RNA binding efficiency and the rate of the catalytic step (**Figure 4a,b**).

Kinetic constants were determined for the wild-type Dcp1/Dcp2 complex and the Nudix domain in isolation, since larger fragments of yeast Dcp2 are poorly behaved in the absence of Dcp1. Remarkably, k_{max} for the Nudix domain was reduced 1000-fold relative to the decapping complex while K_m was increased only 2-fold (**Figures 4c-inset, 4d and Table 1**). Direct binding experiments with non-hydrolyzable capped RNA indicate K_m is K_d (**Figure 4 e,f**). These results reveal that Dcp1 and its interaction domain strongly enhance the catalytic step while the Nudix domain acts as the substrate interaction platform, providing a basal level of cap hydrolysis.

If the Nudix domain acts as a platform for RNA binding, then mutation of channel residues should increase K_m. To test this prediction, we determined k_{max} and K_m for alanine substitutions of channel residues within the Dcp1/Dcp2 complex. All of the

channel mutations that reduced m7GDP formation in the end-point decapping assay for both the isolated Nudix domain and the decapping complex resulted in an increased K_m (**Figures 3a,b and 4c,d**). Consistent with this result, mutation of residues lining the dorsal surface that had the largest effect on K_m reduced RNA binding as detected by ^{15}N HSQC NMR (**Figure S7**). These data indicate that the channel promotes RNA binding by distributing relatively weak interactions over a large interaction surface.

Residues lining the channel also affected the catalytic step of decapping. Mutation of residues within or near the nucleotide binding cavity reduced k_{max}. Mutation of the conserved residue K135 resulted in a 300-fold reduction in k_{max} and a nearly 1000-fold reduction on catalytic efficiency (k_{max}/K_m), consistent with an essential role in catalysis (**Figure 4c-inset and Table 1**). This mutation also reduced product specificity, generating both m7GDP and m7GTP, consistent with K135 playing a direct role in chemistry (**Figure S8**). Mutation of K100 and Y222 had modest effects on the catalytic step, reducing k_{max} only 1.5-fold (**Figures 4c and Table 1**). In contrast, mutation of residues lining the dorsal surface (R170/R229, K212/R229 K216/R229) unexpectedly increased k_{max}; however, the catalytic efficiencies of these mutants were all reduced relative to the wild-type complex due to large defects in substrate binding (**Figure 4c and Table 1**). These results indicate that a subset of residues within the nucleotide binding cavity play an essential role in decapping chemistry while those on the dorsal surface primarily modulate affinity.

The cap is recognized during the catalytic step

In principle specificity for the m7G of the cap could be conferred during binding or the catalytic step. To distinguish between these possibilities, we determined K_m and k_{max} for RNA containing an unmethylated 5' terminal GpppG structure. Importantly, the rate of the catalytic step, k_{max}, was reduced 15-fold for unmethylated RNA compared to the N7-methylated counterpart (**Figures 4c and S9**). In contrast, K_m for unmethylated GpppG RNA increased only three-fold relative to RNA containing the N7-methyl cap (**Figure 4d and Table 1**). In agreement with these findings, comparison of K_d obtained by gel-shift analysis for non-hydrolyzable capped RNA with that containing 5' monophosphate indicates that binding of the decapping complex to RNA is unaffected by presence of the cap structure (**Figure 4e and S10**). These results indicate that specificity for the methylated nucleobase is conferred predominantly during the catalytic step, not binding.

The fact that K_m for N7-methylated substrate is equal to the K_d for non-hydrolyzable counterpart implies that the off-rate for substrate exceeds k_{max} and that the catalytic step is rate-limiting under single-turnover conditions. This, together with the finding that the affinities for non-hydrolyzable capped and 5' monophosphate RNA are nearly equal suggest the rate of product release is also fast relative to the catalytic step. This point was confirmed by a chase experiment where the dissociation of radiolabeled 5' monophosphate RNA from the decapping complex was monitored in the presence of excess unlabelled competitor (**Figure S10**). From these results, we conclude that the

catalytic step is rate-limiting for decapping under multiple turnover conditions since it is slow relative to substrate and product release.

The channel is structurally adaptable

Given that the dorsal surface of the Nudix domain binds the RNA body, one would predict this region of the enzyme to be structurally adaptable since the 5' UTR of eukaryotic mRNA varies in length, sequence and secondary structure. Slow (μs-ms) conformational dynamics play a significant role in structural adaptation by nucleic acid binding proteins, protein-folding, allostery and enzyme catalysis (Eisenmesser et al., 2002; Kalodimos et al., 2004; Korzhnev et al., 2004; Volkman et al., 2001). Accordingly, we probed for these motions using Carr-Purcell-Meiboom-Gill (CPMG) experiments applied to the Nudix domain containing ^{13}C labeled methyl groups of Ile(δ_1), Leu and Val (Skrynnikov et al., 2001). Analysis of CPMG relaxation dispersion profiles reveals a cluster of ILV methyl groups that experience ms-μs dynamics within the dorsal surface (**Figures 5a and S11**). Consistent with these data, Y222 - a conserved residue required for decapping *in vitro* - is broadened beyond detection by ms-μs dynamics (Deshmukh et al., 2007) (**Figure 5b**). In contrast, residues lining the canonical nucleotide binding cleft and the hydrophobic core of the protein are not dynamic on the μs-ms timescale (**Figure 5c**). With the exception of I147 that is within the Nudix box helix (α1), all of the methyl groups undergoing ms-μs dynamics line the RNA body binding site and have similar values of the exchange rate constant suggesting a concerted motional process (**Figures 5c and S11**). These results support the notion that structural adaptability may play an important role in mRNA recognition by Dcp2.

67

DISCUSSION

We addressed how Dcp2 engages substrate RNA and how decapping activity is controlled at the level of protein interactions. Dcp2 is a dumbbell shaped protein with the N-terminal domain binding Dcp1 and the C-terminal Nudix domain acting as a catalytic center (She et al., 2006). We find that the Nudix domain forms the base of an RNA binding channel that runs between the domain interface and resolves interactions with the cap and the RNA body through a bipartite interaction surface. This result is in accord with previous biochemical studies indicating Nudix domain binds RNA (Piccirillo et al., 2003). Importantly, the role of Dcp1 and its interaction domain is to enhance chemistry, not RNA binding. Instead, the channel formed by the Nudix domain promotes the interaction with substrate by distributing weak ionic interactions over a large interaction surface.

The bipartite surface formed by the Nudix domain encodes specific interactions with the cap and non-specific interactions with the RNA body. NMR mapping experiments reveal that the dorsal surface of the Nudix domain binds uncapped RNA independent of sequence whereas the nucleotide binding cavity engages cap only when linked to the RNA. Biochemical and genetic analysis reveal that the dorsal surface and nucleotide binding cavity perform distinct catalytic functions. Alanine substitutions of residues near (K100) or within (K135) the nucleotide binding cavity reduce the catalytic step of decapping, consistent with these residues forming specific contacts to promote chemistry. In contrast, residues lining the dorsal surface (R170, R229, K212 and K216)

68

reduce RNA binding and slightly enhance the catalytic step when mutated to alanine, suggesting some degree of non-productive binding due to non-specific interactions with substrate in the wild-type complex. In yeast, lesions within the nucleotide binding cavity produce stronger phenotypes than those on the dorsal RNA binding surface, consistent with the view that the Dcp1/Dcp2 complex functions as a dedicated catalytic center within a larger mRNP that forms additional contacts with substrate.

Several observations suggest the control of decapping by the Dcp1/Dcp2 complex occurs during the catalytic step. First, we show that the catalytic step is rate limiting for catalysis since it is slow relative to substrate and product release. Second, Dcp1 and its interaction domain enhance the rate of catalytic step but do not affect RNA binding. Third, specificity for the cap structure is conferred exclusively during the catalytic step. Our results do not distinguish whether k_{max} reflects the rate of chemistry per se, or if it is comprised of sub-steps that occur after binding, including the rate of chemistry. The latter could include translocation after non-specific RNA binding, a conformational change that occurs upon cap recognition or a combination of both steps. An important area for future work will be to define further the catalytic step and how it is modulated by additional components of the decapping mRNP.

Our data suggest that the RNA body promotes decapping by binding to the dorsal surface of the Nudix domain of Dcp2, increasing the local concentration of the cap for formation of weak, but specific interactions. Modeling of capped RNA into the structure of Dcp2 indicates roughly 10 nucleotides are required for binding to the dorsal surface

(data not shown), yet *in vitro* decapping efficiency increases for increasing lengths of RNA (Cohen et al., 2005; Steiger et al., 2003; van Dijk et al., 2002). Length dependent interaction kinetics observed in nucleic acid binding proteins are a hallmark of non-specific interactions that promote restricted diffusion processes such as scanning (Berg et al., 1981). This would allow for efficient location of the cap structure within P-bodies in a process analogous to that described for the Lac repressor as it migrates along non-specific DNA in search of a specific operator (Kalodimos et al., 2004; Winter et al., 1981). In support of this view, residues within the dorsal surface bind RNA non-specifically, are mobile on the ms-μs timescale and promote decapping *in vitro*. These data suggest that mobility performs a functional role by allowing structural accommodation of diverse mRNA sequences along the pathway to forming a specific complex with cap.

NMR mapping and kinetic analyses combined with high-resolution structural studies provide a model for substrate binding and the conformational transitions that accompany different steps in the catalytic cycle. We propose that in the active complex, the triphosphate moiety of the cap is positioned near K135 which lines the nucleotide binding cavity and plays an essential role in decapping chemistry, possibly by stabilizing the departure of m7GDP. The remainder of the RNA body traverses a narrow groove between the NTD and Nudix domain with cap proximal nucleotides binding the dorsal surface (**Figure 6**). Consistent with this proposal, an ATP crystallization additive is observed in the *S. pombe* Dcp1/2 co-crystal structure with the β-phosphate oriented

towards the catalytic lysine with additional molecules of ATP binding the dorsum of the Nudix domain (She and co-workers, accompanying manuscript-in revision).

A key result is that Dcp1 and its interaction domain (the NTD) contribute roughly 1000-fold to the catalytic step of decapping, but do not affect RNA binding. Importantly, crystallographic and SAXS analysis of the *S. pombe* decapping complex reveals that the NTD and Dcp1 are far removed from the Nudix domain in the absence of ATP but form a compact structure upon nucleotide binding (She and co-workers, accompanying manuscript-in revision). These observations are consistent with the idea that the structural modules of the complex are uncoupled in the ground state with cap recognition inducing transient formation of the active complex during the catalytic step. Dcp1 and the NTD could stabilize the closed, active form through additional contacts with the cap or the Nudix domain. A prediction of this model is that hydrolysis would trigger opening of the complex, allowing product release and additional rounds of catalysis. Importantly, the position of the substrate recognition channel defined here would allow for control of decapping activity by protein interactions that bias a dynamic equilibrium between open and closed forms. Downstream factors such as Xrn1 could positively regulate decapping by preventing feedback inhibition through accumulation of the 5' monophosphate products at concentrations above the K_d.

It is instructive to compare the mode of cap recognition by the decapping complex with canonical cap binding proteins, such as VP39, eIF4E and CBC20/80, which bind cap in the absence of proximal nucleotides through a classic mode of cap recognition where

m7G is sandwiched between two aromatic residues (Hodel et al., 1998; Hodel et al., 1997; Marcotrigiano et al., 1997; Matsuo et al., 1997; Mazza et al., 2002). Specificity is achieved through a cation-pi interaction between the alkylated nucleobase and protein, allowing relatively tight binding in the absence of additional nucleotides (Lockless et al., 1998; Niedzwiecka et al., 2002; Worch et al., 2005). In contrast, Dcp2 is a member of a growing list of proteins that bind cap only in the presence of the RNA body. These include PABP, YB-1 and VCX-A all of which inhibit decapping and promote either mRNA translation or storage (Evdokimova et al., 2006; Evdokimova et al., 2001; Jiao et al., 2006; Khanna and Kiledjian, 2004). Our results indicate that specificity for m7G is achieved during the catalytic step and are consistent with a non-canonical mode of recognition. This could be achieved by contacts within or outside of the Nudix domain, as described by crystallographic studies of Nudix hydrolases with substrate analogues (Gabelli et al., 2001). High-resolution structural studies with non-hydrolyzable capped RNA in complex with Dcp2 will be required to test this idea and remain a challenge for the future.

The weak interaction of Dcp2 with the cap and the requirement for access to 5' proximal nucleotides has implications for the control of decapping. Translation of the majority of transcripts depends on cap recognition by the eIF4F complex. The 5' end of these messages would be blocked by the cap binding subunit (eIF4E) and other components of the translation machinery, including the ribosome, which would safeguard a translating message from precocious decapping. Decapping requires translational repression, which serves to clear the 5' end of the transcript and allows binding to the

channel within the core of the decapping mRNP. Transcripts may evade decapping by binding the repression mRNP, which includes eIF4E, preventing access to the cap. Alternatively, we propose that non-canonical cap binding proteins inhibit decapping by masking 5' proximal nucleotides, preventing access to the channel and formation of the active decapping complex. Thus, access to the cap and adjacent nucleotides act as a critical checkpoint in mRNA stability, underscoring how the dynamic assembly of multi-protein complexes on the 5' end determines its fate.

METHODS

Construction of Dcp2 plasmids and mutagenesis

The Nudix domain of *S. cerevisiae* Dcp2 (100-245) was PCR amplified from pRP1072 and cloned as a C-terminal fusion to IgG binding domain of protein G (GB1) using the vector GB1-pET30a and the restriction enzymes BamHI and XhoI to generate the C-terminal His-tagged fusion protein. The GB1-Dcp1/Dcp2(1-245) co-expression vector was prepared by PCR amplification of yeast Dcp2 (1-245) from pRP1072 and inserted into pET-DUET using EcoRI and BamHI. Full length Dcp1 was PCR amplified from pRP785 and was fused to GB1 in tandem with a Tobacco Etch Virus protease site (GB1-t-DCP1) in the vector pHis-GB1-parallel (Card and Gardner, 2005) using EcoRI and NotI. GB1-t-Dcp1 was PCR amplified and cloned into pET-DUET containing yDcp2 (1-245) using NdeI and BglII. The final construct contains an N-terminal His tag on Dcp2 and a N-terminal GB1 tag on Dcp1. A yeast expression vector containing full length Dcp2 (pRP1207) was provided as a gift from Dr. Roy Parker. Point mutations were prepared using the Quickchange (Strategene) or Phusion Site-directed mutagenesis kit (Finnzyme). DNA sequences for wild-type and mutants were confirmed by dideoxy sequencing of all protein coding regions.

Decapping assays

All assays were carried out with enzyme in at least 10-fold excess of substrate. Reaction buffer consisted of 50 mM Tris-Cl , 50 mM NH_4Cl, 1mM DTT, 0.1 mg/ml RNase free BSA and 0.01% NP-40 pH 8.3 containing 2000 cpm/μl (roughly 0.1-10nM) cap-

radiolabeled RNA. End-point assays were performed at 20 °C with 100 nM enzyme incubated with 38nt cap-radiolabeled MFA2 RNA for 5 minutes. The reaction buffer contained either 0.2 mM $MnCl_2$ and 2mM Mg-acetate for assays on the Nudix domain or 5 mM $MgCl_2$ for assays on the Dcp1:Dcp2 complex. Kinetic assays were performed at 4 °C on a 29nt cap-radiolabeled RNA in buffer containing $MgCl_2$ as the sole source of divalent metal so that the reactions could be followed by manual pipetting. All decapping reactions were initiated with enzyme and 6 μl aliquots withdrawn at variable times followed by quenching with 1μl of 0.5 M EDTA. An aliquot (4 μl) of the quenched reaction was spotted onto PEI-F cellulose TLC plates (J.T. Baker), developed in 0.75 M LiCl and visualized by phosphorimaging. Migration of m7GDP and GDP were verified by UV shadowing with cold standards. The fraction of m7GDP released was calculated as counts-per-minute m7GDP divided by that for the total radiolabeled RNA observed on the TLC plate (m7GDP, GDP and Origin). Further details on the kinetic assay, protein and RNA production and the direct binding assays are described in the Supplementary Material.

Yeast Methods

The yeast DCP2Δ strain was constructed from HFY107 (DCP2/Dcp2::HIS3) diploid by transforming with the URA plasmid pRS316-DCP2 followed by sporolution, tetrad dissection and selection on synthetic complete media lacking histidine and uracil. The haploid cells were cured of pRSS316-Dcp2 with 5-FOA generating yRG1763 {MAT a *leu2-3, 112 trp-1 can1-100 ura3-1 ade2-1 his3-11,15 DCP2::HIS3*} and the DCP2 disruption was verified by PCR (Ganesan and Jacobson, 2007). For complementation

assays, a URA-CEN plasmid (pRP1207) harboring wild-type or mutant full-length Dcp2 was transformed into yRG1763 using the Lithium-acetate method (Gietz and Woods, 2002). A single transformant was transferred to synthetic media lacking uracil containing 2% glucose (w/v) and grown to OD_{600} 0.5-0.6. Cultures were then diluted to OD_{600} 0.1 with 5 subsequent 1:4 serial dilutions with media in 96 well plates. 3 μL of each dilution was then plated onto SC-URA agar plates and grown at both 25 °C (control) as well at 37 °C.

NMR Methods

The structure of the Nudix domain was solved using a rapid structure determination protocol, using Ile, Leu, Val labeling scheme as described (Medek et al., 2000). Backbone and Ile(δ1), Leu and Val side chain resonances of GB1-yDcp2(100-245) were assigned in 20 mM phosphate buffer containing 100 mM NaCl, 100 mM Na_2SO_4, 50 mM Arg, 50 mM Glu, 5 mM DTT, and 5 mM EDTA at pH 7.0 as described (Deshmukh et al., 2007). Under these conditions, the sample was stable for several weeks at 0.5mM whereas in the absence of RNA and in low salt buffer, the NMR sample precipitates over the time course of one hour. HSQC binding experiments were carried out in a buffer consisting of 100 mM KCl, 2 mM DTT, 10 mM $MgCl_2$ and 50 mM HEPES pH 7.0 since it was found that both phosphate and sulfate inhibit decapping (data not shown). Further details of the RNA binding experiments, the structure determination and the relaxation experiments are provided in the Supplementary Material.

ACKNOWLEDGEMENTS

REFERENCES

Amrani, N., Sachs, M.S., and Jacobson, A. (2006). Early nonsense: mRNA decay solves a translational problem. Nat Rev Mol Cell Biol 7, 415-425.

Anderson, P., and Kedersha, N. (2006). RNA granules. J Cell Biol 172, 803-808.

Andrei, M.A., Ingelfinger, D., Heintzmann, R., Achsel, T., Rivera-Pomar, R., and Luhrmann, R. (2005). A role for eIF4E and eIF4E-transporter in targeting mRNPs to mammalian processing bodies. RNA 11, 717-727.

Bailey, S., Sedelnikova, S.E., Blackburn, G.M., Abdelghany, H.M., Baker, P.J., McLennan, A.G., and Rafferty, J.B. (2002). The crystal structure of diadenosine tetraphosphate hydrolase from Caenorhabditis elegans in free and binary complex forms. Structure 10, 589-600.

Baker, N.A., Sept, D., Joseph, S., Holst, M.J., and McCammon, J.A. (2001). Electrostatics of nanosystems: application to microtubules and the ribosome. Proc Natl Acad Sci U S A 98, 10037-10041.

Barbee, S.A., Estes, P.S., Cziko, A.M., Hillebrand, J., Luedeman, R.A., Coller, J.M., Johnson, N., Howlett, I.C., Geng, C., Ueda, R.*, et al.* (2006). Staufen- and FMRP-containing neuronal RNPs are structurally and functionally related to somatic P bodies. Neuron 52, 997-1009.

Beelman, C.A., Stevens, A., Caponigro, G., LaGrandeur, T.E., Hatfield, L., Fortner, D.M., and Parker, R. (1996). An essential component of the decapping enzyme required for normal rates of mRNA turnover. Nature 382, 642-646.

Behm-Ansmant, I., Rehwinkel, J., Doerks, T., Stark, A., Bork, P., and Izaurralde, E. (2006). mRNA degradation by miRNAs and GW182 requires both CCR4:NOT deadenylase and DCP1:DCP2 decapping complexes. Genes Dev 20, 1885-1898.

Berg, O.G., Winter, R.B., and von Hippel, P.H. (1981). Diffusion-driven mechanisms of protein translocation on nucleic acids. 1. Models and theory. Biochemistry 20, 6929-6948.

Bessman, M.J., Frick, D.N., and O'Handley, S.F. (1996). The MutT proteins or "Nudix" hydrolases, a family of versatile, widely distributed, "housecleaning" enzymes. J Biol Chem 271, 25059-25062.

Brengues, M., Teixeira, D., and Parker, R. (2005). Movement of eukaryotic mRNAs between polysomes and cytoplasmic processing bodies. Science 310, 486-489.

Card, P.B., and Gardner, K.H. (2005). Identification and optimization of protein domains for NMR studies. Methods Enzymol 394, 3-16.

Chen, C.Y., and Shyu, A.B. (1995). AU-rich elements: characterization and importance in mRNA degradation. Trends Biochem Sci 20, 465-470.

Cohen, L.S., Mikhli, C., Jiao, X., Kiledjian, M., Kunkel, G., and Davis, R.E. (2005). Dcp2 Decaps m2,2,7GpppN-capped RNAs, and its activity is sequence and context dependent. Mol Cell Biol 25, 8779-8791.

Coller, J., and Parker, R. (2004). Eukaryotic mRNA decapping. Annu Rev Biochem 73, 861-890.

DeLano, W.L. (2002). The PyMol Molecular Graphics System, D. Scientific, ed. (Palo Alto, CA, USA).

Deshmukh, M.V., Oku, Y., and Gross, J.D. (2007). Backbone and ILV resonance assignments of the catalytic domain of the yeast mRNA deapping enzyme, Dcp2. J Biomol NMR In press.

Dunckley, T., and Parker, R. (1999). The DCP2 protein is required for mRNA decapping in Saccharomyces cerevisiae and contains a functional MutT motif. EMBO J 18, 5411-5422.

Eisenmesser, E.Z., Bosco, D.A., Akke, M., and Kern, D. (2002). Enzyme dynamics during catalysis. Science 295, 1520-1523.

Eulalio, A., Behm-Ansmant, I., and Izaurralde, E. (2007). P bodies: at the crossroads of post-transcriptional pathways. Nat Rev Mol Cell Biol 8, 9-22.

Evdokimova, V., Ruzanov, P., Anglesio, M.S., Sorokin, A.V., Ovchinnikov, L.P., Buckley, J., Triche, T.J., Sonenberg, N., and Sorensen, P.H. (2006). Akt-mediated YB-1 phosphorylation activates translation of silent mRNA species. Mol Cell Biol 26, 277-292. Evdokimova, V., Ruzanov, P., Imataka, H., Raught, B., Svitkin, Y., Ovchinnikov, L.P., and Sonenberg, N. (2001). The major mRNA-associated protein YB-1 is a potent 5' cap-dependent mRNA stabilizer. EMBO J 20, 5491-5502.

Farmer, B.T., 2nd, Constantine, K.L., Goldfarb, V., Friedrichs, M.S., Wittekind, M., Yanchunas, J., Jr., Robertson, J.G., and Mueller, L. (1996). Localizing the NADP+ binding site on the MurB enzyme by NMR. Nat Struct Biol 3, 995-997.

Fenger-Gron, M., Fillman, C., Norrild, B., and Lykke-Andersen, J. (2005). Multiple processing body factors and the ARE binding protein TTP activate mRNA decapping. Mol Cell 20, 905-915.

Ferraiuolo, M.A., Basak, S., Dostie, J., Murray, E.L., Schoenberg, D.R., and Sonenberg, N. (2005). A role for the eIF4E-binding protein 4E-T in P-body formation and mRNA decay. J Cell Biol 170, 913-924.

Gabelli, S.B., Bianchet, M.A., Bessman, M.J., and Amzel, L.M. (2001). The structure of ADP-ribose pyrophosphatase reveals the structural basis for the versatility of the Nudix family. Nat Struct Mol Biol 8, 467-472.

Gabelli, S.B., Bianchet, M.A., Ohnishi, Y., Ichikawa, Y., Bessman, M.J., and Amzel, L.M. (2002). Mechanism of the Escherichia coli ADP-ribose pyrophosphatase, a Nudix hydrolase. Biochemistry 41, 9279-9285.

Ganesan, R., and Jacobson, A. (2007). Personal Communication.

Gietz, R.D., and Woods, R.A. (2002). Transformation of yeast by lithium acetate/single-stranded carrier DNA/polyethylene glycol method. Methods Enzymol 350, 87-96.

Hilgers, V., Teixeira, D., and Parker, R. (2006). Translation-independent inhibition of mRNA deadenylation during stress in Saccharomyces cerevisiae. RNA 12, 1835-1845.

Hodel, A.E., Gershon, P.D., and Quiocho, F.A. (1998). Structural basis for sequence-nonspecific recognition of 5'-capped mRNA by a cap-modifying enzyme. Mol Cell 1, 443-447.

Hodel, A.E., Gershon, P.D., Shi, X., Wang, S.M., and Quiocho, F.A. (1997). Specific protein recognition of an mRNA cap through its alkylated base. Nat Struct Biol 4, 350-354.

Jiao, X., Wang, Z., and Kiledjian, M. (2006). Identification of an mRNA-decapping regulator implicated in X-linked mental retardation. Mol Cell 24, 713-722.

Kalodimos, C.G., Biris, N., Bonvin, A.M., Levandoski, M.M., Guennuegues, M., Boelens, R., and Kaptein, R. (2004). Structure and flexibility adaptation in nonspecific and specific protein-DNA complexes. Science 305, 386-389.

Khanna, R., and Kiledjian, M. (2004). Poly(A)-binding-protein-mediated regulation of hDcp2 decapping in vitro. EMBO J 23, 1968-1976.

Koradi, R., Billeter, M., and Wuthrich, K. (1996). MOLMOL: ap program for display and analysis of macromolecular structures. J Mol Graphics 14, 51-55.

Korzhnev, D.M., Salvatella, X., Vendruscolo, M., Di Nardo, A.A., Davidson, A.R., Dobson, C.M., and Kay, L.E. (2004). Low-populated folding intermediates of Fyn SH3 characterized by relaxation dispersion NMR. Nature 430, 586-590.

Lockless, S.W., Cheng, H.T., Hodel, A.E., Quiocho, F.A., and Gershon, P.D. (1998). Recognition of capped RNA substrates by VP39, the vaccinia virus-encoded mRNA cap-specific 2'-O-methyltransferase. Biochemistry 37, 8564-8574.

Lykke-Andersen, J. (2002). Identification of a human decapping complex associated with hUpf proteins in nonsense-mediated decay. Mol Cell Biol 22, 8114-8121.

Maquat, L.E. (2004). Nonsense-mediated mRNA decay: splicing, translation and mRNP dynamics. Nat Rev Mol Cell Biol 5, 89-99.

Marcotrigiano, J., Gingras, A.C., Sonenberg, N., and Burley, S.K. (1997). Cocrystal structure of the messenger RNA 5' cap-binding protein (eIF4E) bound to 7-methyl-GDP. Cell 89, 951-961.

Matsuo, H., Li, H., McGuire, A.M., Fletcher, C.M., Gingras, A.C., Sonenberg, N., and Wagner, G. (1997). Structure of translation factor eIF4E bound to m7GDP and interaction with 4E-binding protein. Nat Struct Biol 4, 717-724.

Mazza, C., Segref, A., Mattaj, I.W., and Cusack, S. (2002). Large-scale induced fit recognition of an m(7)GpppG cap analogue by the human nuclear cap-binding complex. EMBO J 21, 5548-5557.

Medek, A., Olejniczak, E.T., Meadows, R.P., and Fesik, S.W. (2000). An approach for high-throughput structure determination of proteins by NMR. J Biolmol NMR 18, 229-238.

Mildvan, A.S., Xia, Z., Azurmendi, H.F., Saraswat, V., Legler, P.M., Massiah, M.A., Gabelli, S.B., Bianchet, M.A., Kang, L.W., and Amzel, L.M. (2005). Structures and mechanisms of Nudix hydrolases. Arch Biochem Biophys 433, 129-143.

Niedzwiecka, A., Marcotrigiano, J., Stepinski, J., Jankowska-Anyszka, M., Wyslouch-Cieszynska, A., Dadlez, M., Gingras, A.C., Mak, P., Darzynkiewicz, E., Sonenberg, N., et al. (2002). Biophysical studies of eIF4E cap-binding protein: recognition of mRNA 5' cap structure and synthetic fragments of eIF4G and 4E-BP1 proteins. J Mol Biol 319, 615-635.

Parker, R., and Sheth, U. (2007). P bodies and the control of mRNA translation and degradation. Mol Cell 25, 635-646.

Piccirillo, C., Khanna, R., and Kiledjian, M. (2003). Functional characterization of the mammalian mRNA decapping enzyme hDcp2. RNA 9, 1138-1147.

Rehwinkel, J., Behm-Ansmant, I., Gatfield, D., and Izaurralde, E. (2005). A crucial role for GW182 and the DCP1:DCP2 decapping complex in miRNA-mediated gene silencing. RNA11, 1640-1647.

Sali, A., and Blundell, T.L. (1993). Comparative protein modelling by satisfaction of spatial restraints. J Mol Biol 234, 779-815.

Schier, A.F. (2007). The maternal-zygotic transition: death and birth of RNAs. Science 316, 406-407.

She, M., Decker, C.J., Chen, N., Tumati, S., Parker, R., and Song, H. (2006). Crystal structure and functional analysis of Dcp2p from Schizosaccharomyces pombe. Nat Struct Mol Biol 13, 63-70.

She, M., Decker, C.J., Sundramurthy, K., Liu, Y., Chen, N., Parker, R., and Song, H. (2004). Crystal structure of Dcp1p and its functional implications in mRNA decapping. Nat Struct Mol Biol 11, 249-256.

Sheth, U., and Parker, R. (2003). Decapping and decay of messenger RNA occur in cytoplasmic processing bodies. Science 300, 805-808.

Skrynnikov, N.R., Mulder, F.A.A., Hon, B., Dahlquist, F.W., and Kay, L.E. (2001). Probing Slow Time Scale Dynamics at Methyl-Containing Side Chains in Proteins by Relaxation Dispersion NMR Measurements: Application to Methionine Residues in a Cavity Mutant of T4 Lysozyme. J Am Chem Soc 123, 4556-4566.

Steiger, M., Carr-Schmid, A., Schwartz, D.C., Kiledjian, M., and Parker, R. (2003). Analysis of recombinant yeast decapping enzyme. RNA 9, 231-238.

Stevens, A., and Maupin, M.K. (1987). A 5'----3' exoribonuclease of Saccharomyces cerevisiae: size and novel substrate specificity. Arch Biochem Biophys 252, 339-347.

van Dijk, E., Cougot, N., Meyer, S., Babajko, S., Wahle, E., and Seraphin, B. (2002). Human Dcp2: a catalytically active mRNA decapping enzyme located in specific cytoplasmic structures. EMBO J 21, 6915-6924.

Volkman, B.F., Lipson, D., Wemmer, D.E., and Kern, D. (2001). Two-state allosteric behavior in a single-domain signaling protein. Science 291, 2429-2433.

Wang, Z., Jiao, X., Carr-Schmid, A., and Kiledjian, M. (2002). The hDcp2 protein is a mammalian mRNA decapping enzyme. Proc Natl Acad Sci U S A 99, 12663-12668.

Winter, R.B., Berg, O.G., and von Hippel, P.H. (1981). Diffusion-driven mechanisms of protein translocation on nucleic acids. 3. The Escherichia coli lac repressor--operator interaction: kinetic measurements and conclusions. Biochemistry 20, 6961-6977.

Worch, R., Niedzwiecka, A., Stepinski, J., Mazza, C., Jankowska-Anyszka, M., Darzynkiewicz, E., Cusack, S., and Stolarski, R. (2005). Specificity of recognition of mRNA 5' cap by human nuclear cap-binding complex. RNA 11, 1355-1363.

Zhou, P., Lugovskoy, A.A., and Wagner, G. (2001). A solubility-enhancement tag (SET) for NMR studies of poorly behaving proteins. J Biomol NMR 20, 11-14.

FIGURE CAPTIONS

Figure 1: The Nudix domain of yDcp2 forms a channel between the catalytic and Dcp1 binding domains. (a) Alignment of the Nudix domain structure of yDcp2 determined by NMR with the crystal structure of *S. pombe* Dcp2 (cyan, 2A6T.pdb (She et al., 2006)) containing both the Nudix domain (CTD) and the N-terminal Dcp1 binding domain (NTD). The backbone RMSD for aligned secondary structural elements is 1.9 Å. The dorsal view is depicted. (b) Ribbon diagram of the yDcp2 Nudix domain. The Nudix box is colored red and helices lining the dorsal surface are colored blue. The view is rotated slightly about the y-axis relative to (a). (c) Electrostatic surface of the yeast Dcp2 homology model based on fission yeast crystal structure . Left: dorsal view as in (a); right: channel view obtained by rotation of -110º about y-axis and 60º about the x-axis relative to dorsal view. The scale is -4KT/e to 4KT/e. (d) The domain surfaces of the yDcp2 homology model are color-coded to allow comparison to the electrostatic surface; channel view with the NTD (residues 1-100) colored cyan and the Nudix domain (residues 101-245) colored grey. The homology model was generated using Modeller 8.2.1 (Sali and Blundell, 1993); panels (a) and (b) were generated using Molmol (Koradi et al., 1996); all other structure figures were generated with Pymol (DeLano, 2002) with electrostatic surfaces calculated using APBS (Baker et al., 2001).

Figure 2: Substrate RNA binds the dorsal surface and nucleotide binding cavity of the Nudix domain. (a) Residue specific chemical shift perturbations observed upon binding 29nt non-hydrolyzable capped RNA with yDcp2 at 1:1 stoichiometry color coded onto

surface of the Nudix domain. The change in chemical shift $\delta\Delta$ was calculated as $[(\Delta N*0.17)^2 + \Delta H^2]^{0.5}$ as described (Farmer et al., 1996). Asterisks indicate regions not assigned due to exchange broadening. Views as in Fig 1c. (b) Overlay ^{15}N HSQC spectral excerpt comparing chemical shifts of free enzyme (red) to that bound to 29nt 5' OH (green) and non-hydrolyzable capped RNA (blue) indicate differential perturbations on the Nudix box (residue E153) but not on the dorsal surface (residue S232). The cross-peak labeled *l*, derives from the linker between GB1 and the Nudix domain (c) Ribbon diagram of the yeast Dcp2 Nudix domain with residues lining the substrate binding surface depicted as sticks. (d) Alignment of Nudix domains of yDcp2 and Ap4APase from *C. elegans* in complex with AMP (1KTG (Bailey et al., 2002)). Same view as right panel of (a) depicting canonical nucleotide binding cavity with residues E153 and E198 of Dcp2.

Figure 3: Residues lining the substrate binding surface affect endpoint decapping *in vitro* and function of yDcp2 in yeast. Cap hydrolysis monitored by TLC of decapping reactions in the presence of 38nt MFA2 cap-radiolabeled RNA and (a) recombinant Nudix domain of yDcp2 or (b) the Dcp1/Dcp2 complex . Wild type and alanine substitutions are indicated along with fraction m7GDP released. Assays carried out in buffer containing either Mn^{2+} or Mg^{2+} for Nudix domain or Dcp1/Dcp2 complex, respectively. (c) *In vivo* function of plasmid borne copies of wild-type and mutant DCP2 genes assayed by complementation of temperature sensitive growth defect in DCP2Δ strain. Top-panel: growth of DCP2Δ strain containing empty vector control (vector) versus wild-type Dcp2 on URA-CEN plasmid. Bottom-panels: growth of DCP2Δ strain

containing wild-type or indicated alanine substitutions within plasmid encoded full-length DCP2. All mutants were folded as judged by CD analysis and mutant complexes co-purify by size exclusion chromatography (**Figure S5**).

Figure 4: Kinetic analysis of decapping enzyme complex reveals cap specificity, the role of Dcp1 and the substrate binding channel. (a) Representative TLC time course data for wild-type complex (2 μM). Location of m7GDP and GDP are indicated by arrows. GDP is produced from reactions due to incomplete N7-methylation by guanylyl transferase during substrate preparation. (b) Time courses of the fraction m7GDP released at variable enzyme concentrations (1 μM ●, 2 μM ○, 3 μM ▼, 4 μM △, 5 μM ■, 7 μM ❑ and 9 μM ◆) and corresponding fits to obtain the first order rate constant k_{obs} for wild-type complex. (c) Graph of mean k_{obs}, with standard deviation for n≥2 independent experiments, versus enzyme concentration for wild-type and mutant Dcp1/Dcp2 complexes used to obtain K_m and k_{max} (wild-type ●, K100 ○, R133 ▼, K135 △, R170/229 ◇, K212/R229 ❑, K216/R229 ◆ and wild-type complex with GpppG RNA ■). Inset: data for the K135 complex and the Nudix domain which are between 300 and 1000-fold less active than the wild-type complex. (d) Bar graph of mean K_m, with standard deviation for n≥2 independent experiments, for wild-type and mutant complexes and the Nudix domain, color-coded to correspond to data in (c). (e) Gel mobility shift assay of GB1-Dcp1/Dcp2 complex with a 29 nt 2' OMe non-hydrolyzable capped RNA . The protein concentration was decreased from 20.9 μM by factors of two. (f) Fraction RNA shifted versus concentration of GB1-Dcp1:Dcp2 complex for 29nt 2' OMe non-hydrolyzable capped RNA ● and 5' monophosphate RNA ■. The equilibrium

dissociation constants for non-hydrolyzable capped and 5' monophosphate RNA were estimated to be 2.1 μM and 3.0 μM respectively. All assays were carried out with 5 mM MgCl$_2$ as sole source of metal ion.

Figure 5: The dorsal surface fluctuates on the ms-μs timescale. (a) Representative relaxation dispersion curves obtained on the Nudix domain of yDcp2 labeled with ^{1}H/^{13}C at methyl positions of Ile(δ$_1$), Leu, Val recorded at 600 MHz (blue) and 800 MHz (red) field strengths, respectively. The δ$_1$ methyl group of Box B residue Leu 223 is severely broadened by ms-μs dynamics while that of Ile147 within the Nudix box is less affected. Errors in R$_2$ were propagated using standard procedures with uncertainty in individual peak intensities taken from the NMRPipe peak detection algorithm (insert NMRPipe reference here) (b) Sequence alignment of a conserved region within the dorsal surface (Box B) from several species. (c) Rates of dynamical interconversion between two states (k$_{ex}$) encoded in sphere diameters mapped onto C$_β$ positions of Ile, Leu and Val within the structure of the Nudix domain. Cyan spheres denote measurable ms-μs motions while grey spheres indicate methyl groups that are not dynamic on ms-μs timescales.

Figure 6: Model of RNA binding by yDcp2. (a) Residues lining the surface of the Nudix domain serve as the base of a channel that runs between the Dcp1 binding domain and the catalytic center. (b) Chemical shift changes of 29nt non-hydrolyzable capped RNA mapped onto homology model of yDcp2. (c) Proposed path of the RNA body based on NMR mapping, biochemical and genetic data.
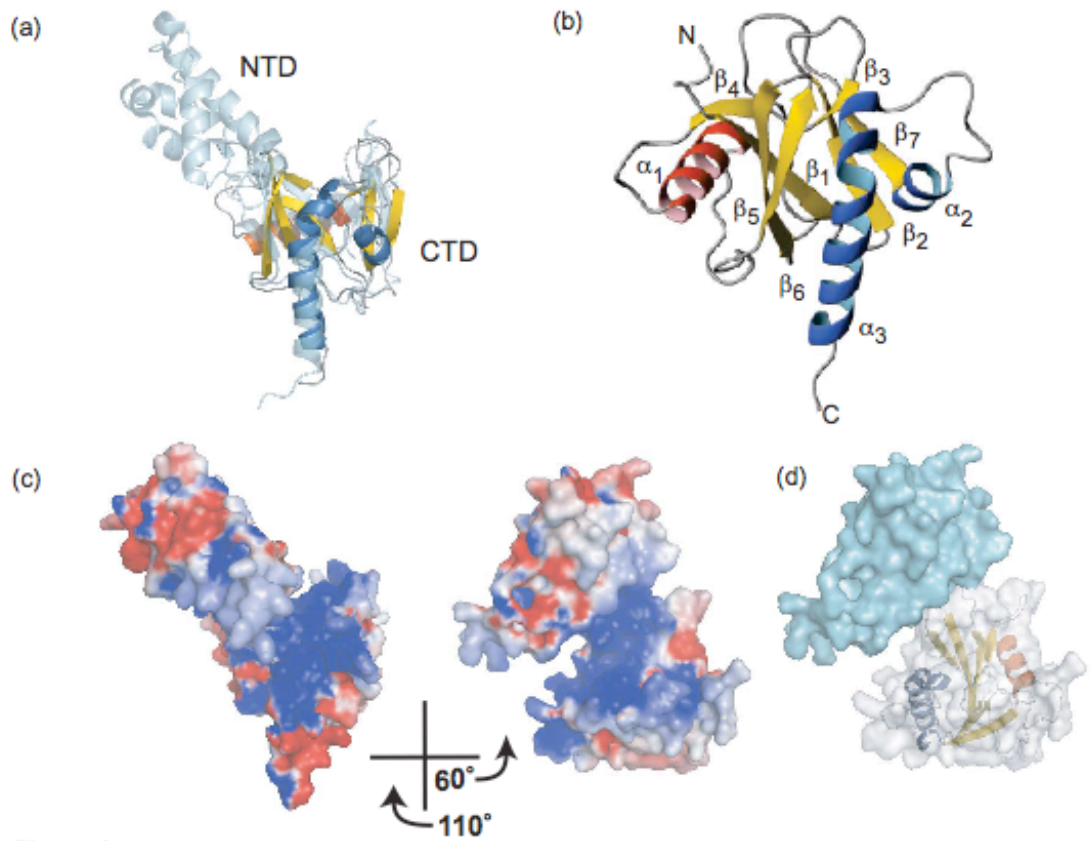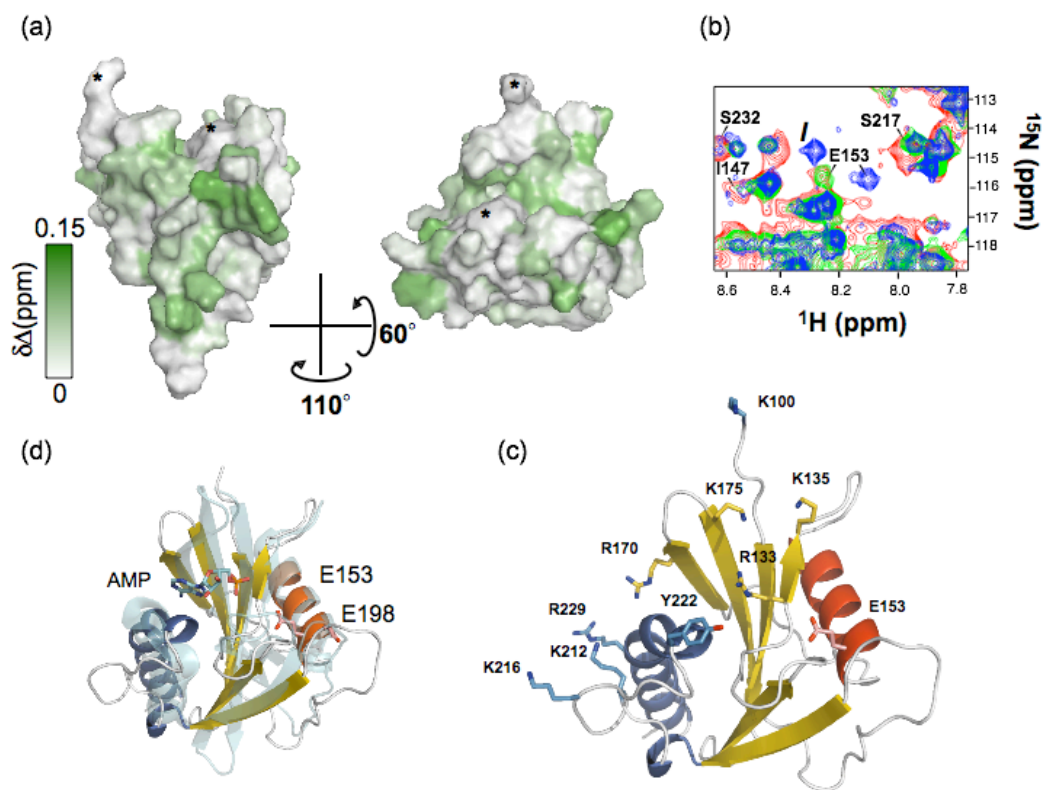
FIGURE 1

FIGURE 2
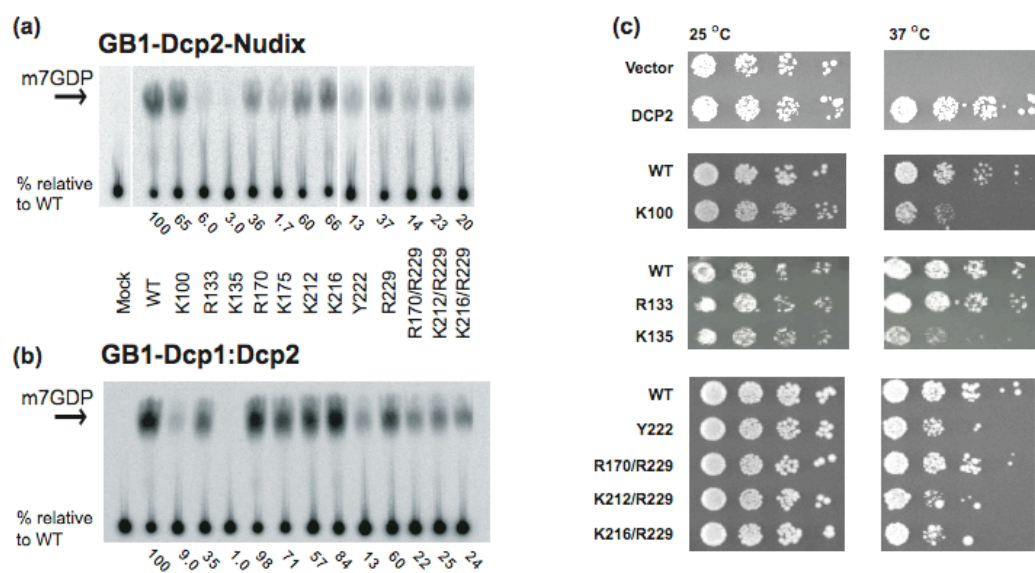
FIGURE 3
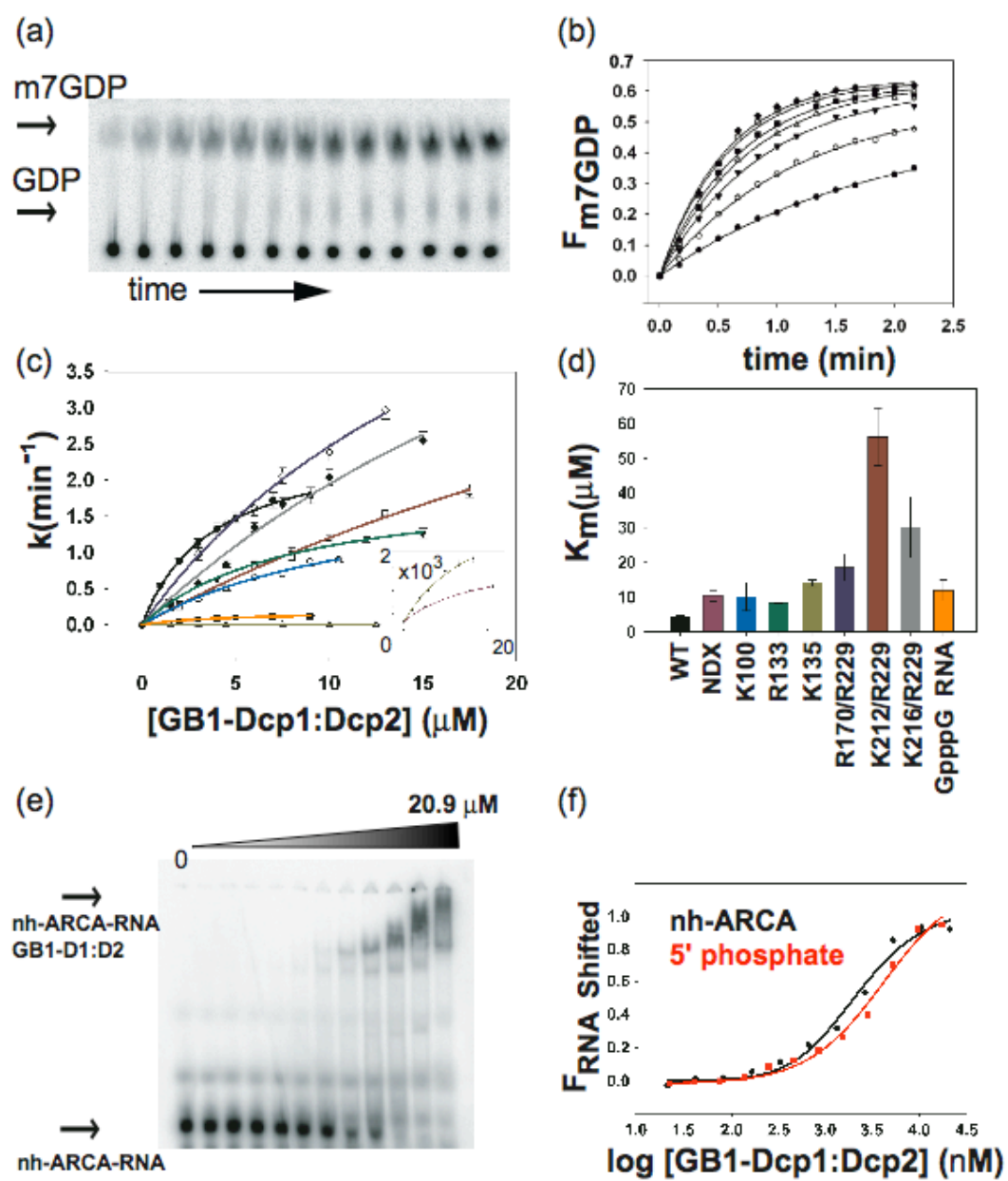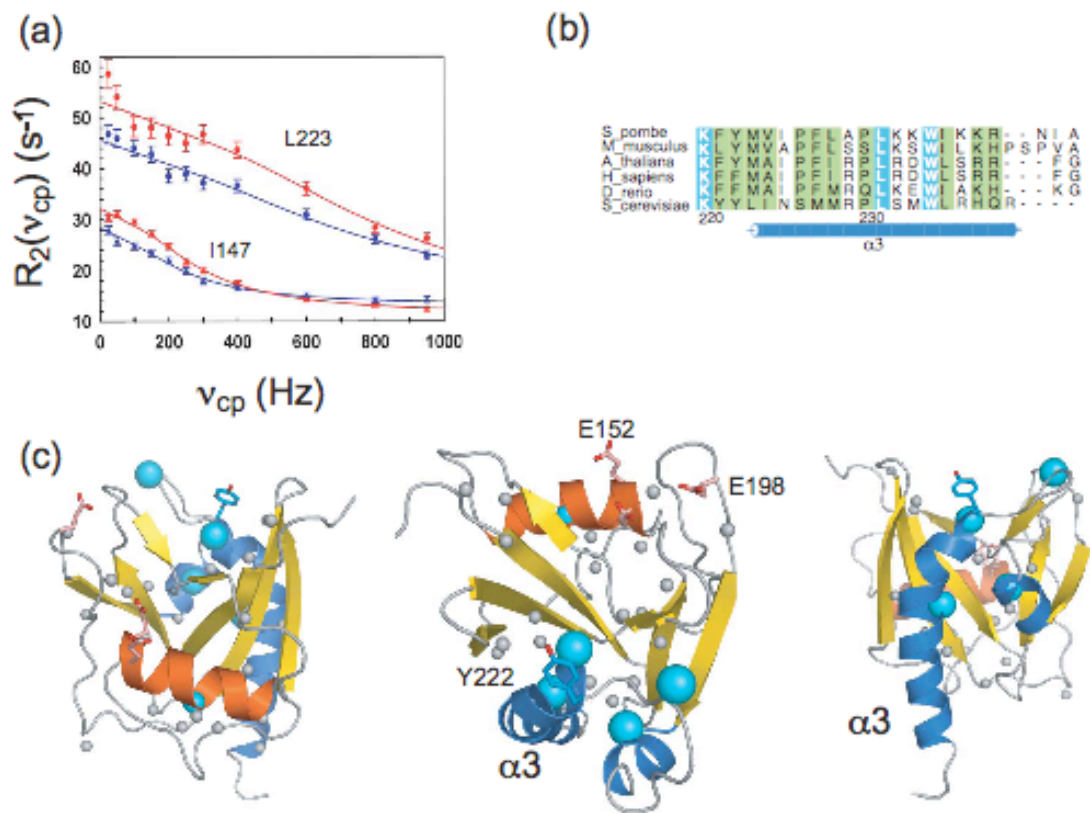
FIGURE 4

FIGURE 5
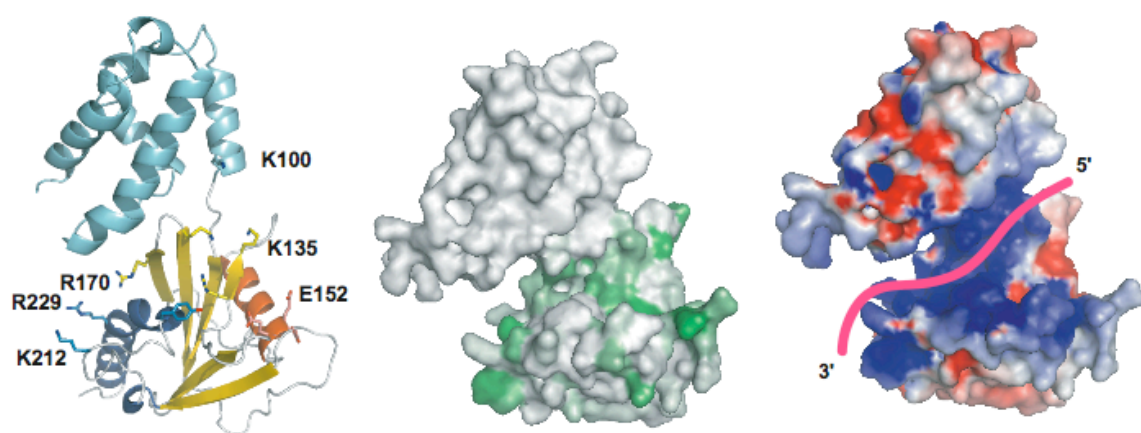
FIGURE 6

	k_{max} (min^{-1})	K_m (μM)	k_{max}/K_m (min^{-1}/μM)	k_{max}/K_m (wt/mut)
m7GpppG RNA				
Wild-type complex	2.2± 0.5	4.2±0.5	0.53	1
K100	1.6±0.5	10.1±4.0	0.16	3
R133	2.1± 0.2	8.2±0.2	0.25	2
K135	0.7x10^{-3}±0.1x10^{-3}	14.0±0.9	0.5x10^{-3}	1130
Y222	1.6± 0.3	4.7±0.8	0.35	1.5
R170/R229	7.2±0.7	18.5±3.8	0.37	1.5
K212/R229	7.1±0.1	56.2±8.4	0.08	8
K216/R229	6.2±3.9	30.1±8.7	0.21	3
Nudix domain	0.2x10^{-3}±0.4x10^{-4}	10.3±1.7	0.5x10^{-3}	2697
GpppG RNA				
Wild-type complex	0.12±0.3x10^{-2}	11.9±1.7	0.01	50

Table 1: Kinetic constants measured for wild-type, mutant Dcp1/Dcp2 complexes and Nudix domain. The mean and standard deviations are reported for n≥2 independent experiments. m7GpppG and GpppG RNA denote a 29nt capped RNA containing or lacking the N7-methyl modification.

TABLE 1

SUPPLEMENTARY MATERIAL

METHODS

Protein Expression and Purification of Proteins

GB1-Dcp2 (100-245) and GB1-Dcp1/Dcp2 (1-245) were expressed in E. coli and purified using immobilized metal affinity chromatography using Ni-NTA and Talon resin, respectively. The Nudix domain and decapping enzyme complex were further purified to >95% homogeneity by size-exclusion chromatography using Superdex 75 and Superdex 200 columns (**Figure S5**). Gb1-Dcp2(100-245) and GB1-t-Dcp1/Dcp2(1-245) were expressed in BL21(DE3) and Bl21(DE3)-Rosetta. For enzymology, the proteins were stored at −80 ºC after flash-freezing in buffer containing 50 mM HEPES, 100 mM NaCl, 20 % glycerol, 5mM DTT pH 7.5. This procedure did not reduce activity of the enzyme and was adopted since storage at 4 ºC resulted in reduced activity after several days.

Expression and Purification of GB1-yDcp2 for NMR

E. coli BL21 (DE3) CodonPlus cells (Stratagene) were transformed with pET30a GB1-yDcp2 (100-245) plasmid and GB1-Dcp2(100-245) was over-expressed by inducing with 1mM IPTG at 20°C for 18 hrs. Harvested cells were lysed (in 20 mM HEPES (pH 7.5), 300 mM NaCl, 0.5 % NP-40, 10 mM PMSF, 10 mM β-mercaptoethanol), sonicated and purified over a nickel-NTA affinity column (Qiagen) followed by gel filtration on a Sephadex 75 column (GE Biosciences). Uniform ^{13}C/^{15}N and ^{2}H samples were prepared using M9 D_2O media with ^{13}C glucose and ^{15}N NH_4Cl as the sole carbon and nitrogen

sources, respectively. A sample with methyl groups of Ile(δ1), Leu and Val were ^{13}C/^{1}H labeled with or without ^{1}H Phe in an otherwise perdeuterated environment using M9 D$_2$O media with ^{2}H labeled glucose, supplementing media with γ-^{13}C labeled α-ketoacid precursors to ILV and unlabelled Phe prior to induction as described (Gross et al., 2003 ; Medek et al., 2000).

RNA Preparation

Cap-radiolabeled RNA was prepared from a gel purified 29nt RNA that was transcribed in vitro using T7 polymerase using DNA oligonucleotide templates with the top strand sequence TAATACGACTCACTATAG containing the T7 polymerase promoter and the bottom strand containing the coding sequence UUA GTG TTA TGT CGT GCT GTA ATC TGC CCT ATA GTG AGT CGT ATT A (Milligan et al., 1987). The tandem 5' U contains a 2' OMe modification to reduce non-template mediated addition (Kao et al., 2001). Capping was carried out using ^{32}P(α) GTP, recombinant vaccinia virus guanylyl transferase in the presence of S-adenosyl methionine (SAM) as described (Haley et al., 2003). Cap-radiolabeled RNA was gel purified prior to use. Nuclease P1 treatment and TLC analysis indicated the purified substrate preparation contained roughly 60% m7GpppG and 40% GpppG cap RNA (data not shown). Capped radiolabeled RNA lacking the N7-methyl modification (GpppG RNA) was prepared and purified just as the m7GpppG labeled RNA except 1mM S-adenosyl homocysteine was used in the capping reaction instead of SAM.

Non-hydrolyzable capped and 5' monophosphate RNA were prepared co-transcriptionally using T7 RNA polymerase and oligonucleotide template primers supplemented with 1mM of each NTP in addition to either 4mM GMP or cap analogue as described (Sampson and Uhlenbeck, 1988). Non-hydrolyzable anti-reverse capped analogue (ARCA, 2' OMe m7GppCH$_2$pG) was prepared as described (Kalek et al., 2006). The in vitro transcribed RNAs were purified to single nucleotide resolution using denaturing PAGE followed by electroelution (Schleicher and Schuell). The 15nt MFA2 5' OH RNA was purchased from Dharmacon, judged to be greater than 95% by denaturing PAGE and used without further purification. For gel mobility shift assays, cold capped RNA or 5' monophosphate RNA was radiolabeled at the 3' end using α-^{32}P cordycepin-5' triphosphate and yeast poly(A) polymerase (USB) following the manufacturer's protocol.

Gel Mobility Shift Assay

Non-hydrolyzable capped RNA containing 2' OMe m7GppCH$_2$pG or 5' monophosphate RNA were radiolabeled with cordycepin and incubated at 4 °C with serial dilutions of GB1-Dcp1/His6-Dcp2(1-245) in binding buffer containing 10% glycerol, 50 mM NH$_4$Cl, 0.01 % NP40, 0.1 mg/ml BSA, 1 mM DTT, 5 mM MgCl$_2$ and 50 mM Tris-Cl pH 8.0 for 1 hour. The final concentration of radiolabeled RNA in each sample was 10 nM. Aliquots were loaded onto an electrophoresing native 6% polyacrylamide gel (19:1 acrylamide:bis-acrylamide) in 1xTris-Glycine buffer and run for 3 hours at 4 °C. The gel was dried, visualized by phosphorimagery and the fraction RNA bound (F) was quantified. K$_d$ was estimated by fitting the fraction RNA shifted F=E$_T$/(E$_T$+K$_d$) versus

total enzyme (E_T) using non-linear regression. The chase experiment was performed at 4 °C by preincubating 20 μM GB1-Dcp1/His6-Dcp2(1-245) with radiolabeled 5' monophosphate RNA in binding buffer as above. The chase was initiated by addition of an equal volume of either 80-fold excess cold-competitor 5' monophosphate RNA or binding buffer as control. Reactions were followed by manual pipetting with aliquots withdrawn at 15s time intervals that were immediately loaded onto an electrophoresing native gel as described above.

Kinetic Assays

The fraction m^{7}GDP (F) released was plotted versus time and fit to the equation: $F(t) = F_{ep}[1-\exp(-k_{obs}t)]$ using non-linear regression with the end-point (F_{ep}) and first-order rate constant for product formation (k_{obs}) as fit-parameters. Reactions were followed for $>3/k_{obs}$, except for the very slow reactions from the K135A mutation , the Nudix domain and reactions with unmethylated GpppG RNA. For N7-methyl capped substrates, good first-order fits were obtained with end-points between 0.5-0.6. The reactions for K135A and the Nudix domain were linear over the time-course of an hour, and an endpoint of 0.55 was assumed to obtain the observed rate constant from the initial rate. The end-point of 0.55 arises from fraction of unmethylated GpppG RNA contained within our capped RNA preparation. Rates for GpppG capped RNA prepared using SAH were fit assuming an end-point of unity. Rates determined from different enzyme concentrations were fit to the equation: $k_{obs}= k_{max}E_T/(K_m+E_T)$ to obtain k_{max} and K_m, with k_{max} the apparent rate of the catalytic step and K_m corresponding to $(k_{off}+ k_{max})/k_{on}$. The rate of the catalytic step is denoted k_{max} to emphasize that this can be different from k_{cat} measured under multiple

turnover conditions. The latter contains contributions from catalysis and the rate of product release whereas the former reports exclusively on the catalytic step. Note that in the single turnover limit, the presence of capped RNA lacking the N7-methyl modification does not alter the observed rates since these are independent of substrate concentration. For example, very similar values of k_{max} are obtained for GpppG RNA prepared using SAH and the residual GpppG RNA within our N7-methyl capped RNA preparations (**Figure S9**). However, the K_m value of the former was consistently elevated relative to the latter, though the effect on K_m was typically less than 3-fold and does not alter any of our conclusions.

NMR Spectroscopy

Spectra were recorded at 25 ℃ on Bruker Avance 500, Varian Inova 600 or Bruker Avance 800 MHz spectrometers outfitted cryogenic probes. Backbone, C', N, C_β and $C\alpha$ resonances and sidechain methyl Ile(δ1), Leu and Val groups were obtained as described (Deshmukh et al., 2007). Short range NOEs were provided by an ^{15}N edited NOESY-HSQC (τ_m= 80 ms) recorded on ^{15}N labeled GB1-yDcp2(100-245) (Talluri and Wagner, 1996). Long range HN-HN NOEs were obtained from a 3D HSQC-NOESY-HSQC (200 ms) (Grzesiek et al., 1995) experiment recorded on a ^{2}H/^{15}N/^{13}C labeled sample; Methyl-Methyl and Methyl-HN NOEs were obtained from a ^{13}C edited 3D HMQC-NOESY (τ_m= 150 ms) and 3D section of ^{13}C-^{15}N edited 3D HMQC-NOESY-HSQC (τ_m =150ms) experiments with either ^{13}C or ^{1}H frequency labeling in F1 on a sample that was ^{13}C/^{1}H ILV labeled in a uniform ^{15}N/^{2}H background. Aromatic/methyl NOEs were obtained on a sample of GB1-yDcp2(100-245) where Phe was protonated and methyl groups of Val,

Leu and Ile(δ1) where ^{13}C/^{1}H enriched in an otherwise deuterated environment using a ^{13}C HMQC-NOESY in D$_2$O as described (Medek et al., 2000). Phe resonances were assigned by 2D NOESY (τ_m=100 ms) and ^{1}H-^{1}H TOCSY. Residual dipolar couplings were extracted from differences in resonance displacements obtained from interleaved 2D ^{15}N HSQC and TROSY experiments conducted in isotropic and oriented phase using 3% polyethylene glycol C12E5-hexanol (r = 0.96) (Kontaxis et al., 2000; Ruckert and Otting, 2000). χ_1 torsion angles for aliphatic and aromatic side chains were extracted from ^{3}J$_{NC\gamma}$ measured by TROSY-modified quantitative spin-echo difference experiments on a ^{2}H/^{15}N/^{13}C labeled sample (Hu and Bax, 1997; Hu et al., 1997; Pervushin et al., 1998).

Structure Calculations

A total of 50 structures were calculated from an extended template using experimentally determined distance and torsion angle data (Supplemental Table 1, Figure S1) using restrained molecular dynamics in conjunction with simulated annealing implemented in cartesian space within the program XPLOR-NIH (Schwieters et al., 2003). During latter stages of refinement, hydrogen bonds derived from H/D exchange experiments were supplied for regular secondary structures. The lowest energy structure without any distance and dihedral angle violations of 0.5Å and 5° was subsequently refined using a hybrid torsion-angle/rigid body dynamics protocol (Chou et al., 2000) using NH residual dipolar couplings , NOE derived distances, hydrogen bonds with TALOS (Cornilescu et al., 1999) and experimentally derived torsion angles. The axial and rhombic components of the alignment tensor of yDcp2(100-245) were used in refinement and obtained by fitting the experimental derived HN dipolar couplings to a homology model based on the

crystal structure (2A6T.pdb, (She et al., 2006)) of the *S. pombe* enzyme using the program PALES (Zweckstetter and Bax, 2000). Structure quality was accessed with PROCHECK-NMR (Laskowski et al., 1996).

RNA Binding Experiments

Assignments of GB1-yDcp2 in RNA binding buffer (100 mM KCl, 2 mM DTT, 10 mM MgCl$_2$ and 50 mM HEPES pH 7.0) were obtained by a series of titrations since phosphate, sulfate and metal all bind in fast-exchange. The RNA binding site was first determined for a 15nt MFA2 RNA by titration at molar ratios (RNA:enzyme) of 0:1, 0.5:1, 1:1 and 2:1. Fast exchange binding in RNA binding buffer allowed unambiguous determination of the binding site for the RNA body. Assignments for a random 29nt 5' OH RNA were obtained by comparison with the 1:1 15 nt MFA2 RNA:enzyme complex, since these RNAs generated similar shift changes. Experiments with non-hydrolyzable capped RNA were carried out at 1:1 ratio of RNA to enzyme.

Relaxation measurements

Relaxation-compensated constant-time CPMG experiments were performed on ^{13}C/^{1}H methyl labeled Ile(δ1), Leu and Val GB1-yDcp2(100-245) (Skrynnikov et al., 2001). All data were recorded at 23°C at spectrometer frequencies of 600 MHz and 800 MHz. Fitting was done using the cpmg_fitd8 program courtesy of D. Korzhnev (U. Toronto, L.E. Kay lab). Dispersion curves for ν_{CPMG} (Hz) = 25, 50, 100, 150, 200, 250, 300, 400, 600, 800, 950 were fit to the modified Carver-Richards two-site exchange equation (Korzhnev et al., 2004) assuming intermediate exchange for all residues except for Leu

231 which was fit using the fast-exchange limit. In the fast-exchange limit only the product p_a p_b $\Delta\omega^2$ and k_{ex} can be fit (Luz and Meiboom, 1963). This was realized by fixing p_a and p_b to 0.5 each and allowing $\Delta\omega$ and k_{ex} to vary. We determined the parameter α (Millet et al., 2000) to choose which equation to use for fitting; fast exchange was assumed for $\alpha > 1.5$.

The modified Carver-Richards equation is given by:

$$R_{2a}^{eff}(\nu_{CP}) = \tfrac{1}{2}(R_{2a} + R_{2b} + k_a + k_b - 2\nu_{CP}\cosh^{-1}[D_+\cosh(\eta_+) - D_-\cos(\eta_-)])$$
$$- \tfrac{1}{4n\delta}\ln(Q)$$

with

$$D_{\pm} = \tfrac{1}{2}\left[\pm 1 + \frac{\psi + 2\Delta\omega^2}{(\psi^2 + \xi^2)^{1/2}}\right]$$
$$\eta_{\pm} = \frac{\sqrt{2}}{4\nu_{CP}}[\pm\psi + (\psi^2 + \xi^2)^{1/2}]^{1/2}$$
$$\psi = (R_{2a} - R_{2b} + k_a - k_b)^2 - \Delta\omega^2 + 4k_a k_b$$
$$\xi = 2\Delta\omega(R_{2a} - R_{2b} + k_a - k_b)$$

and n, δ, and Q defined in (Korzhnev et al., 2004).

SUPPLEMENTAL REFERENCES

Chou, J.J., Li, S., and Bax, A. (2000). Study of conformational rearrangement and refinement of structural homology models by the use of heteronuclear dipolar couplings. J Biomol NMR 18, 217-227.

Cornilescu, G., Delaglio, F., and Bax, A. (1999). Protein backbone angle restraints from searching a database for chemical shift and sequence homology. J Biomol NMR 13, 289-302.

Deshmukh, M.V., Oku, Y., and Gross, J.D. (2007). Backbone and ILV resonance assignments of the catalytic domain of the yeast mRNA decapping enzyme, Dcp2. J Biomol NMR In press.

Gross, J.D., Geleev, V., and Wagner, G. (2003). A sensitive and robust method for obtaining intermolecular NOEs between sidechains in large protein complexes. J Biomol NMR 25, 235-242.

Grzesiek, S., Wingfield, P., Stahl, S., Kaufman, J.D., and Bax, A. (1995). Four-dimensional ^{15}N-separated NOESY of slowly tumbling perdeuterated ^{15}N-enriched protein. J Am Chem Soc 117, 9594-9595.

Haley, B., Tang, G., and Zamore, P.D. (2003). In vitro analysis of RNA interference in Drosophila melanogaster. Methods 30, 330-336.

Hu, J.-S., and Bax, A. (1997). Chi1 angle information from a simple two-dimensional NMR experiment that identifies trans 3JNCy couplings in isotopically enriched proteins. J Biolmol NMR 9, 323-328.

Hu, J.-S., Grzesiek, s., and Bax, A. (1997). Two-dimensional NMR methods for determining chi1 angles of aromatic residues in proteins from three-bond Jc'cg and JNCg couplings. J Am Chem Soc 119, 1803-1804.

Kalek, M., Jemielity, J., Darzynkeiwicz, Z.M., Bojarska, E., Stepinski, J., Stolarski, R., Davis, R.G., and Darzynkeiwicz, E. (2006). Enzymatically stable 5' mRNA cap analogs: Synthesis and binding studies with human DcpS decapping enzyme. Bioorg Med Chem 14, 3223-3230.

Kao, C., Rudisser, S., and Zheng, M. (2001). A simple and efficient method to transcribe RNAs with reduced 3' heterogeneity. Methods 23, 201-205.

Kontaxis, G., Clore, G.M., and Bax, A. (2000). Evaluation of cross-correlation effects and measurement of one-bond couplings in proteins with short transverse relaxation times. J Magn Reson 143, 184-196.

Korzhnev, D.M., Kloiber, K., and Kay, L.E. (2004). Multiple-quantum relaxation dispersion NMR spectroscopy probing millisecond time-scale dynamics in proteins: theory and application. J Am Chem Soc 126, 7320-7329.

Laskowski, R.A., Rullmannn, J.A., MacArthur, M.W., Kaptein, R., and Thornton, J.M. (1996). AQUA and PROCHECK-NMR: programs for checking the quality of protein structures solved by NMR. J Biomol NMR 8, 477-486.

Luz, Z., and Meiboom, S. (1963). Nuclear magnetic resonance study of the protolysis of trimethylammonium ion in aqueous solution-order of the reaction with respect to solvent. J Chem Phys 39, 366-270.

Medek, A., Olejniczak, E.T., Meadows, R.P., and Fesik, S.W. (2000). An approach for high-throughput structure determination of proteins by NMR. J Biolmol NMR 18, 229-238.

Millet, O., Loria, J.P., Kroenke, C.D., Pons, M., and A.G. Palmer, 3rd. (2000). The Static Magnetic Field Dependence of Chemical Exchange Linebroadening Defines the NMR Chemical Shift Time Scale. J Am Chem Soc 122, 2867-2877.

Milligan, J.F., Groebe, D.R., Witherell, G.W., and Uhlenbeck, O.C. (1987). Oligoribonucleotide synthesis using T7 RNA polymerase and synthetic DNA templates. Nucleic Acids Res 15, 8783-8798.

Pervushin, K.V., Wider, G., and Wuthrich, K. (1998). Single transition-to-single transition polarization transfer (ST2-PT) in 15N-1H TROSY. J Biol Mol NMR 12, 345-348.

Ruckert, M., and Otting, G. (2000). Alignment of biological macromolecules in novel nonionic liquid crystalline media for NMR experiments. J Am Chem Soc 122, 7793-7797.

Sampson, J.R., and Uhlenbeck, O.C. (1988). Biochemical and physical characterization of an unmodified yeast phenylalanine transfer RNA transcribed in vitro. Proc Natl Acad Sci U S A 85, 1033-1037.

Schwieters, C.D., Kuszewski, J.J., Tjandra, N., and Clore, G.M. (2003). The Xplor-NIH NMR molecular structure determination package. J Magn Reson 160, 65-73.

She, M., Decker, C.J., Chen, N., Tumati, S., Parker, R., and Song, H. (2006). Crystal structure and functional analysis of Dcp2p from Schizosaccharomyces pombe. Nat Struct Mol Biol 13, 63-70.

Skrynnikov, N.R., Mulder, F.A.A., Hon, B., Dahlquist, F.W., and Kay, L.E. (2001). Probing slow time scale dynamics at methyl-containing sidechains in proteins by

relaxation dispersion NMR measurements: application to methionine residues in a cavity mutant of T4 lysozyme. J Am Chem Soc 123, 4556-4566.

Talluri, S., and Wagner, G. (1996). An optimized 3D NOESY-HSQC. J Magn Reson B 112, 200-205.

Zweckstetter, M., and Bax, A. (2000). Prediction of sterically induced alignment in a dilute liquid crystalline phase: Aid to protein structure determination by NMR. J Am Chem Soc 122, 3791-3792.

SUPPLEMENTAL FIGURE LEGENDS

Figure S1: Structure and activity of GB1-yDcp2(100-245) . (a) Solution structure of yDcp2(100-245) displayed as a superposition of 10 lowest energy structures without any NOE distance and dihedral angle violations greater than 0.5 Å and 5°, respectively. (b) 15N HSQC of GB1-yDcp2(100-245) (red) overlayed that of GB1 (blue) . (c) Activity of GB1-yDcp2(100-245). Lane 1: GB1 alone, Lane 2: GB1-yDcp2(100-245) and Lane 3: an aliquot of the reaction from Lane 2 was incubated with Nucleotide Diphosphate Kinase (NDPK) and ATP which converts GDP to GTP, indicating a small amount of m7GMP product formed by GB1-yDcp2(100-245). Decapping assay performed in buffer containing manganese as described in Material and Methods.

Figure S2: Comparison of electrostatic surface of *S. pombe* Dcp2 (2A6T.pdb) (a,b) with homology model of *S. cerevisiae* Dcp2(1-245) (c,d). Surfaces displayed at -4KT/e (red) to 4.0 KT/e (blue) color range. Views are same as Figure 1c of main text.

Figure S3: Sequence alignment of Dcp2. The N-terminal regions of Dcp2 from *S. pombe* (residues 1-245), *A. thaliana* (residues 1 260), *M. musculus* (residues 1-250), *H. sapiens* (residues 1-250), *D. rerio* (residues 1-250) and *S. cerevisiae* (residues 1-245) were aligned. Box A and Box B are identified; residues mutated to alanine are marked with *. Secondary structural elements derived from NMR structure of yDcp2 are colored while those predicted from the homology model of yDcp2 (based on *S. pombe*

106

crystal structure) are colored black. Parenthesis indicate secondary structural labels from main text.

Figure S4: Binding of various RNA oligonucleotides to GB1-yDcp2(100-245) by NMR. (a) 15N HSQC showing chemical shift perturbation of 15nt MFA2 containing 5' OH (15MFA2) at 0:1(red), 1:1(green) and 2:1(blue) RNA:Enzyme ratio. (b) Chemical shift changes of 15nt MFA2 RNA mapped onto surface of yDcp2 (2:1 RNA: enzyme) with dorsal view as in Figure 1 of main text (left) and that rotated by 90 degrees about the horizontal axis (right). (c) Comparison of induced chemical shift changes for 15MFA2 RNA, (d) a random 29nt 2' OMe non-hydrolyzable capped RNA (29RND) and (e) shifts induced by 5' OH 29RND versus 15MFA2 RNA. For (c)-(e), the RNA:enzyme ratio is 1:1 ; a and b secondary structures depicted as rectangles and arrows; and the B1 domain of protein G is depicted as a green rectangle.

Figure S5: Mutations within the Nudix domain of yDcp2 do not alter the solution structure of the enzyme. (a) Circular Dichroism and (b) SDS-PAGE analysis of recombinant wild-type and mutant GB1-Dcp2(100-245). (c) SDS-PAGE analysis of recombinant GB1-Dcp1/Dcp2(1-245) after co-purification by gel filtration chromatography. Gels of recombinant proteins were stained with Coomassie Brilliant Blue.

Figure S6: Complementation assay for single alanine substitutions within Dcp2

Figure S7: 15N HSQC spectra of wild-type and dorsal surface mutants of GB1-yDcp2(100-245) alone (blue) and in complex with 15 nt 5' OH MFA2 RNA (red). The RNA:protein ratio is 2:1 and the protein concentrations are 100mM. Below each spectrum are excerpts showing RNA binding to the dorsal surface residues indicated in the left panel. The arrow below the spectral excerpts indicates that the spectra are ordered horizontally as K_m increases. The 15nt RNA binds in fast-exchange, so the degree of resonance shift reports on the population of bound RNA.

Figure S8: Decapping kinetics for Nudix domain and the Dcp1/K135A-Dcp2 complex. (a) Representative decapping time course for 6mM GB1-fused Nudix domain and (b) corresponding plot of fraction m7GDP released versus time for different enzyme concentrations. (c) Decapping time course for 8mM GB1-Dcp1/K135A-Dcp2 complex and (d) corresponding plot of fraction m7GDP released versus time. (e) Observed rate (k) plotted versus enzyme concentration. The mean and standard deviations are reported for n≥2 independent experiments. Arrows indicate position of products, which were verified by UV shadowing of cold-standards. Assays performed as described in main text for Figure 4 with Mg^{2+} as sole metal ion.

Figure S9: Decapping kinetics of GpppG labeled 29nt RNA, which lacks the N-7 methyl modification. (a) Time-course for fraction GDP released from a 60/40 % mixture of m7GpppG and GpppG capped RNA (top) and 100% GpppG capped RNA (bottom). (b) Fraction GDP released versus time for enzyme concentrations of 2, 3, 4, 5, 7 and 9 mM decapping complex and (c) observed rates plotted versus total concentration of decapping

complex for the "mixed" methylated RNA substrate. The fitted k_{max} and K_m are 0.15/min and 2.7mM respectively. (d) Observed rates for homogeneous preparation of 100% GpppG RNA plotted against total concentration of decapping complex. The fitted k_{max} and K_m are 0.12 and 10.7 mM respectively. The mean and standard deviations are reported for n≥2 independent experiments.

Figure S10: Interaction of non-hydrolyzable ARCA substrate and product 5' monophosphate RNA with the decapping complex (GB1-Dcp1:Dcp2). Native gel shift assay with (a) 29nt non-hydrolyzable capped RNA as described in main text and (b) the same RNA containing a 5'monophosphate RNA. Concentrations of GB1-Dcp1/Dcp2 complex were reduced by serial dilution in binding buffer from 20.9 or 15.6 mM for non-hydrolyzable substrate or 5'monophosphate RNA , respectively. (c) Overlay of fraction RNA shifted versus concentration of decapping complex duplicated from main text Figure 4f. (d) Chase experiment: radiolabeled 29nt RNA was pre-incubated with 20mM GB1-Dcp1:Dcp2 complex (C) and either diluted with an equal volume of buffer (M) or excess cold-competitor (chase). Aliquots of the chase reaction were loaded onto an electrophoresing native gel at 15-second time-intervals.

Figure S11: (a) Representative relaxation dispersion data for residues contained within the distal RNA binding site containing Box B (residues 220-240) and adjacent helix of the Nudix domain. (b) Table of fitted relaxation parameters as described in Supplementary Methods. Errors in R_2 were propagated using standard procedures with uncertainty in individual peak intensities taken from the NMRPipe peak detection

algorithm.

Supplemental Table 1: NMR structural statistics[a]

NOE distance restraints	
Intraresidue	34
Medium range [(i-j) ≤ 4]	142
Long range [(i-j) > 4]	109
Total	285
Hydrogen Bonds	34
Dihedral angle restraints	294
Residual Dipolar Couplings (NH)	55
Ramachandran plot[b]	
(residues 105-240)	
Most favored region	87.5%
Additionally allowed region	11.3%
Generously allowed region	0.5%
Disallowed region	0.4%
R.M.S.D. from ideal geometry	
Bonds (Å)	0.001
Angles (°)	0.38
Impropers (°)	0.217
R.M.S.D. from mean structure	
Backbone	0.73
Heavy atoms	1.28
Q(Saupe, NH RDC)	0.16

[a]The 10 structures with lowest energy selected from 50 calculated final structures by NIH-XPLOR (Schwieters *et. al*. 2003) contain no distance violations greater than 0.5 Å and no dihedral angle violations > 5°.
[b]Data obtained by using the program PROCHECK-NMR (Laskowski *et al*., 1996)

(a)

(b)

(c)

FIGURE S1

(a) (b)

(c) (d)
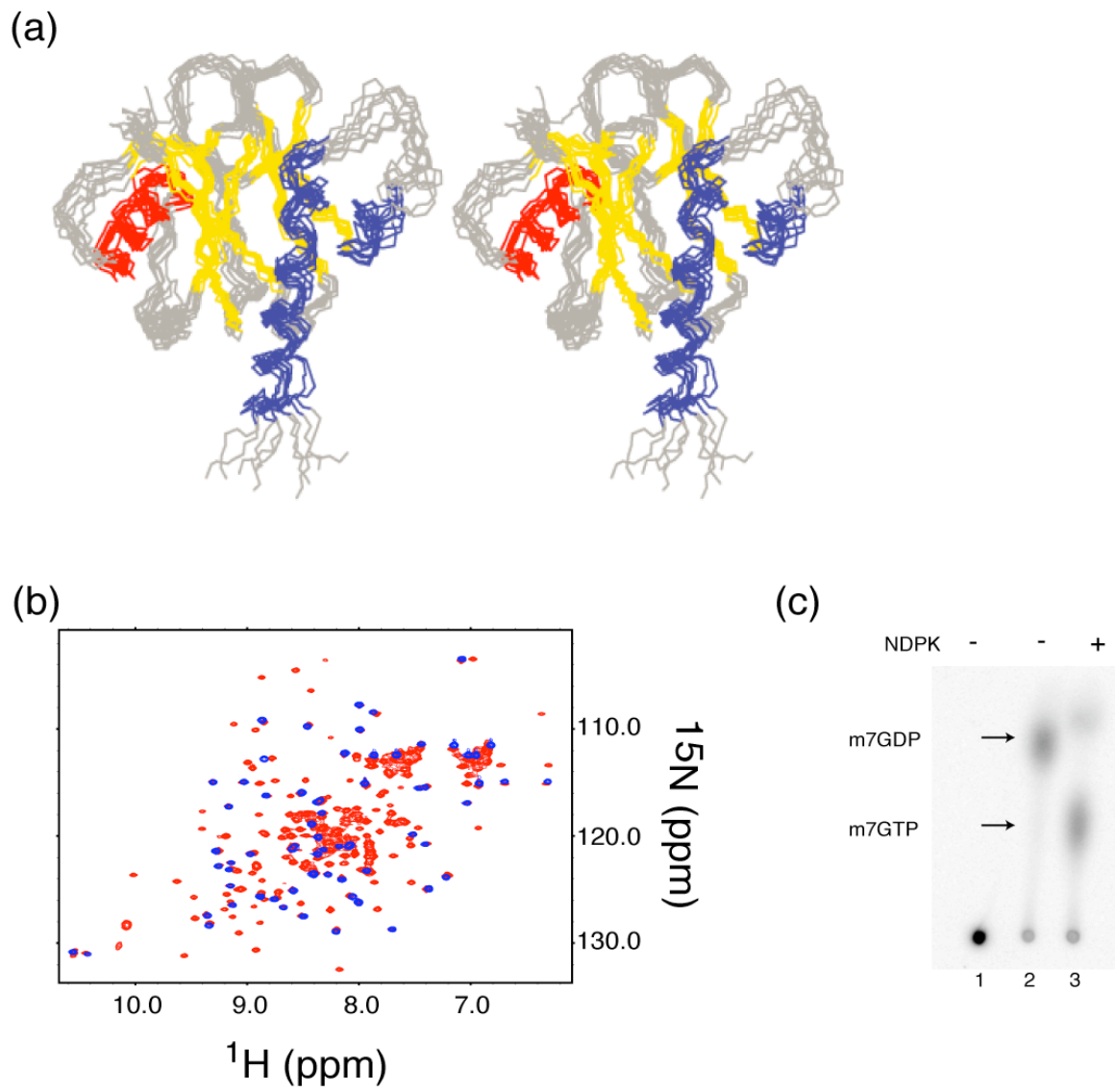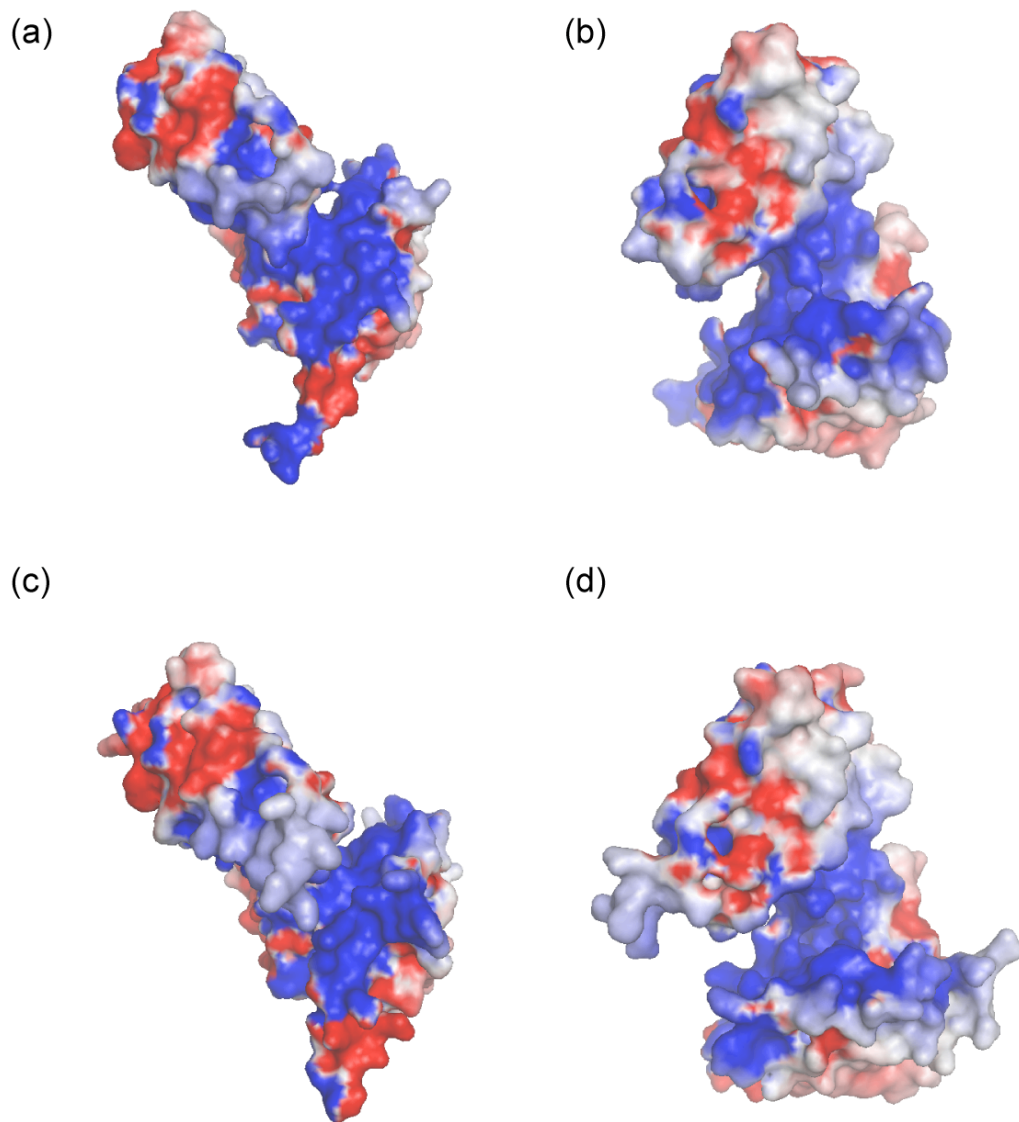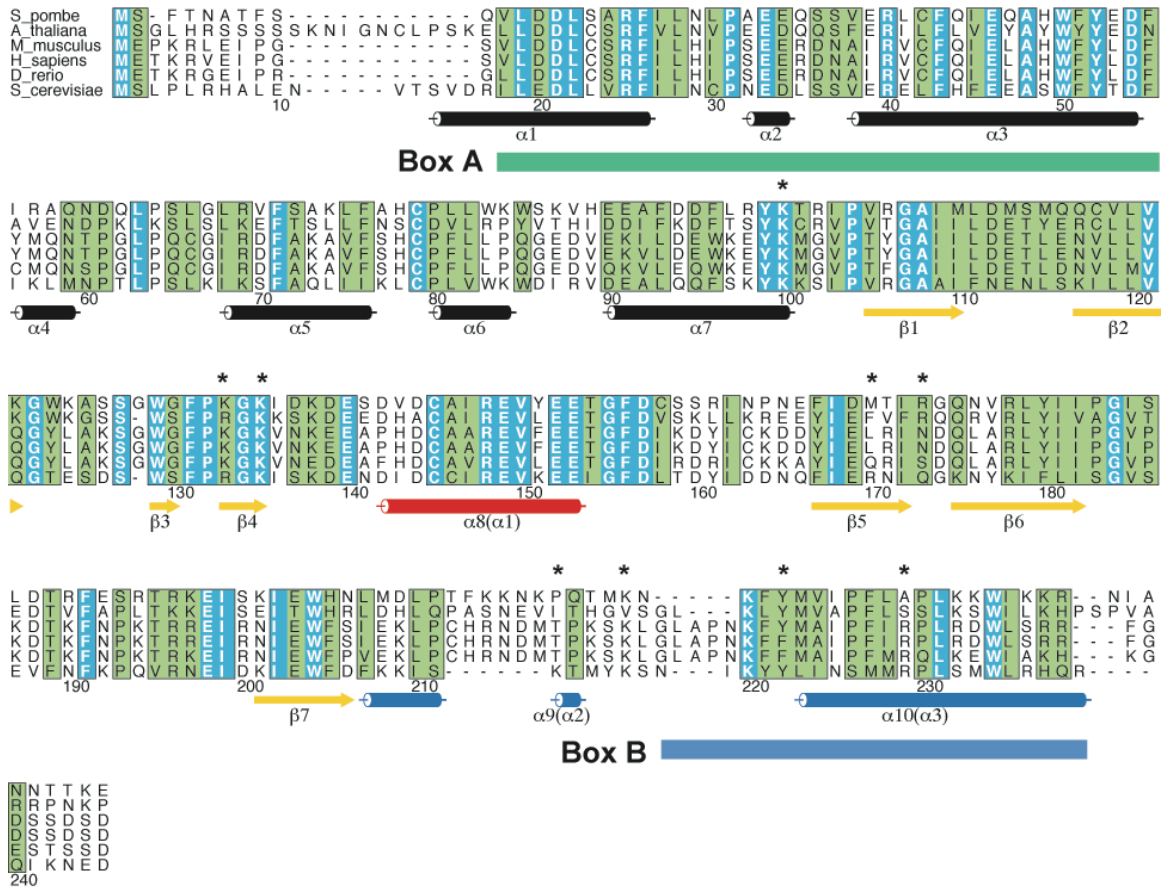
FIGURE S2

FIGURE S3

FIGURE S4

(a)

(b)

(c)
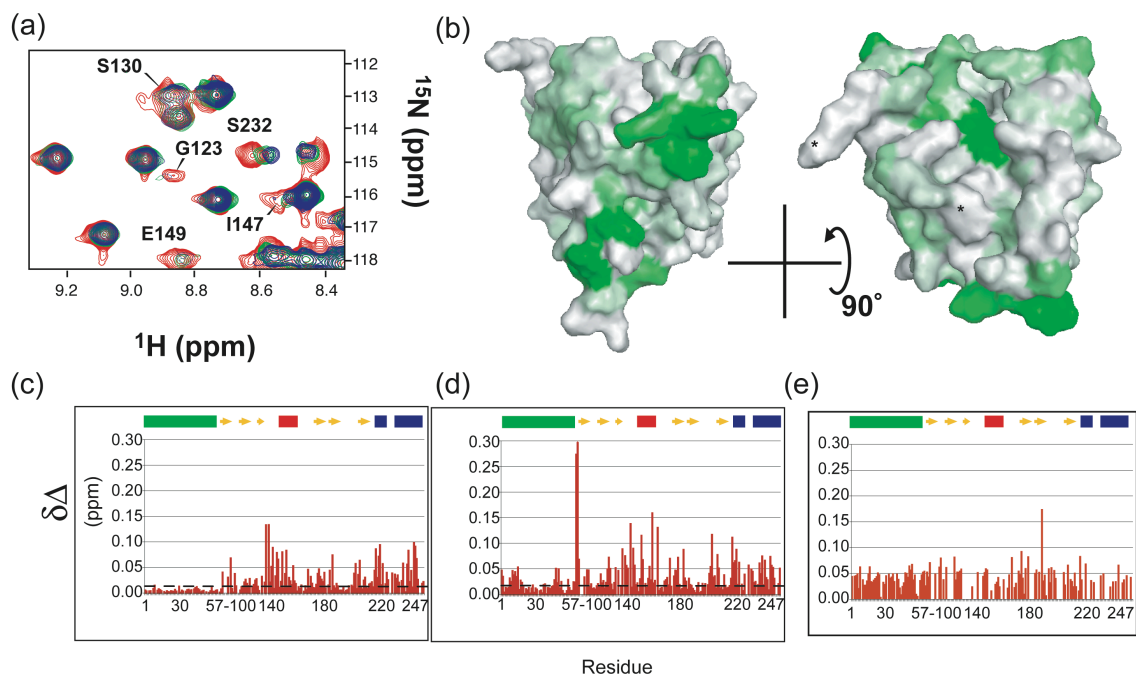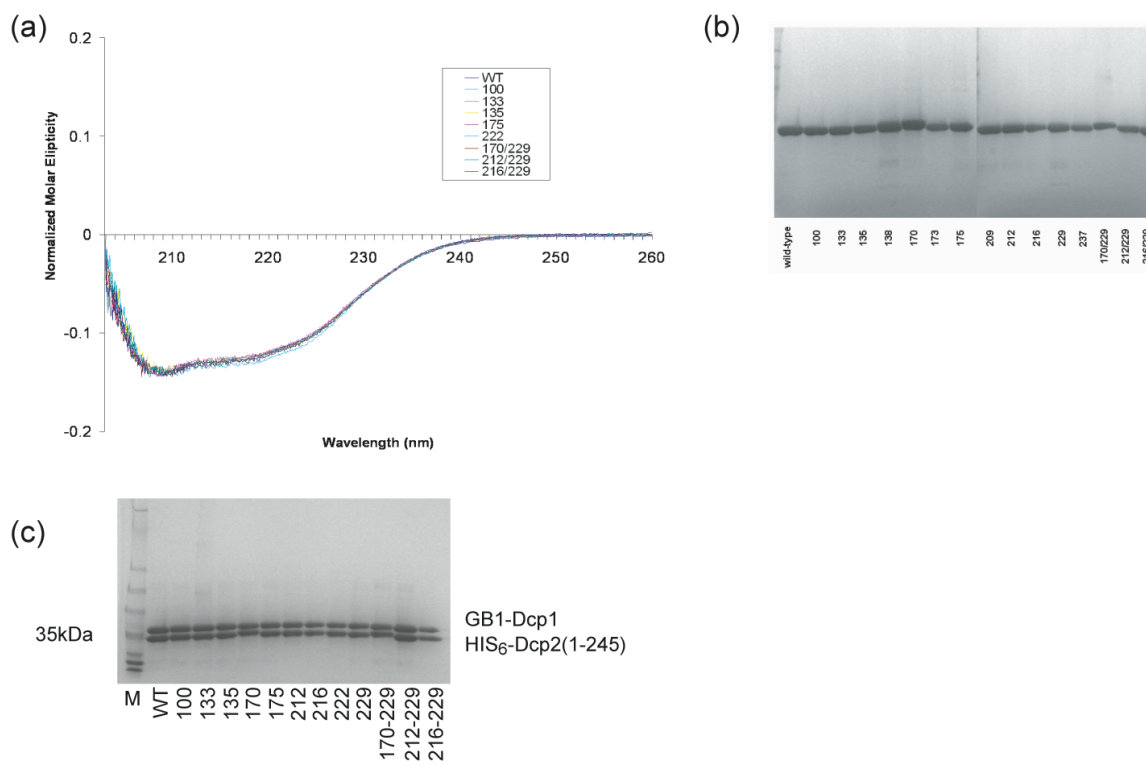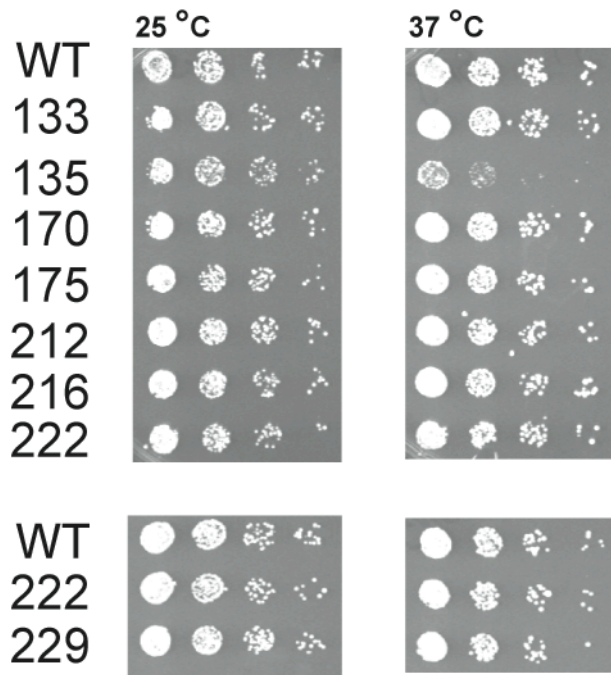
FIGURE S5

FIGURE S6
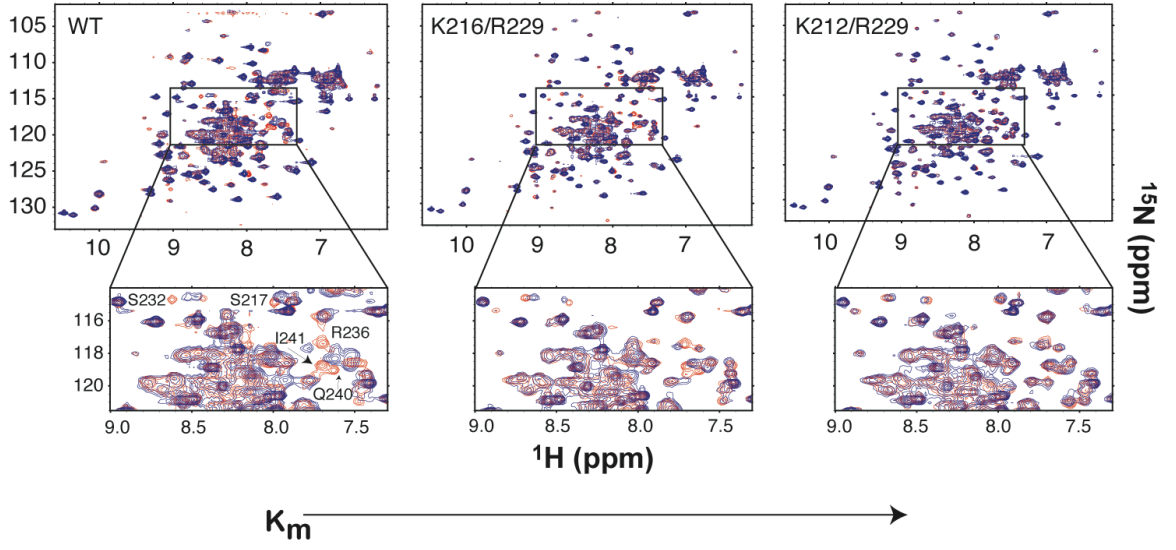
FIGURE S7

FIGURE S8

FIGURE S9

(a) 20.9 μM

nh-ARCA-RNA GB1-D1:D2

nh-ARCA-RNA

(b) 15.6 μM

5' phosphate GB1-D1:D2

5' phosphate

(c)

nh-ARCA
5' phosphate

F_{RNA} Shifted

log [GB1-Dcp1:Dcp2] (nM)

(d)

5' phosphate GB1-D1:D2

5' phosphate

C M 15 135

chase (seconds)

FIGURE S10

(a)
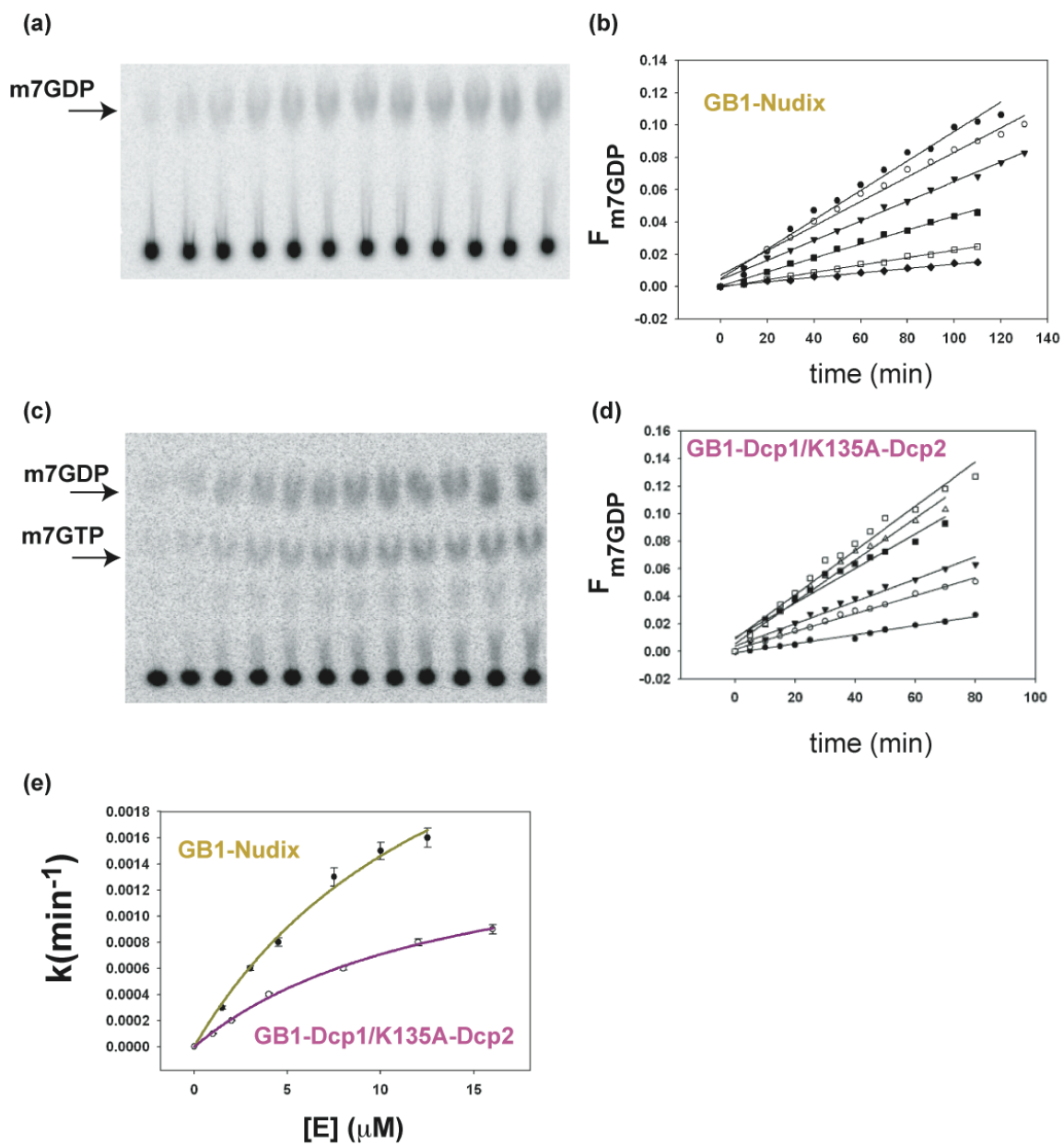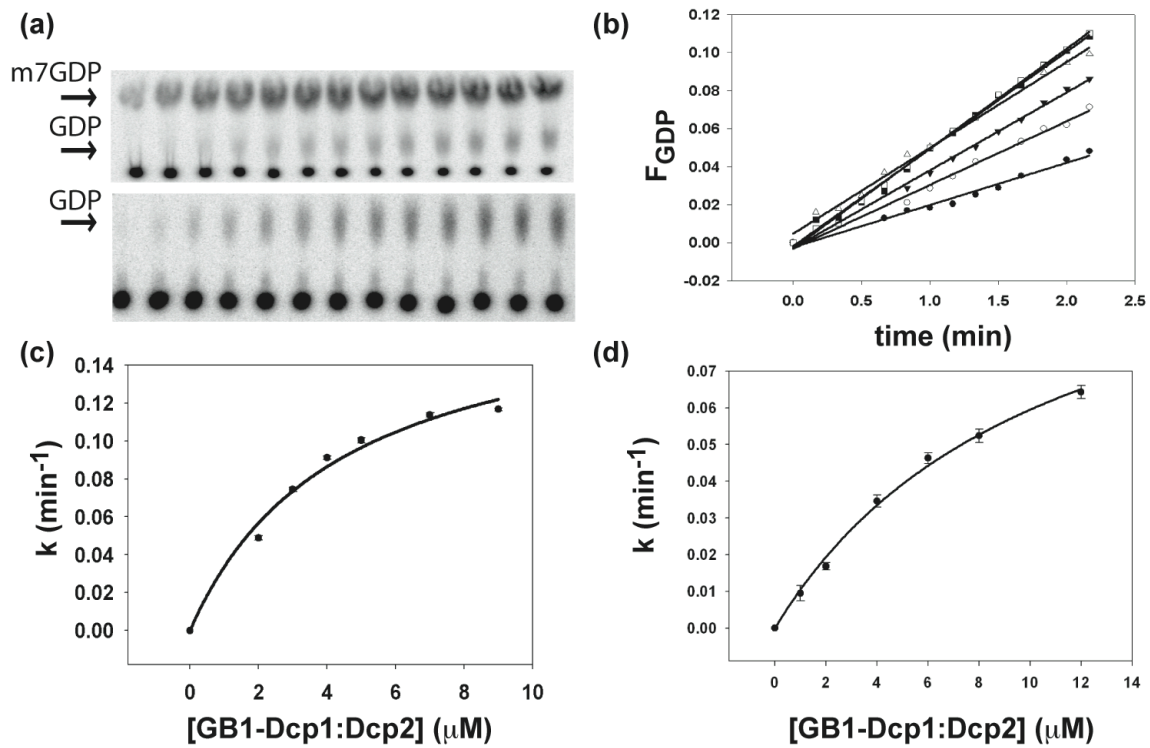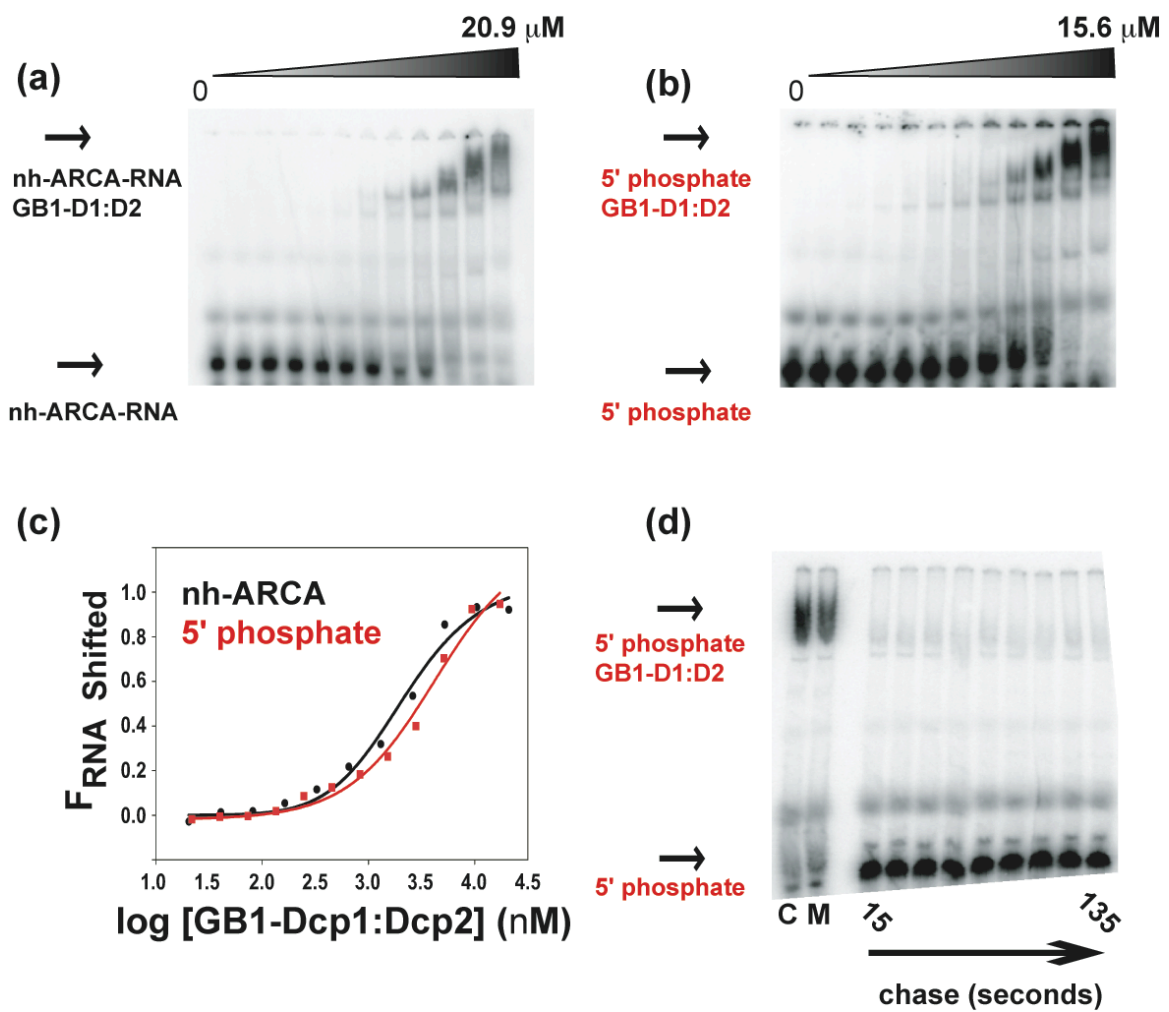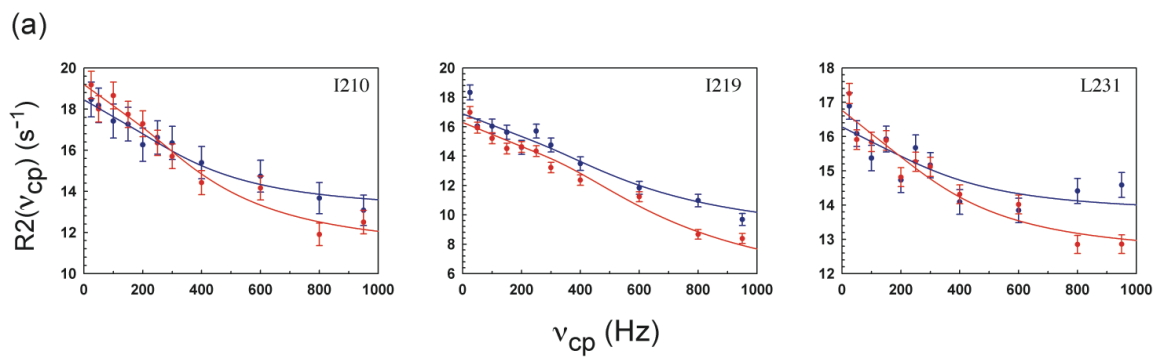
(b)

Residue	$R_{2a,600}$ (s⁻¹)	$R_{2a,800}$ (s⁻¹)	α	k_{ex} (s⁻¹)	Δω(ppm)	P_b	P (χ²)
Ile 147	13.2 ± 0.20	11.3 ± 0.26	0.96	1166 ± 89	1.01 ± 0.05	0.033 ± 0.002	0.761
Ile 210	13.0 ± 0.30	11.1 ± 0.50	0.744	2031 ± 471	1.23 ± 0.23	0.011 ± 0.003	0.962
Ile 219	8.4 ± 0.92	4.64 ± 1.54	-0.021	2768 ± 798	2.29 ± 0.31	0.008 ± 0.001	0.002
Leu 223	13.4 ± 3.55	8.38 ± 5.90	1.05	3527 ± 790	2.83 ± 0.32	0.025 ± 0.002	0.331

Residue	$R_{2a,600}$ (s⁻¹)	$R_{2a,800}$ (s⁻¹)	α	k_{ex} (s⁻¹)	$p_a p_b \Delta\omega^2$ (s⁻²)	P (χ²)
Leu 231	19.3 ± 0.29	18.0 ± 0.45	2.19	2460 ± 574	0.0067 ± 0.002	0.002

FIGURE S11

CHAPTER 5:

Conclusions

Cap hydrolysis by Dcp2 is a critical step in the life of eukaryotic mRNAs as removal of the cap is a prerequisite for 5'-3' decay. In yeast, decapping is catalyzed by the evolutionally conserved Dcp1-Dcp2 complex, comprised of the catalytic subunit, Dcp2, in complex with Dcp1, an obligate *in vivo* activator. Dcp2 is a dumbbell shaped protein with the N-terminal domain binding Dcp1 and the C-terminal Nudix domain acting as a catalytic center. Decapping is highly regulated and requires the coordinated assembly of a multiprotein decapping mRNP. However, the mechanism of substrate recognition and how decapping is regulated by protein interactions have remained elusive as *in vitro* assays to dissect enzyme activity are unavailable. The goal of this study is to characterize the mechanism of mRNA decapping by Dcp2 and the role of activators.

To address this goal, we have developed a kinetic assay to monitor decapping by the heterodimeric yeast Dcp1/Dcp2 complex. Kinetic constants related to RNA binding and the rate of the catalytic step were determined with recombinant enzyme and cap radiolabeled RNA substrate, allowing substrate specificity and the role of activating factors to be firmly established. Using NMR spectroscopy and kinetic analyses we show that yeast Dcp2 interacts with the cap and RNA body using a bipartite surface that forms an extensive, highly charged channel from the active site to the dorsal side of the protein. The Nudix domain forms the base of this channel, which extends between the catalytic and Dcp1 binding domains.

 Biochemical and genetic analysis reveal that the dorsal surface and cap proximal nucleotide binding cavity perform distinct catalytic functions. The dorsal surface promotes the interaction with substrate by distributing weak, nonspecific ionic interactions over a large interaction surface. The interaction with cap is weak but

specific as alanine substitutions of amino acids near or within the cap-binding cavity reduce the catalytic activity of Dcp2 while minimally affecting RNA binding. Our data also suggest that the RNA body promotes decapping by binding and increasing the local concentration of the cap to promote catalysis. Thus, activation of the decapping mRNP is restricted by access to cap proximal nucleotides, a feature that could act as a checkpoint in mRNA metabolism.

Importantly, the role of Dcp1 and its interaction domain is to enhance chemistry, not RNA binding. The catalytic step is stimulated by Dcp1 and its interaction domain, likely through a substrate induced conformational change. This is suggested by several observations. We show that the catalytic step is rate limiting for catalysis since it is slow relative to substrate binding and product release. Also, specificity for the cap structure is conferred exclusively during the catalytic step. As our results do not distinguish whether catalysis reflects exclusively the rate of chemistry or if it is comprised of all sub-steps that occur after binding, including the rate of chemistry, k_{max} could include a conformational change that occurs upon cap recognition. This is further supported by crystallographic and SAXS analysis of the *S. pombe* decapping complex reveals that in the absence of nucleotide, the Dcp1/Dcp2 complex adopts and extended open conformation where the regulatory domain of Dcp2 bound to Dcp1 is far removed from the Nudix domain but forms a compact structure upon ATP binding. This dynamic conformation equilibrium represents a possible control point for decapping activity as protein interactions with activators could shift the balance by promoting the closed, active form of the enzyme.

To address this we began studies on a known activator of decapping, Edc3. We determined that Edc3 binding to Dcp2 is mediated by a short peptide sequence located C-terminal to the catalytic domain of Dcp2. This sequence is required for Edc3 to stimulate decapping activity of Dcp2 *in vitro*. These results suggest a model for Dcp2 recruitment to specific mRNAs where regions outside the catalytic core promote the formation of different complexes involved in mRNA decapping.

APPENDIX I:

Enhancers of decapping

Identification and analysis of the interaction between Edc3 and Dcp2 in

Saccharomyces cerevisae

Yuriko Harigaya[1], Brittnee N. Jones[2], Denise Muhlrad[1], John D. Gross[3] and Roy Parker[1]*

[1]Department of Molecular and Cellular Biology and Howard Hughes Medical Institute,

University of Arizona, Tucson, AZ, 85721-0106, USA;

[2]Program in Chemistry and Chemical Biology, [3]Department of Pharmaceutical

Chemistry, University of California, San Francisco, 600 16th Street, San Francisco, CA

94107, USA

*Corresponding author:

Mailing address: Department of Molecular and Cellular Biology and Howard Hughes

Medical Institute, University of Arizona, Tucson, AZ, 85721-0106, USA

Phone: 520-621-9347

Fax: 520-621-4524

E-mail: rrparker@u.arizona.edu

Running title: Mapping the interaction between Edc3 and Dcp2

128

ABSTRACT

Cap hydrolysis is a critical control point in the life of eukaryotic mRNAs and catalyzed by the evolutionally conserved Dcp1-Dcp2 complex. In *Saccharomyces cerevisae*, decapping is modulated by several factors including the Lsm family protein Edc3, which directly binds to Dcp2. We show that Edc3 binding to Dcp2 is mediated by a short peptide sequence located C-terminal to the catalytic domain of Dcp2. This sequence is required for Edc3 to stimulate decapping activity of Dcp2 *in vitro*, and for Dcp2 to efficiently accumulate in P-bodies. Deletion of the sequence results in a subtle but significant defect in turnover of a reporter transcript, which is exacerbated by weak hypomorphic mutations in Dcp1. Deletion of this region also up-regulates the *RPS28B* mRNA, indicating that interaction of Dcp2 and Edc3 is required for the degradation of this mRNA. In contrast, degradation of the *YRA1* pre-mRNA, whose decay is enhanced by Edc3, is not affected by removal of this region, suggesting that the effect of Edc3 on *YRA1* is independent of its interaction with Dcp2. These results suggest a model for Dcp2 recruitment to specific mRNAs where regions outside the catalytic core promote the formation of different complexes involved in mRNA decapping.

INTRODUCTION

mRNA degradation plays an important role in control of gene expression. Removal of the 5' N7-methyl guanosine (^{m7}G) cap structure is a critical step in many mRNA decay pathways and occurs following deadenylation in one of the major pathways of mRNA degradation (Parker and Song, 2004). Decapping is catalyzed by a decapping holoenzyme consisting of the catalytic Dcp2 subunit and the co-activating Dcp1, which are conserved throughout eukaryotes (Franks and Lykke-Andersen, 2008). Dcp2 contains a Nudix/MutT motif, which binds to both the ^{m7}G cap and mRNA body, and is critical for decapping catalysis (Dunckley and Parker, 1999; Lykke-Andersen, 2002; Wang et al., 2002; van Dijk et al., 2003). Recent kinetic and structural studies using the Dcp proteins from *S. cerevisiae* and *S. pombe* have indicated that Dcp1 strongly stimulates Dcp2 catalytic activity by binding the N-terminal region of Dcp2 (residues 1-101 in *S. cerevisiae*) and inducing a conformational change in Dcp2 so that the N-terminal region is brought to the proximity of the C-terminal catalytic domain (residues 102-245 in *S. cerevisiae*), which contains the Nudix/MutT motif (She et al., 2006; Deshmukh et al., 2008; She et al., 2008).

In principle, three sequential events are required for mRNA engaged in translation to be eventually routed to decapping. First, the eukaryotic initiation factor eIF4E that protects the ^{m7}G cap should be displaced from the mRNA (Schwartz and Parker, 2000). Sequentially, the Dcp1-Dcp2 decapping complex needs to be recruited onto the mRNA. Finally, the decapping complex catalyzes the removal of the ^{m7}G cap

structure, which appears to require an activation step enhancing the catalytic function of Dcp2 (Dunckley et al., 2001). Several factors are thought to function in these processes to promote decapping including the DEAD-box helicase RCK/p54/Me31B/CGH-1/Dhh1, the RNA binding Lsm1-7 complex, the RNA binding protein Pat1, the Lsm family proteins Edc3 and Rap55/Edc4/Tral/CAR-1/Scd6, all of which are evolutionarily conserved (Decker and Parker, 2006; Decourty et al., 2008; Franks and Lykke-Andersen, 2008). In yeast, Dhh1 and Pat1 appear to promote decapping at least in part by eliciting translational repression, which either directly or indirectly involves displacement of eIF4E (Coller and Parker, 2005). Other proteins appear to affect decapping by directly activating the decapping enzyme. For example, the Edc1 and Edc2 proteins can directly activate the decapping enzyme by unknown mechanisms (Dunckley et al., 2001; Schwartz et al., 2003; Steiger et al., 2003). Similarly, the Edc3 protein does not appear to function in translation repression and instead directly binds and activates Dcp2 (P. Rajyaguru, T. Nissan and R. P., submitted for publication).

Edc3 is an interesting protein for a variety of reasons. In *Saccharomyces cerevisiae*, Edc3 is dispensable for efficient decapping of certain reporter transcripts (Kshirsagar and Parker, 2004) and also for maintenance of steady-state levels of most transcripts (Badis et al., 2004; Dong et al., 2007). However, Edc3 becomes critical for efficient mRNA degradation of the reporter transcripts when the decapping enzyme is compromised by mutations either in Dcp1 or in Dcp2 (Kshirsagar and Parker, 2004). Deletion of *EDC3* also causes a synthetic growth defect when combined with another Lsm protein Scd6 (Decourty et al., 2008; Wilmes et al., 2008), suggesting some

redundancy in Edc3 function. Edc3 is also required for the specific degradation of some mRNAs. For example, the efficient degradation of the *RPS28B* mRNA and *YRA1* pre-mRNAs requires Edc3 (Badis et al., 2004; Dong et al., 2007). Moreover, in *Drosophila* S2 cells, Edc3 is required for the degradation of a subset of miRNA targets (Eulalio et al., 2007). Edc3 contains three functional domains: an N-terminal divergent Lsm (Sm-like) domain, which binds Dcp2 (Decker et al., 2007) (P. Rajyaguru, T. Nissan and R. P., submitted for publication), a central FDF domain, which binds Dhh1 (Decker et al., 2007; Tritschler et al., 2009), and a C-terminal YjeF-N domain, which self-interacts and promotes Edc3 dimerization (Decker et al., 2007; Ling et al., 2008). Taken together, these results indicate the Edc3 is a core component of the decapping machinery that can both generally affect the activity of the decapping enzyme and be recruited for the regulation of specific mRNAs. An unresolved question is how Edc3 interacts with Dcp2 and the consequences of that interaction for general mRNA decapping and the control of specific mRNAs.

In this work, we demonstrate that a short peptide sequence just C-terminal of the Nudix domain of Dcp2 interacts with Edc3. This peptide region is required for the binding of Dcp2 to the Lsm-FDF domain of Edc3, for the stimulation of Dcp1/Dcp2 decapping activity by Edc3 *in vitro*, and for efficient accumulation of Dcp2 into P-bodies *in vivo*. Deletion of the peptide sequence causes a significant up-regulation of a known substrate of Edc3-mediated decay, *RPS28B* mRNA, and results in a subtle but significant defect in decapping of the *MFA2pG* reporter mRNA, which is exacerbated by weak hypomorphic mutations in Dcp1. Surprisingly, degradation of the *YRA1* pre-mRNA,

whose decay is enhanced by Edc3, is not affected by removal of this region suggesting that the effect of Edc3 on *YRA1* is independent of its interaction with Dcp2. Our results also imply that this region of Dcp2 may represent an important site for the binding of additional decapping regulators.

MATERIALS AND METHODS

Yeast Strains

Yeast strains used in this study are listed in **Table 1**. All strains are in the

yRP840/yRP841 background (Hatfield et al., 1996). The strains yRP2702, yRP2703,

yRP2706, yRP2708, yRP2709 and yRP2710 were constructed from yRP841 by a PCR-

based method using oligonucleotides oRP1450, oRP1449, oRP1461, oRP1463, oRP1464,

oRP1462 and oRP1451 (Longtine et al., 1998). The strains yRP2704 and yRP2705 were

constructed from yRP1515 using oligonucleotides oRP1450, oRP1449 and oRP1451.

Plasmids

Plasmids used in this study are listed in **Table 2**. Plasmid pRP1891, 1892 and 1893 were

constructed in multiple steps. First, pRP1667 (a gift from C. J. Decker) was digested

with restriction enzymes *Sac*I and *Hind*III to isolate the DNA fragment containing the

GPD promoter, the *Nru*I restriction site, a GFP open reading frame and the *ADH1*

terminator. The fragment was cloned into corresponding sites in pRS416 (Sikorski and

Hieter, 1989) to generate pRP1902. DNA fragments containing the 514-bp upstream

region of *DCP2* and a sequence encoding residues 1-970, 1-300 and 1-247 of Dcp2 were

PCR amplified from the genome using a forward primer oRP1440 and reverse primers

oRP1441, oRP1442 and oRP1443. The resultant fragments were digested with restriction

enzymes *Sac*I and *Bam*HI and cloned into corresponding sites in pRP1902 to generate

pRP1891, 1892 and pRP1893.

To generate pRP1903, a DNA fragment containing the 514-bp upstream region of *DCP2* was PCR amplified from the genome using primers oRP1440 and oRP1458. The resultant fragment was digested with restriction enzymes *Sac*I and *Nru*I and cloned into corresponding sites in pRP1902. Note that the plasmid contains a 7-bp random sequence downstream of the *Nru*I site.

To generate pRP1894 and pRP1895, DNA sequences encoding residues 243-970 and 327-970 of Dcp2 were amplified from the genome with the initiation codon using forward primers oRP1459 and oRP1460 and a reverse primer oRP1441. The resultant fragments were digested with restriction enzymes *Sac*I and *Nru*I and cloned into corresponding site in pRP1903. Note that the plasmids contain a 6-bp random sequence upstream of the *Nru*I site.

To generate pRP1904, a DNA fragment containing the 514-bp upstream region of *DCP2*, the initiation codon and a sequence encoding residues of 102-300 of Dcp2 were PCR amplified from the plasmid pRP1278 (a gift from C. J. Decker) using primers oRP1440 and oRP1442. The resultant DNA fragment was digested with restriction enzymes *Sac*I and *Bam*HI and cloned into corresponding sites in pRP1902. pRP1905 was constructed essentially in the same way using primers oRP1440 and oRP1443.

pRP1896 was constructed in multiple steps. First, a DNA fragment was PCR amplified from pRP1207 (She et al., 2006) using a primer pair of oRP1447 and oRP1442. A second PCR reaction was performed using a primer pair of oRP1440 and oRP1448.

The two PCR fragments were then mixed and fused by PCR amplification using primers oRP1440 and oRP1442. The resultant fragment was digested with restriction enzymes *Sac*I and *Bam*HI and cloned into corresponding sites in pRP1902. pRP1906, pRP1908 and pRP1909 were constructed essentially in the same way.

pRP1907 was constructed in multiple steps. First, a DNA fragment was PCR amplified from pRP1207 (She et al., 2006) using a primer pair of oRP1467 and oRP1442. A second PCR reaction was performed using a primer pair of oRP1440 and oRP1468. The two PCR fragments were then mixed and fused by PCR amplification using primers oRP1440 and oRP1442. The resultant fragment was used as template in PCR amplification using a primer pair of oRP1465 and oRP1442. The resultant fragment was then mixed with another fragment amplified from pRP1207 (She et al., 2006) using oRP1466 and oRP1440, and the two fragments were fused by PCR using primers oRP1440 and oRP1442. The resultant fragment was digested with restriction enzymes *Sac*I and *Bam*HI and cloned into corresponding sites in pRP1902. pRP1910 was constructed essentially in the same way.

To generate pRP1897 and pRP1898, DNA fragments encoding residues 1-300 and 1-247 of Dcp2 were PCR amplified from pRP1207 (She et al., 2006)   using a forward primer oRP1444 and reverse primers oRP1445 and oRP1446 respectively, digested with restriction enzymes *Nde*I and *Bam*HI, and cloned into corresponding sites in pRP784 (pPROEX-1, GibcoBRL).

Plasmids pRP1453, 1450 and 1449 were constructed in multiple steps. First, the DNA fragment containing the 3' region of the *DCP2* gene was PCR amplified from pRP1207 (She et al., 2006) using primers oRP1471 and oRP1472, digested with restriction enzymes *Sac*I and *Bam*HI, and cloned into corresponding sites in pRP10 (Heaton et al., 1992), to generate pRP1454. Second, the DNA fragment containing the promoter region of *DCP2* and N-terminal portions of the coding region (residues 1-300, 1-247 and 1-227) were PCR amplified using a forward primer oRP1473 and reverse primers oRP1474, oRP1475 and oRP1476, digested with restriction enzymes *Sac*I and *Bgl*II, and cloned into corresponding sites in pRP1454.

To generate pRP1899, a DNA fragment was PCR amplified from pRP1896 using primers oRP1444 and oRP1445, digested with restriction enzymes *Nde*I and *Bam*HI and cloned into corresponding sites in pRP784.

Oligonucleotides

Oligonucleotides used in this study are listed in **Table S1**.

Cell growth conditions

For microscopy and Western blot analysis (**Fig. 1B, 1C and 7B**), cells were grown at 30°C in synthetic complete medium (SC) lacking uracil but containing 2% glucose as a carbon source, until OD_{600} of 0.3-0.35 was reached. Cells were subsequently harvested by centrifugation, washed, resuspended in synthetic complete medium (SC) lacking uracil and a carbon source, and incubated in a shaking water bath at 30°C for 10 minutes. For

Northern blot analysis, cells were grown either at 30°C in SC medium lacking uracil or tryptophan but containing 2% galactose (**Fig. 4B, 4C, 5, 6A and 7D**) or at 24°C in YP media containing 2% galactose (**Fig. 4D and 6B**) until OD_{600} of 0.3-0.35 was reached.

Microscopy

Microscopy was performed essentially as described previously (Buchan et al., 2008). All images are acquired using a Deltavision RT microscope system running softWoRx 3.5.1 software (Applied Precision, LLC), using an objective (UPlan sapo 100 x, 1.4 NA, Olympus). They were collected using software (SoftWoRx) as 1024 by 1024 pixel files with a camera (CoolSNAP HQ, Photometrics) using 1 by 1 binning. A Z-series with 10 to 11 image planes and a step size of 0.8 μm was taken. All images were deconvolved using standard softWoRx deconvolution algorighms (enhanced ratio, medium noise filtering, 10 cycles). ImageJ (National Institute of Health) was used to adjust all images to equal contrast ranges.

Protein purification, *in vitro* protein-protein interaction assays and Western blot analysis

His-tagged Dcp2 (1-300), Dcp2 (1-247) and Dcp2 (1-300) harboring the L255A K256A mutation were expressed in *E. coli* BL21 from plasmids pRP1897, pRP1898 and pRP1899. Purification of His-Dcp2 (1-300) and His-Dcp2 (1-247) was performed essentially as described previously (She et al., 2006). The GST-tagged Lsm-FDF domain of Edc3 was expressed in *E. coli* BL21 from the plasmid pRP1444 (a gift from C. J. Decker) and was purified using Glutathione Sepharose 4B (GE Healthcare) after lysis in

PBS buffer containing 1 mM DTT, 1% Triton X-100, 0.1 mM PMSF and complete

protease inhibitor (Roche).

Binding experiments were performed at 4°C in 400 μL of binding buffer (50

mM HEPES, pH 7.0, 100 mM NaCl, 1 mM DTT, 2 mM $MnCl_2$, 2 mM $MgCl_2$, 1% Triton

X-100, 10% glycerol, and 10 mg/ml BSA), essentially as described previously (Decker et

al., 2007). Each protein was added to the binding reaction at a final concentration of

approximately 0.5 μM. Glutathione Sepharose 4B was used to pull-down GST-Lsm-

FDF. Western analysis was performed by a standard method using monoclonal anti-His

antibody (1:2000, Novagen 70796) and polyclonal anti-GST antibody (1:2000,

Pharmacia 27-4577-01).

For Western analysis of GFP- and HA-tagged Dcp2, total yeast extract was

prepared as described previously (Keogh et al., 2006). GFP- and HA-tagged versions of

Dcp2 proteins were detected using monoclonal anti-GFP antibody (1:1000, Covance

MMS-118P) and monoclonal anti-HA 12CA5 antibody (1:2500, Roche 1666606)

respectively. For a loading control, the endogenous Pgk1 proteins were detected using

monoclonal anti-Pgk1 antibody (1:2000, Molecular Probes A-6457).

Northern blot analysis

Total RNA was extracted by a hot phenol method. Northern blot analysis was conducted

as previously described (Caponigro et al., 1993). The amount of *MFA2pG*, *CYH2*, *YRA1*

and *RPS28B* mRNA was quantified by oRP140, oRP1300, oRP1456 and oRP1439

respectively using the Typhoon phosphoimager (Molecular Dynamics). As a loading control, the signal recognition particle 7S RNA (*SCR1*), a stable RNA polymerase III transcript, was detected by oRP100.

In vitro decapping assays

Decapping reactions were carried out at 4°C under single-turnover conditions where enzyme is in at least 10-fold excess of substrate. The 343-nt ^{32}P cap-radiolabeled *MFA2* RNA substrate was prepared as described (LaGrandeur and Parker, 1998). Reaction buffer consisted of 50 mM Tris-Cl, 50 mM NH$_4$Cl, 1 mM DTT, 0.1 mg/ml RNase-free BSA, and 0.01% NP-40 (pH 8.3) containing roughly 0.05–5 nM substrate. Assays were performed using 50 nM Dcp1:Dcp2 (1-245) and Dcp1:Dcp2 (1-315) in complex with 500 nM His-Edc3 (**Figure S2**). Decapping complexes in the presence or absence of Edc3 were incubated at 4°C for 30 minutes prior to initiation of the reactions. Time courses were monitored and analyzed as described (Jones et al., 2008). Dcp1/Dcp2(1–245) and Dcp1/Dcp2(1-315) were co-expressed in *E. coli* and purified as described (Deshmukh et al., 2008). The constructs contain an N-terminal GB1-tag on Dcp1 and an N-terminal His-tag on Dcp2.

RESULTS

Residues 248 to 300 of Dcp2 mediate its accumulation in P-bodies

To identify the important functional domains of Dcp2, we first examined the ability of

Dcp2 proteins harboring a series of deletions in the N-terminus and/or C-terminus to

assemble into P-bodies (PBs). Although yeast Dcp2 consists of 970 residues, it has been

shown that residues 1 to 300 are sufficient for decapping *in vivo* (Dunckley and Parker,

1999). Moreover, the N-terminal globular domain and the Nudix domain at residues 1 to

245 is known to be sufficient for decapping activity *in vitro* (Fig. 1A) (Deshmukh et al.,

2008). The truncated Dcp2 proteins were expressed from its own promoter with a C-

terminal GFP tag on low copy centromeric plasmids in wild-type cells, in which an intact

genomic copy of *DCP2* is present. We then observed the location of Dcp2 during

glucose starvation, which is known to induce PB formation in yeast (Teixeira et al.,

2005).

We observed that amino acids 1-300 of Dcp2 were sufficient for recruitment into

P-bodies, which were similar to foci formed by full-length Dcp2 (**Fig. 1B**). By contrast,

the region 1-247 of Dcp2 was significantly impaired in accumulation in foci (**Fig. 1B**),

suggesting that the residues 247-300 of Dcp2 are important for its targeting and/or

maintenance of Dcp2 in P-bodies. Surprisingly, the region 243-970 of Dcp2, which lacks

almost the entire domain sufficient for decapping *in vitro*, could accumulate in foci,

whereas the region 327-970 was unable to do so (**Fig. 1B**). We were not able to test if

the region 248-300 of Dcp2 is sufficient for its PB accumulation, because the region 248-

300 of Dcp2 fused to GFP was not stably expressed in yeast cells (data not shown).

Taken together, these observations support the idea that the region 248-300 of Dcp2

contains an element that mediates its accumulation in P-bodies.

The absence of a given Dcp2 fusion protein in P-bodies could be either due to a

reduction in its cellular concentration, or due to a loss of specific protein-protein or

protein-RNA interactions. To distinguish these possibilities, we examined the fusion

proteins by western analysis (**Fig. 1C**). We did observe that the level of Dcp2 (1-247)-

GFP was somewhat reduced as compared to that of Dcp2 (1-300)-GFP. Likewise, Dcp2

(327-970)-GFP was reduced as compared to Dcp2 (243-970)-GFP. These observations

have raised the possibility that these constructs retain the intrinsic property to efficiently

accumulate in P-bodies but fail to do so simply due to the reduction in their cellular

concentration. However, we also observed that a mutant Dcp2 construct (LAKA) that

was impaired in accumulation in P-bodies (**Fig. 7C**, see below) was expressed at a level

comparable to that of Dcp2 (1-300)-GFP (**Fig. 1C**). Moreover, both regions 102-300 and

102-247 of Dcp2 tagged with GFP were expressed well and only the GFP fusion of the

region 102-300 accumulated in intensive foci (data not shown). Taken together, we

interpret these observations to indicate that reductions of Dcp2 (1-247)-GFP in foci

formation is due, at least in part, to a loss of specific interactions that are dependent on

the 248-300 region of the protein.

The region 248-300 of Dcp2 is required for binding to Edc3 *in vitro*

One possible explanation for why residues 248-300 are required for the accumulation of

Dcp2 in P-bodies is that the region mediates interaction of Dcp2 with other P-body

components. Because accumulation of Dcp2 in P-bodies is impaired by deletion of *EDC3*

and because the region 1-300 of Dcp2 can interact with both the Lsm (amino acids 1-85)

and FDF (amino acids 86-231) domains of Edc3 *in vitro* (Decker et al., 2007), we

suspected that the lesion of residues 248-300 might affect the interaction between Dcp2

and Edc3. We tested this possibility by direct binding experiments with purified

recombinant proteins.

We observed that a purified His-tagged Dcp2 (1-247) could not be pulled-down

by GST-tagged Lsm-FDF of Edc3 (amino acids 1-231), whereas His-tagged Dcp2 (1-

300) could be efficiently pulled-down, consistent with a previous result (**Fig. 2**) (Decker

et al., 2007). Together with the cytological data, the result suggests that the residues 248-

300 of Dcp2 are critical, and may be sufficient, for the interaction between Dcp2 and the

decapping activator Edc3.

The region 248-300 of Dcp2 is required for stimulation of decapping activity by

Edc3 *in vitro*

Purified Edc3 can stimulate decapping of the Dcp1-Dcp2 (1-300) complex *in vitro* (P.

Rajyaguru, T. Nissan, R. P., submitted for publication). If the interaction of residues

248-300 of Dcp2 with Edc3 is functionally important, we would predict that Dcp2

lacking this region would no longer be stimulated by Edc3 *in vitro*. To test this

possibility, we examined the ability of recombinant Edc3 to stimulate decapping *in vitro* of both the Dcp1:Dcp2 (1-245) complex and the Dcp1:Dcp2 (1-315) complex. In a single-turnover assay (see Materials and Methods), we observed that Edc3 was unable to stimulate the activity of Dcp1:Dcp2 (1-245), but did stimulate the activity of the Dcp1:Dcp2 (1-315) (**Fig. 3**). We observed at least a five-fold stimulation of activity upon addition of excess Edc3. These results are consistent with the idea that binding of Edc3 to Dcp2 through the residues 248-300 of Dcp2 is required for Edc3 to stimulate the activity of Dcp2.

The region 248-300 of Dcp2 promotes the function of Dcp2 *in vivo*

To determine the significance of the region 248-300 of Dcp2 *in vivo*, we first analyzed the growth phenotype in the presence and absence of the residues 248-300 of Dcp2. It has been reported that deletion of *DCP2* results in lethality in a certain yeast strain background (Giaever et al., 2002) and causes a growth defect in other strain backgrounds (Dunckley and Parker, 1999; Deshmukh et al., 2008). We expressed either full-length or C-terminally truncated Dcp2 proteins (1-300, 1-247 and 1-227) in a viable *dcp2Δ* strain and assessed relative growth rates by serial dilution spotting (**Fig. 4A**). As expected, Dcp2 (1-227), which lacks a portion of the highly conserved region and is completely defective for decapping *in vivo* (see below), was unable to complement the growth defect in *dcp2Δ*. Consistent with the previous result (Dunckley and Parker, 1999), Dcp2 (1-300) could complement the growth defect in *dcp2Δ* as efficiently as the full-length Dcp2 protein. Importantly, the growth of *dcp2Δ* cells expressing Dcp2 (1-247) was slightly but consistently slower than that of *dcp2Δ* cells expressing full-length Dcp2 or Dcp2 (1-300)

(**Fig. 4A**). We also observed the same trends with strains, in which C-terminal regions of the chromosomal *DCP2* gene were deleted with or without C-terminal 3x HA tags (**Fig. S1**). The observed phenotype was unlikely to be due to a reduction in Dcp2 protein levels, since the level of the Dcp2 (1-247)-3HA protein was similar to that of the Dcp2 (1-300)-3HA protein (**Fig. S1**). These results suggest that the region 248-300 of Dcp2 enhances the function of Dcp2 *in vivo*.

We then analyzed the mRNA decay phenotype in the presence and absence of the residues 248-300 of Dcp2. For this purpose, we first used the *MFA2pG* reporter mRNA, which is an unstable transcript containing a highly structured poly(G) sequence that blocks 5' to 3' degradation (Decker et al., 2007). To determine the impact of the residues 248-300 of Dcp2 on decapping *in vivo*, we expressed the region 1-300, 1-247 and 1-227 of Dcp2 in *dcp2Δ* and examined the steady-state levels of the poly(G) fragment (pG), which is a 5' to 3' degradation intermediate of the *MFA2pG* mRNA and indicative of efficient decapping (Hatfield et al., 1996; Cao and Parker, 2003). We observed substantial accumulation of the pG fragment in the cells carrying the region 1-300 or 1-247 of Dcp2 but not in the cells carrying the region 1-227 of Dcp2 or an empty vector (**Fig. 4B**). Quantification of the signals revealed that deletion of the residues 301-970 resulted in a decreased amount of the pG fragment (i.e., increased ratio of the full-length mRNA to the fragment) and that additional deletion of the residues 248-970 lead to a further decrease in the amount of the pG fragment. We also observed the same trends in strains containing chromosomal truncations of *DCP2* either with or without 3x HA tags (**Fig. S1**). On the other hand, deletion of *EDC3* did not affect the accumulation of the pG

fragment, consistent with a previous observation that the half-life of the *MFA2pG* mRNA in *edc3Δ* is comparable to that in wild-type cells (**Fig. 4C**) (Kshirsagar and Parker, 2004). These results suggest that both the region 248-300 and 301-970 additively subtly promote decapping *in vivo*. Moreover, because deletion of *EDC3* does not affect the degradation of the *MFA2pG* mRNA, but deletion of the 248-300 region does to some extent, it suggests that the 248-300 region of Dcp2 has additional functions in addition to binding to Edc3.

Deletion of the region 248-300 of Dcp2 shows a synthetic decapping defect with weak hypomorphic mutations in Dcp1

Although Edc3 is dispensable for maintenance of appropriate steady-state levels of most transcripts in wild-type strains, it becomes essential for fully efficient decapping of two reporter mRNAs, *MFA2pG* and *PGK1pG* under conditions where function of the decapping complex is compromised by either the *dcp1-2* (R29A D31A) or *dcp2-7* (N60D I68V D142V) mutation (Kshirsagar and Parker, 2004). If the residues 248-300 of Dcp2 indeed mediate the functional interaction of Dcp2 and Edc3 *in vivo*, lesion of those residues would be predicted to cause the same phenotype as deletion of *EDC3* does. To test this possibility, we examined the decapping of the *MFA2pG* reporter transcript in the following strains; *DCP1 dcp2(Δ301-970)*, *DCP1 dcp2(Δ248-970)*, *dcp1-2 dcp2 (Δ301-970)* and *dcp1-2 dcp2 (Δ248-970)*. We performed the analysis at a low temperature, where the temperature sensitive *dcp1-2* allele by itself does not cause noticeable defect in turnover of the *MFA2pG* mRNA. We observed that in the presence of the residues 248-300 of Dcp2, the *dcp1-2* mutation had at best a marginal effect on *MFA2pG* mRNA (**Fig.**

4D). By contrast, in the absence of the residues 248-300, the decapping defect was significantly exacerbated by the *dcp1-2* mutation as assessed by the ratio of the full length mRNA to the decay fragment of the *MFA2pG* transcript (**Fig. 4D**). These observations are consistent with the idea that the residues 248-300 of Dcp2 at least in part mediate the function of Edc3 *in vivo*.

Dcp2-Edc3 interaction is required for control of the *RPS28B* mRNA decay, but not for the decay of the *YRA1* pre-mRNA

The Edc3 protein has been specifically shown to be required for the autoregulation of the *RPS28B* mRNA and the *YRA1* pre-mRNA (Badis et al., 2004; Dong et al., 2007). In principle, those mRNA-specific roles of Edc3 could be due to its direct interaction with Dcp2, or could be due to other functions of Edc3. To determine how Edc3 modulates the *RPS28B* mRNA and the *YRA1* pre-mRNA, we examined the control of these mRNAs in strains lacking the 248-300 region of Dcp2. If the effect of Edc3 on *RPS28B* mRNA or *YRA1* pre-mRNA is modulated by its direct interaction with Dcp2, then we would expect increased levels of these mRNAs in the *dcp2Δ* strain expressing the region 1-247 of Dcp2 similar to those in a *edc3Δ* strain. In contrast, if Edc3 regulates the decay of these mRNAs independent of its direct interaction with Dcp2, then the levels of the mRNAs would be unchanged in the Dcp2 (1-247) strain.

We observed a 1.6-fold up-regulation of the *RPS28B* mRNA in the *dcp2Δ* strain expressing Dcp2 (1-247), whereas the mRNA level in *dcp2Δ* expressing Dcp2 (1-300) was comparable to that in *dcp2Δ* expressing full-length Dcp2 (**Fig. 5A**). We interpret this

observation to indicate that the regulation of *RPS28B* mRNA by Edc3 requires its interaction with Dcp2, although the effect of removing the residues 248-300 of Dcp2 was somewhat smaller as compared to the effect observed in the *edc3Δ* strain (**Fig. 5B**) (Badis et al., 2004; Ling et al., 2008).

An interesting result was that the *YRA1* pre-mRNA was not significantly up-regulated by lesion of the residues 248-300 of Dcp2 (**Fig. 5C**), although its levels were increased significantly by deletion of *EDC3* (**Fig. 5C**) (Dong et al., 2007). We interpret this observation to argue that the modulation of *YRA1* pre-mRNA by Edc3 is independent of its direct interaction with Dcp2.

The region 248-300 of Dcp2 is dispensable for nonsense-mediated decay

The nonsense-mediated decay pathway (NMD) targets mRNAs with premature termination codons (PTCs) for rapid decay. In yeast, the decay process of NMD is initiated by decapping (Muhlrad and Parker, 1994). To determine if the region 248-300 of Dcp2 is required for this decay pathway, we analyzed the steady-state levels of a known NMD substrate, the *CYH2* pre-mRNA, which is inefficiently spliced and contains a PTC (He et al., 1993). The level of the *CYH2* pre-mRNA in the *dcp2Δ* strains expressing the region 1-247 of Dcp2 was comparable to those in the strains expressing either full-length or region 1-300 of Dcp2 (**Fig. 6A**). Moreover, even in the *dcp1-2* background, *dcp2 (Δ248-970)* and *dcp2 (Δ301-970)* showed comparable levels of the *CYH2* pre-mRNA (**Fig. 6B**). These results suggest that the region 248-300 is dispensable for NMD, which is consistent with the idea that the region 248-300 of Dcp2 is a binding

platform for Edc3, given that Edc3 is dispensable for NMD as assessed by degradation of the *CYH2* pre-mRNA (Kshirsagar and Parker, 2004).

Structural features and conservation of the region 248-300

Although the yeast Dcp2 consists of 970 residues, the region outside the N-terminal globular domain and the Nudix domain (residues 1-245 of *S. cerevisiae* Dcp2) is not highly conserved among eukaryotes (Wang et al., 2002; van Dijk et al., 2003). To try to identify important functional residues in this region, we performed a BLAST search of *DCP2* across several fungal species (*Saccharomyces cerevisiae*, *Candida glabrata*, *Ashbya gossypii*, *Kluveromyces waltii*, *Debaryomyces hansenii*, *Pichia stipitis*, and *Candida albicans*). This analysis revealed that the conservation extends to the 280th residue of *S. cerevisiae* Dcp2 and abruptly disappears in the region C-terminal to the 280th residue (**Fig. 7A**). Interestingly, the conservation in this region appeared to be concentrated in two blocks, one from 245-261 and a second conserved region between 264-278. Consistent with the two possible significant regions of conservation, the putative homolog from another fungal organism *Lodderomyces elongisporus* contains a spacer sequence that splits the homologous sequence into two parts at the 266th and 267th residues of *S. cerevisiae* (data not shown). Moreover, a secondary structure prediction identified two putative helical structures at residues 249-259 and 270-278 (Cole et al., 2008) (data not shown).

To assess the significance of this conservation at the primary sequence level, we examined the effects of mutations at the conserved residues on accumulation of Dcp2 in

P-bodies during glucose deprivation. We observed that amino acid substitutions at highly conserved residues (single mutations E252A, D268A, double mutations L255A K256A, E252A D268A, R271A L273A, and a quadruple mutation L255A K256A R271A L273A) reduced accumulation of Dcp2 in P-bodies to various extents (**Fig. 7B**). The expression level of the protein carrying the L255A K256A mutation, which appeared to have the greatest effect on PB accumulation, was comparable to that of the wild-type protein, suggesting that the reduction in PB accumulation was unlikely to be due to a decreased protein level (**Fig. 1C**). These results identify specific amino acids in this peptide region that modulate the function of this protein-protein interaction domain.

We then tested if the mutation affects the binding of Edc3 to Dcp2 *in vitro*. A purified His-tagged Dcp2 (1-300) harboring the L255A K256A mutation could not be pulled-down by GST-tagged Lsm-FDF of Edc3 (**Fig. 7C**). This demonstrates that these residues are directly required for Edc3-Dcp2 interaction.

If the L255A and K256A mutations are also important for the interaction between Dcp2 and Edc3 *in vivo*, we would predict that these mutations would compromise the regulation of the *RPS28B* mRNA similarly to the deletion of the residues 248-300 of Dcp2 or loss of Edc3. To examine this possibility, we analyzed the *RPS28B* mRNA levels in *dcp2Δ* strain expressing Dcp2 (1-300)-GFP with or without the L255A K256A mutation and observed that the *RPS28B* mRNA was up-regulated by 2.2 -fold by the mutation (**Fig. 7D**). This is consistent with this region being required for the functional interaction of Edc3 with Dcp2. Interestingly, we observed that the *MFA2pG* mRNA was

150

not noticeably affected by the L255A K256A mutation (**Fig. 7D**), although it is affected by deletion of the region 248-300 of Dcp2 (**Fig. 4 and S1**). This latter result provides additional evidence that the region 248-300 of Dcp2 affects some other aspect of Dcp2 function in addition to binding Edc3 (see discussion).

DISCUSSION

Several observations indicate that residues 248-300 of Dcp2 are required for functional interaction between Dcp2 and the decapping activator Edc3 both *in vitro* and *in vivo*. First, the region is required for binding to Edc3 *in vitro* (**Fig. 2**). Second, the region is required for stimulation of decapping by Edc3 *in vitro* (**Fig. 3**). Third, the region is required for efficient accumulation of Dcp2 in P-bodies (**Fig. 1**). Fourth, deletion of these residues shows a synthetic decapping defect with the *dcp1-2* mutation, as does deletion of *EDC3* (**Fig. 4**). Fifth, deletion of the residues causes up-regulation of *RPS28B* mRNA, as does deletion of *EDC3* (**Fig. 5**). Sixth, amino acids substitutions at residues within this region impair binding between Dcp2 and Edc3 *in vitro* and cause up-regulation of *RPS28B* mRNA *in vivo* (**Fig. 7**). Taken together, these observations indicate that Edc3 interacts with this small peptide region, which allows Edc3 to activate the decapping activity of Dcp2.

An unresolved issue is exactly how binding of Edc3 to this region activates the activity of Dcp2. The 248-300 region of Dcp2 is located C-terminal to the catalytic domain of Dcp2 and is not required for decapping activity (**Fig. 3**) (Deshmukh et al., 2008). In the crystal structure of the Dcp1:Dcp2 complex from *S. pombe*, the corresponding region (residues 246-266) forms an alpha helix that extends along the backside of Dcp2 (She et al., 2008) and connects the N- and C-terminal domains of Dcp2. This structure raises several possibilities for how Edc3 binding at this site could affect activity. First, the region 248-300 of Dcp2 might negatively regulate the catalytic

activity normally, and binding of Edc3 might liberate Dcp2 from the inhibitory effect, although this possibility is inconsistent with the notion that the closed form of the Dcp1-Dcp2 complex is the more catalytically active form (Deshmukh et al., 2008; She et al., 2008). Moreover, this model is unlikely since it predicts that Dcp2 (1-245) should be more active than Dcp2 (1-315), which is not observed in comparable preparations of Dcp2 where the rates of decapping are similar (**Fig. 3B**). An alternative mechanism could be that the Edc3 provides additional surfaces for RNA to bind to, thereby increasing the interaction of Dcp2 with the substrate. However, this appears unlikely since the Lsm domain of Edc3 is sufficient to activate Dcp2 and yet does not appear by itself to have RNA binding activity (Ling et al., 2008) (P. Rajyaguru, T. Nissan and R. P., submitted for publication). Future mechanistic studies will be required to determine the details of this interaction and activation of decapping activity.

Several observations suggest that the region 248-300 of Dcp2 might interact with other regulators of decapping. First, deletion of the residues 248-300 of Dcp2 did not completely phenocopy the deletion of *EDC3*. Specifically, deletion of the region causes a subtle but consistent growth defect, whereas deletion of *EDC3* does not result in a noticeable growth defect (**Fig. 4A**) (Kshirsagar and Parker, 2004). Second, the decapping defect of the *MFA2pG* mRNA caused by lesion of the region of Dcp2 is greater than that caused by deletion of *EDC3* (**Fig. 4B, C and D**). In this regard, it would be interesting to test if the residues 248-300 of Dcp2 also mediate binding to other decapping regulators. Specifically, another Lsm protein Scd6 would be a potent candidate, because a recent

study in yeast identifies Scd6 as a factor functioning redundantly with Edc3 in decapping (Decourty et al., 2008).

Our results also suggest that Edc3 functions in two different mechanisms to modulate the decay of specific mRNAs. Specifically, because the deletion of residues 248-300 in Dcp2 phenocopies an *edc3Δ* for the auto-regulation of *RPS28B*, the interaction of Dcp2 and Edc3 appears to be required for Edc3 to promote the degradation of the *RPS28B* mRNA (**Fig. 5A and B**). This is consistent with the earlier proposed model whereby binding of the Rps28B protein to the 3' UTR of *RPS28B* mRNA would recruit Edc3 and the decapping enzyme to promote its degradation (Badis et al., 2004). In contrast, the interaction of Edc3 and Dcp2 does not appear to be required for the auto-regulation of the *YRA1* pre-mRNA (**Fig. 5C**). This may suggest that specific features of this mRNA allow Dcp2 to act on it independent of its direct interaction with Edc3.

It is rather surprising that the Edc3-binding platform is located outside the conserved domain (residues 1-245) of Dcp2, given that both Dcp2 and Edc3 are evolutionarily conserved among eukaryotes. An important question is whether this type of sequence also exists in the Dcp2 proteins from other organisms. The Dcp2 homologs from various organisms including human commonly contain divergent C-terminal extensions that are of very different length (Wang et al., 2002; van Dijk et al., 2003). Although the conservation at the primary sequence level in the C-terminal regions appears to be restricted to certain fungal species, the use of regions outside the catalytic domain as docking platforms for its regulators could be a universal feature of decapping

enzymes. Alternatively, it is possible that other organisms have evolved a different strategy to maintain the integrity of the decapping complex. The existence of organism-specific decapping regulators might support this idea. For example, homologs of yeast Edc1 and Edc2, whose functional significance as decapping regulators has been demonstrated both *in vivo* and *in vitro* (Dunckley et al., 2001; Schwartz et al., 2003), have not been recognized in higher eukaryotic genomes. On the other hand, Hedls/Ge-1/Edc4, which is essential for stable association of human Dcp1 and Dcp2, does not have obvious homolog in yeast, and yeast Dcp1 and Dcp2 can form a stable complex by themselves (Fenger-Gron et al., 2005). In any case, it is currently an open question if the C-terminal extensions of Dcp2 that exist in diverse organisms play an important role in the binding of decapping regulators.

In this work, we have identified a region of Dcp2 that mediates a functional interaction between Dcp2 and Edc3 both *in vivo* and *in vitro*. Although our results have extended the understanding of how Edc3 activates Dcp2, numerous questions still remain for the future study. As describe above, it would be interesting to determine if other decapping regulators also bind to Dcp2 through this domain and, if so, to examine if these interactions can occur simultaneously or exclusively. To obtain deeper insights into functions of the decapping complex, it would be also important to determine the structure of this short peptide sequence in complex with Edc3 and possibly with other decapping regulators. Our results also support the notion that the decapping complex could function in multiple distinct manners depending on each mRNP context. Therefore, it would be important to determine the specific modes of interactions among the decapping factors in

each mRNP context and, eventually, in a specific local cellular context including

macromolecular structures such as P-bodies.

ACKNOWLEDGMENTS

REFERENCES

Badis, G., Saveanu, C., Fromont-Racine, M., Jacquier, A., 2004. Targeted mRNA degradation by deadenylation-independent decapping. Mol Cell. 15**,** 5-15.

Buchan, J. R., Muhlrad, D., Parker, R., 2008. P bodies promote stress granule assembly in Saccharomyces cerevisiae. J Cell Biol. 183**,** 441-55.

Cao, D., Parker, R., 2003. Computational modeling and experimental analysis of nonsense-mediated decay in yeast. Cell. 113**,** 533-45.

Caponigro, G., Muhlrad, D., Parker, R., 1993. A small segment of the MAT alpha 1 transcript promotes mRNA decay in Saccharomyces cerevisiae: a stimulatory role for rare codons. Mol Cell Biol. 13**,** 5141-8.

Cole, C., Barber, J. D., Barton, G. J., 2008. The Jpred 3 secondary structure prediction server. Nucleic Acids Res. 36**,** W197-201.

Coller, J., Parker, R., 2005. General translational repression by activators of mRNA decapping. Cell. 122**,** 875-86.

Decker, C. J., Parker, R., 2006. CAR-1 and trailer hitch: driving mRNP granule function at the ER? J Cell Biol. 173**,** 159-63.

Decker, C. J., Teixeira, D., Parker, R., 2007. Edc3p and a glutamine/asparagine-rich domain of Lsm4p function in processing body assembly in Saccharomyces cerevisiae. J Cell Biol. 179**,** 437-49.

Decourty, L., Saveanu, C., Zemam, K., Hantraye, F., Frachon, E., Rousselle, J. C., Fromont-Racine, M., Jacquier, A., 2008. Linking functionally related genes by sensitive and quantitative characterization of genetic interaction profiles. Proc Natl Acad Sci U S A. 105**,** 5821-6.

Deshmukh, M. V., Jones, B. N., Quang-Dang, D. U., Flinders, J., Floor, S. N., Kim, C., Jemielity, J., Kalek, M., Darzynkiewicz, E., Gross, J. D., 2008. mRNA decapping is promoted by an RNA-binding channel in Dcp2. Mol Cell. 29**,** 324-36.

Dong, S., Li, C., Zenklusen, D., Singer, R. H., Jacobson, A., He, F., 2007. YRA1 autoregulation requires nuclear export and cytoplasmic Edc3p-mediated degradation of its pre-mRNA. Mol Cell. 25**,** 559-73.

Dunckley, T., Parker, R., 1999. The DCP2 protein is required for mRNA decapping in Saccharomyces cerevisiae and contains a functional MutT motif. Embo J. 18**,** 5411-22.

Dunckley, T., Tucker, M., Parker, R., 2001. Two related proteins, Edc1p and Edc2p, stimulate mRNA decapping in Saccharomyces cerevisiae. Genetics. 157**,** 27-37.

Eulalio, A., Rehwinkel, J., Stricker, M., Huntzinger, E., Yang, S. F., Doerks, T., Dorner, S., Bork, P., Boutros, M., Izaurralde, E., 2007. Target-specific requirements for enhancers of decapping in miRNA-mediated gene silencing. Genes Dev. 21**,** 2558-70.

Fenger-Gron, M., Fillman, C., Norrild, B., Lykke-Andersen, J., 2005. Multiple processing body factors and the ARE binding protein TTP activate mRNA decapping. Mol Cell. 20**,** 905-15.

Franks, T. M., Lykke-Andersen, J., 2008. The control of mRNA decapping and P-body formation. Mol Cell. 32**,** 605-15.

Giaever, G., et al., 2002. Functional profiling of the Saccharomyces cerevisiae genome. Nature. 418**,** 387-91.

Hatfield, L., Beelman, C. A., Stevens, A., Parker, R., 1996. Mutations in trans-acting factors affecting mRNA decapping in Saccharomyces cerevisiae. Mol Cell Biol. 16**,** 5830-8.

He, F., Peltz, S. W., Donahue, J. L., Rosbash, M., Jacobson, A., 1993. Stabilization and ribosome association of unspliced pre-mRNAs in a yeast upf1- mutant. Proc Natl Acad Sci U S A. 90**,** 7034-8.

Heaton, B., Decker, C., Muhlrad, D., Donahue, J., Jacobson, A., Parker, R., 1992. Analysis of chimeric mRNAs derived from the STE3 mRNA identifies multiple regions within yeast mRNAs that modulate mRNA decay. Nucleic Acids Res. 20**,** 5365-73.

Jones, B. N., Quang-Dang, D. U., Oku, Y., Gross, J. D., 2008. A kinetic assay to monitor RNA decapping under single- turnover conditions. Methods Enzymol. 448**,** 23-40.

Keogh, M. C., et al., 2006. A phosphatase complex that dephosphorylates gammaH2AX regulates DNA damage checkpoint recovery. Nature. 439**,** 497-501.

Kshirsagar, M., Parker, R., 2004. Identification of Edc3p as an enhancer of mRNA decapping in Saccharomyces cerevisiae. Genetics. 166**,** 729-39.

LaGrandeur, T. E., Parker, R., 1998. Isolation and characterization of Dcp1p, the yeast mRNA decapping enzyme. Embo J. 17**,** 1487-96.

Ling, S. H., Decker, C. J., Walsh, M. A., She, M., Parker, R., Song, H., 2008. Crystal structure of human Edc3 and its functional implications. Mol Cell Biol. 28**,** 5965-76.

Longtine, M. S., McKenzie, A., 3rd, Demarini, D. J., Shah, N. G., Wach, A., Brachat, A., Philippsen, P., Pringle, J. R., 1998. Additional modules for versatile and economical PCR-based gene deletion and modification in Saccharomyces cerevisiae. Yeast. 14**,** 953-61.

Lykke-Andersen, J., 2002. Identification of a human decapping complex associated with hUpf proteins in nonsense-mediated decay. Mol Cell Biol. 22**,** 8114-21.

Muhlrad, D., Parker, R., 1994. Premature translational termination triggers mRNA decapping. Nature. 370, 578-81.

Parker, R., Song, H., 2004. The enzymes and control of eukaryotic mRNA turnover. Nat Struct Mol Biol. 11, 121-7.

Schwartz, D., Decker, C. J., Parker, R., 2003. The enhancer of decapping proteins, Edc1p and Edc2p, bind RNA and stimulate the activity of the decapping enzyme. Rna. 9, 239-51.

Schwartz, D. C., Parker, R., 2000. mRNA decapping in yeast requires dissociation of the cap binding protein, eukaryotic translation initiation factor 4E. Mol Cell Biol. 20, 7933-42.

She, M., Decker, C. J., Chen, N., Tumati, S., Parker, R., Song, H., 2006. Crystal structure and functional analysis of Dcp2p from Schizosaccharomyces pombe. Nat Struct Mol Biol. 13, 63-70.

She, M., Decker, C. J., Svergun, D. I., Round, A., Chen, N., Muhlrad, D., Parker, R., Song, H., 2008. Structural basis of dcp2 recognition and activation by dcp1. Mol Cell. 29, 337-49.

Sikorski, R. S., Hieter, P., 1989. A system of shuttle vectors and yeast host strains designed for efficient manipulation of DNA in Saccharomyces cerevisiae. Genetics. 122, 19-27.

Steiger, M., Carr-Schmid, A., Schwartz, D. C., Kiledjian, M., Parker, R., 2003. Analysis of recombinant yeast decapping enzyme. Rna. 9, 231-8.

Teixeira, D., Sheth, U., Valencia-Sanchez, M. A., Brengues, M., Parker, R., 2005. Processing bodies require RNA for assembly and contain nontranslating mRNAs. Rna. 11, 371-82.

Tritschler, F., Braun, J. E., Eulalio, A., Truffault, V., Izaurralde, E., Weichenrieder, O., 2009. Structural basis for the mutually exclusive anchoring of P body components EDC3 and Tral to the DEAD box protein DDX6/Me31B. Mol Cell. 33, 661-8.

van Dijk, E., Le Hir, H., Seraphin, B., 2003. DcpS can act in the 5'-3' mRNA decay pathway in addition to the 3'-5' pathway. Proc Natl Acad Sci U S A. 100, 12081-6.

Wang, Z., Jiao, X., Carr-Schmid, A., Kiledjian, M., 2002. The hDcp2 protein is a mammalian mRNA decapping enzyme. Proc Natl Acad Sci U S A. 99, 12663-8.

Wilmes, G. M., et al., 2008. A genetic interaction map of RNA-processing factors reveals links between Sem1/Dss1-containing complexes and mRNA export and splicing. Mol Cell. 32, 735-46.

FIGURE LEGENDS

Figure 1. The region 248-300 of Dcp2 mediates its accumulation in P-bodies. (A) Domain architecture of *S. cerevisiae* Dcp2. The N-terminal globular domain is shown in gray. The Nudix domain is shown in black. (B) Localization of truncated Dcp2 proteins. Wild-type cells (yRP840) carrying plasmids expressing truncated Dcp2 proteins C-terminally tagged with GFP (pRP1891, pRP1892, pRP1893, pRP1894 and pRP1895) were used. Cells were cultured to mid-log phase and shifted to media lacking glucose for 10 minutes. A single focal plane image is shown. Bar, 5 μm. (C) The protein levels of truncated Dcp2 proteins. The same strains as described in (B) were cultured to mid-log phase and shifted to media lacking glucose for 10 minutes. Anti-GFP antibody was used in Western blot to detect GFP-tagged proteins. Anti-Pgk1 antibody was used to detect the endogenous Pgk1 protein as a loading control. Arrowheads indicate GFP-tagged proteins. Asterisks indicate non-specific bands.

Figure 2. The region 248-300 of Dcp2 is required for Edc3 binding *in vitro*. (A) Coomassie blue-stained SDS-PAGE showing purified recombinant proteins used in the pull-down assay. (B) An *in vitro* pull-down assay between purified GST-tagged Lsm-FDF domain of Edc3 and His-tagged Dcp2 (amino acids 1-300) or His-Dcp2 (1-247). Glutathione Sepharose was used to pull-down either the GST-tagged Lsm-FDF of Edc3 or the GST portion alone as a control. Anti-His and anti-GST antibody were used in Western blot to detect His-Dcp2 proteins and GST-tagged proteins respectively. The amounts corresponding to the same volume in the binding reaction were loaded for all

samples: T (total), S (supernatant) and P (pellet). Note that the mobility of the GST-Lsm-

FDF was shifted presumably because of the BSA proteins present in the samples.

Asterisk indicates partial degradation products of GST-Lsm-FDF. See materials and

methods for details.

Figure 3. The region 246-315 of Dcp2 is required for decapping stimulation by Edc3 *in*

vitro. (A) Time courses of the fraction m^{7}GDP released by decapping by recombinant

purified GB1-Dcp1:His-Dcp2 (1-245) and GB1-Dcp1:His-Dcp2 (1-315) with and

without recombinant purified His-Edc3 measured under single-turnover conditions using

343-nt *MFA2* RNA substrate. (B) Bar graphs of first-order rate constants k_{obs} fitted to the

time courses depicted in (A).   Error bars represent the standard error.

Figure 4. The region 248-300 of Dcp2 promotes decapping *in vivo*. (A) Deletion of the

region 248-300 causes a subtle but consistent growth defect. Growth phenotype of

yRP1346 (*dcp2Δ*) expressing Dcp2 full-length or truncated proteins from plasmids

pRP1207, pRP1453, pRP1450 or pRP1449 was analyzed by serial dilution spotting.

pRP10 was used as a control vector. Cells were incubated on SC media containing 2%

glucose for 2 days at 30˚C. (B) The region 248-300 of Dcp2 promotes decapping *in vivo*.

Decay intermediates (pG) of the *MFA2pG* reporter mRNA were analyzed in the strain

yRP1346 (*dcp2Δ*) expressing Dcp2 full-length or truncated proteins from plasmids

pRP1207, pRP1453, pRP1450 or pRP1449. pRP10 was used as a control vector. Cells

were grown in SC media containing 2% galactose at 30˚C to express the *MFA2pG*

mRNA from the *GAL* promoter. FL and pG represent the full-length mRNA and the

poly(G) decay intermediate respectively. The ratio of the full-length mRNA to the

poly(G) decay intermediate in each strain relative to the ratio in the strain expressing full-

length Dcp2 is indicated below each lane. The average and standard deviation of values

obtained with four independent transformants is shown. The *SCR1* RNA was detected as

a loading control. (C) Deletion of *EDC3* does not affect the *MFA2pG* mRNA. Cells of

the strains yRP1745 (*edc3Δ*) expressing Edc3 from the plasmid pRP1432 were grown in

SC media containing 2% galactose to mid-log phase at 30˚C. pRP642 was used as a

control vector. The average and standard deviation of values obtained with four

independent transformants is shown. (D) Deletion of the region 248-300 of Dcp2 shows

a synthetic effect with the *dcp1-2* mutation. Cells of the strains yRP2702 (*DCP1*

dcp2(Δ301-970)), yRP2703 (*DCP1 dcp2(Δ248-970)*), yRP2704 (*dcp1-2 dcp2(Δ301-*

970)) and yRP2705 (*dcp1-2 dcp2(Δ301-970)*) were grown in YP media containing 2%

galactose to mid-log phase at 24˚C, which is permissive for the *dcp1-2* temperature

sensitive allele. The ratio of the full-length mRNA to the poly(G) decay intermediate in

each strain relative to the ratio in the *DCP1 dcp2(Δ301-970)* strain is indicated. Three

independent strains were analyzed for each genotype.

Figure 5. The region 248-300 of Dcp2 is required for efficient degradation of *RPS28B*

mRNA but not for degradation of *YRA1* pre-mRNA. (A) Analysis of the *RPS28B*

mRNA. The same RNA samples as described in the figure legend to Fig. 4B were

analyzed. The *RPS28B* level normalized to the *SCR1* RNA level in each strain relative to

the normalized mRNA level in the strain expressing full-length Dcp2 is indicated below

each lane. (B) Up-regulation of the *RPS28B* mRNA by deletion of *EDC3*. The same

RNA samples as described in the figure legend to Fig. 4C were analyzed. (C) Analysis of the *YRA1* pre-mRNA. The same RNA samples as described in the figure legend to Fig. 4B were analyzed. The *YRA1* pre-mRNA level normalized to the *SCR1* RNA level in each strain relative to the normalized pre-mRNA level in the strain expressing full-length Dcp2 is indicated below each lane.

Figure 6. The region 248-300 of Dcp2 is dispensable for NMD. To assess the relative accumulation, the *CYH2* pre-mRNA/mRNA ratio was normalized to the ratio in the *dcp2Δ* strain expression the full-length Dcp2 protein. (A) The same RNA samples as described in the figure legend to Fig. 4B were analyzed. Values represent the average and standard deviation of fold changes obtained with four independent transformants. (B) The same RNA samples as described in the figure legend to Fig. 4C were analyzed. Values represent the average of fold changes obtained with two independent strains.

Figure 7. Mutations in the region 248-300 of Dcp2 impair interaction between Dcp2 and Edc3. (A) Conservation of the sufficiency domain across the seven Dcp2 fungal homologs (*Saccharomyces cerevisiae*, *Candida glabrata*, *Ashbya gossypii*, *Kluveromyces waltii*, *Debaryomyces hansenii*, *Pichia stipitis* and *Candida albicans*). The numbers refer to residues of *S. cerevisiae* Dcp2. (B) Localization of Dcp2 (1-300) with mutations. A wild-type strain (yRP840) expressing C-terminal GFP-tagged Dcp2 (1-300) with or without the mutations (L255A K256A, R271A L273A, L255A K256A R271A L273A, E252A, D268A, E252A D268A) from the plasmid pRP1896, pRP1892, pRP1906, pRP1907, pRP1908, pRP1909 or pRP1910 was cultured as described in the figure legend

to Fig. 1B. A single focal image is shown. Bar, 5 μm. (C) Coomassie blue-stained SDS-PAGE showing purified recombinant proteins used in the pull-down assay (top). An *in vitro* pull-down assay between purified GST-tagged Lsm-FDF domain of Edc3 and His-tagged Dcp2 (amino acids 1-300) or His-Dcp2 (1-300) L255A K256A (bottom). Asterisk indicates partial degradation products of GST-Lsm-FDF. (D) The *MFA2pG* reporter mRNA and the *RPS28B* mRNA were analyzed in yRP1346 (*dcp2Δ*) expressing Dcp2 (1-300)-GFP or Dcp2 (1-300) L255A K256A-GFP from plasmids pRP1892 or pRP1896. Cells were grown in SC media containing 2% galactose at 30°C to express the *MFA2pG* mRNA from the *GAL* promoter. For *MFA2pG*, the ratio of the full-length mRNA to the poly(G) decay intermediate relative to the ratio in the strain expressing wild-type Dcp2 is indicated. For *RPS28B*, the mRNA level normalized to the *SCR1* RNA level relative to the normalized mRNA level in the strain expressing wild-type Dcp2 is indicated. The average and standard deviation of values obtained with three independent transformants is shown.

TABLE 1. Yeast strains used in this study

| Strains	Genotype	Reference
yRP840	*MATa leu2-3,112 trp1 ura3-52 his4-539 cup1::LEU2/PGK1pG/MFA2pG*	(Hatfield et al., 1996)
yRP841	*MATa leu2-3,112 trp1 ura3-52 lys2-201 cup1::LEU2/PGK1pG/MFA2pG*	(Hatfield et al., 1996)
yRP1346	*MATa leu2-3,112 trp1 ura3-52 his4-539 lys2-201 cup1::LEU2/PGK1pG/MFA2pG dcp2Δ::TRP1*	(Dunckley and Parker, 1999)
yRP1515	*MATa leu2-3,112 trp1 ura3-52 his4-539 lys2-201 cup1::LEU2/PGK1pG/MFA2pG dcp1-2::TRP1*	(Dunckley and Parker, 1999)
yRP1745	*MATa leu2-3,112 his4-539 trp1 ura3-52 edc3::NEO cup1::LEU2/PGK1pG/MFA2pG*	(Kshirsagar and Parker, 2004)
yRP2702	*MATa leu2-3,112 trp1 ura3-52 lys2-201 cup1::LEU2/PGK1pG/MFA2pG dcp2(Δ301-970)::kanMX6*	This study
yRP2703	*MATa leu2-3,112 trp1 ura3-52 lys2-201 cup1::LEU2/PGK1pG/MFA2pG dcp2(Δ248-970)::kanMX6*	This study
yRP2704	*MATa leu2-3,112 trp1 ura3-52 his4-539 lys2-201 cup1::LEU2/PGK1pG/MFA2pG dcp1-2::TRP1 dcp2(Δ301-970)::kanMX6*	This study
yRP2705	*MATa leu2-3,112 trp1 ura3-52 his4-539 lys2-201 cup1::LEU2/PGK1pG/MFA2pG dcp1-2::TRP1 dcp2(Δ248-970)::kanMX6*	This study
yRP2706	*MATa leu2-3,112 trp1 ura3-52 lys2-201 cup1::LEU2/PGK1pG/MFA2pG DCP2::kanMX6*	This study
yRP2708	*MATa leu2-3,112 trp1 ura3-52 lys2-201 cup1::LEU2/PGK1pG/MFA2pG DCP2-3HA::kanMX6*	This study
yRP2709	*MATa leu2-3,112 trp1 ura3-52 lys2-201 cup1::LEU2/PGK1pG/MFA2pG dcp2(Δ301-970)-3HA::kanMX6*	This study
yRP2710	*MATa leu2-3,112 trp1 ura3-52 lys2-201 cup1::LEU2/PGK1pG/MFA2pG*	This study

dcp2(Δ248-970)-3HA::kanMX6


TABLE 2. Plasmids used in this study

Number	Description	Sources
pRP250	pRS416, centromeric vector with the *URA3* marker	(Sikorski and Hieter, 1989)
pRP1667	pRS425 (Sikorski and Hieter, 1989) carrying a sequence encoding GFP and the *ADH1* terminator	C. J. Decker
pRP1902	pRS416 carrying a sequence encoding GFP and the *ADH1* terminator	This study
pRP1903	pRP416 carrying the *DCP2* promoter, a sequence encoding GFP and the *ADH1* terminator	This study
pRP1891	pRS416 carrying the *DCP2* promoter, a sequence encoding Dcp2-GFP and the *ADH1* terminator	This study
pRP1892	pRS416 carrying the *DCP2* promoter, a sequence encoding Dcp2(aa1-300)-GFP and the *ADH1* terminator	This study
pRP1893	pRS416 carrying the *DCP2* promoter, a sequence encoding Dcp2(aa1-247)-GFP and the *ADH1* terminator	This study
pRP1894	pRS416 carrying the *DCP2* promoter, a sequence encoding Dcp2(aa243-970)-GFP and the *ADH1* terminator	This study
pRP1895	pRS416 carrying the *DCP2* promoter, a sequence encoding Dcp2(aa327-970)-GFP and the *ADH1* terminator	This study
pRP1278	YCplac33 (Gietz and Sugino, 1988) carrying the *DCP2* promoter, a sequcne encoding Dcp2 (Δaa2-101)-GFP and the *ADH1* terminator	C. J. Decker
pRP1904	pRS416 carrying the *DCP2* promoter, a sequence encoding Dcp2(aa102-300)-GFP and the *ADH1* terminator	This study
pRP1905	pRS416 carrying the *DCP2* promoter, a sequencne encoding Dcp2(aa102-247)-GFP and the *ADH1* terminator	This study
pRP1896	pRS416 carrying the *DCP2* promoter, a sequence encoding Dcp2(aa1-300) L255A K256A-GFP and the *ADH1* terminator	This study
pRP1906	pRS416 carrying the *DCP2* promoter, a sequence encoding Dcp2(aa1-300) R271A K273A-GFP and the *ADH1* terminator	This study

| pRP1907	pRS416 carrying the *DCP2* promoter, a sequence encoding Dcp2(aa1-300) L255A K256A R271A K273A-GFP and the *ADH1* terminator	This study
pRP1908	pRS416 carrying the *DCP2* promoter, a sequence encoding Dcp2(aa1-300) E252A-GFP and the *ADH1* terminator	This study
pRP1909	pRS416 carrying the *DCP2* promoter, a sequence encoding Dcp2(aa1-300) D268A-GFP and the *ADH1* terminator	This study
pRP1910	pRS416 carrying the *DCP2* promoter, a sequence encoding Dcp2(aa1-300) E252A D268A-GFP and the *ADH1* terminator	This study
pRP784	pPROEX-1	GibcoBRL
pRP1897	pPROEX-1 carrying a sequence encoding Dcp2(aa1-300), to express N-terminal His-tagged protein in *E. coli*	This study
pRP1898	pPROEX-1 carrying a sequence encoding Dcp2(aa1-247), to express N-terminal His-tagged protein in *E. coli*	This study
pRP1899	pPROEX-1 carrying a sequence encoding Dcp2(aa1-300) L255AK256A, to express N-terminal His-tagged protein in *E. coli*	This study
pRP1900	pGEX-6P-3, to express GST in *E. coli*	GE Healthcare
pRP1444	pGEX-6P-3 carrying a sequence encoding the LsmFDF domain (aa1-231) of Edc3, to express N-terminal GST-tagged protein in *E. coli*	C. J. Decker
pRP10	centromeric vector with the *URA3* marker	(Heaton et al., 1992)
pRP1207	pRP10 carrying the *DCP2* promoter, a sequence encoding full-length Dcp2 and the *DCP2* terminator	(She et al., 2006)
pRP1453	pRP10 carrying the *DCP2* promoter, a sequence encoding Dcp2(aa1-300) and the *DCP2* terminator	This study
pRP1450	pRP10 carrying the *DCP2* promoter, a sequence encoding Dcp2(aa1-247) and the *DCP2* terminator	This study
pRP1449	pRP10 carrying the *DCP2* promoter, a sequence encoding Dcp2(aa1-227) and the *DCP2* terminator	This study
pRP642	pRS200, centromeric vector with the *TRP1* marker	lab stock
pRP1432	pRS200 carrying the *EDC3* promoter, a sequence encoding Edc3 and the *EDC3* terminator	C. J. Decker
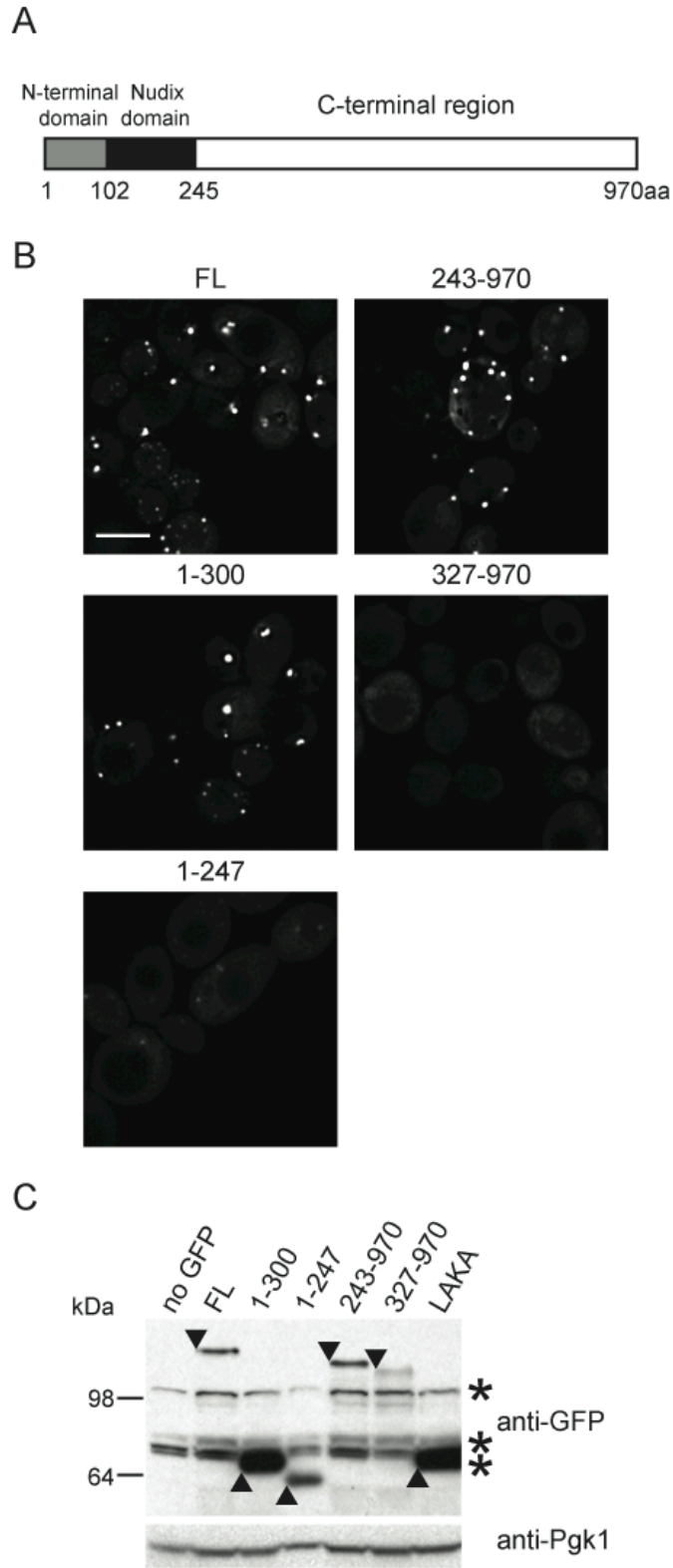
FIGURE 1: The region 248-300 of Dcp2 mediates its accumulation in PBs
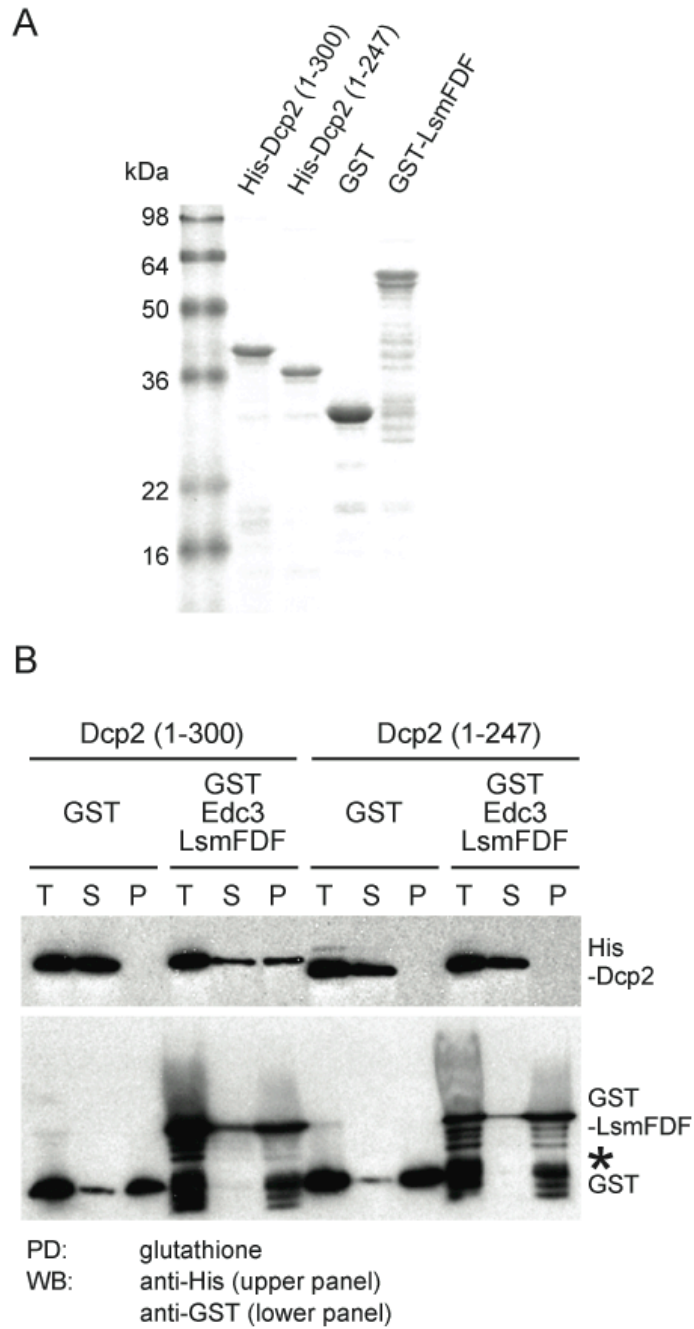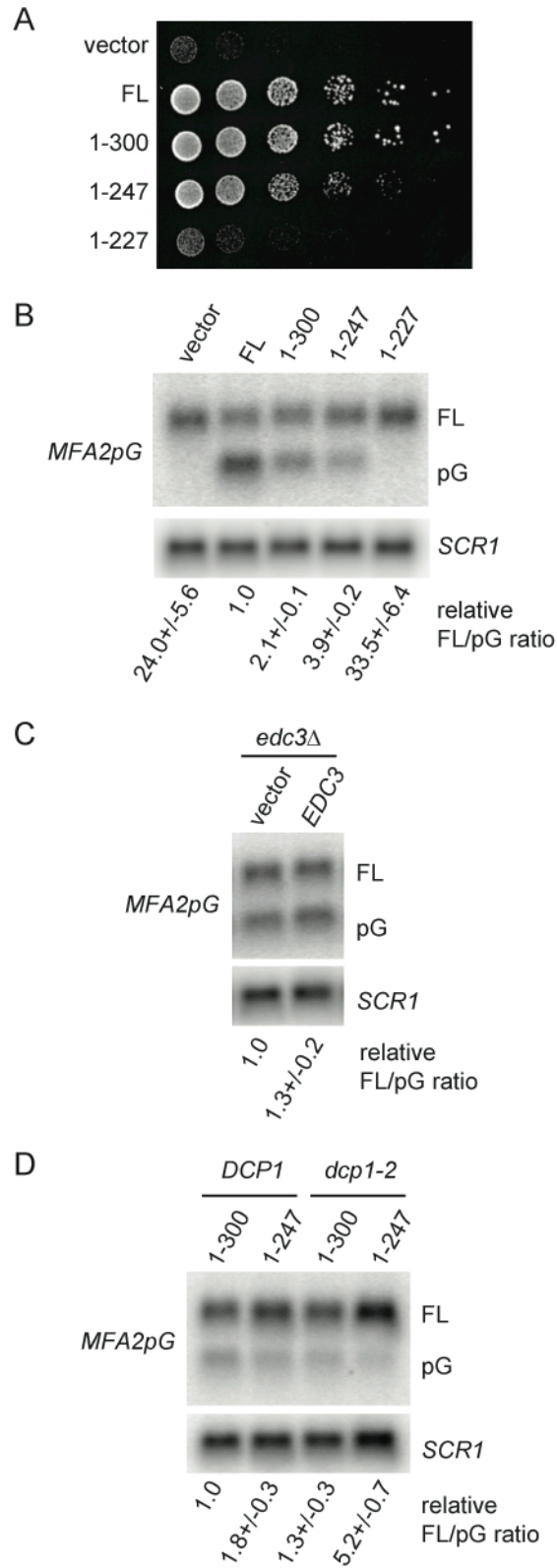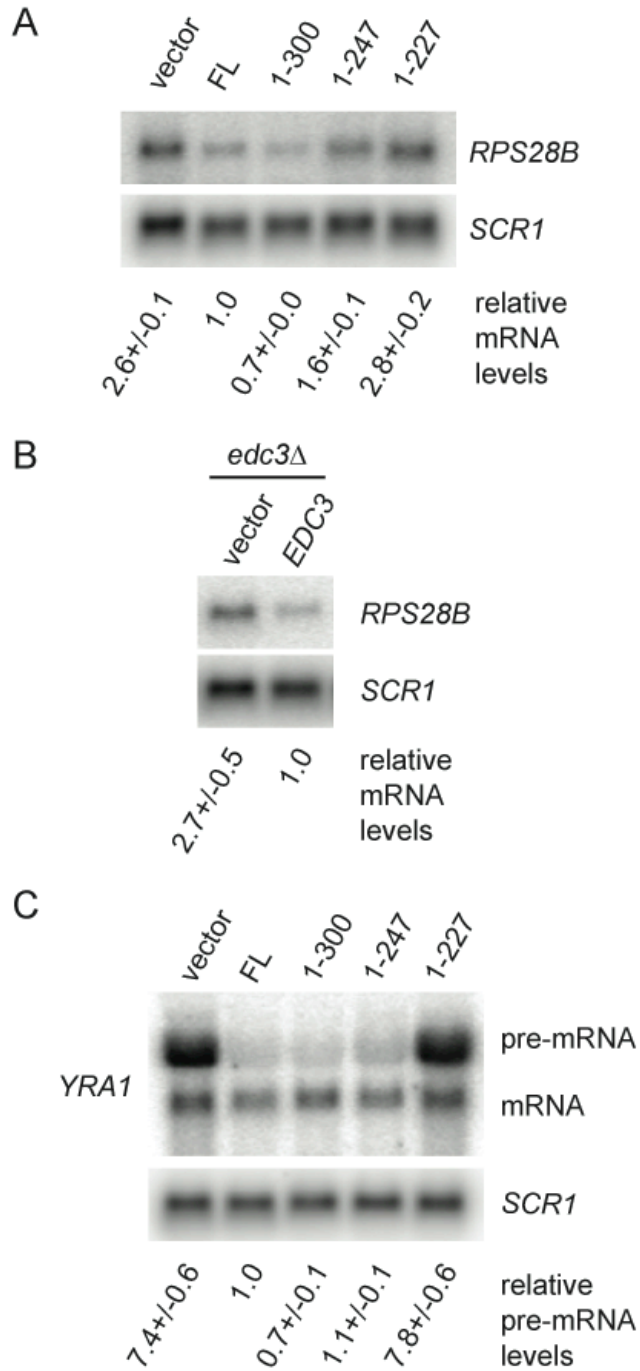
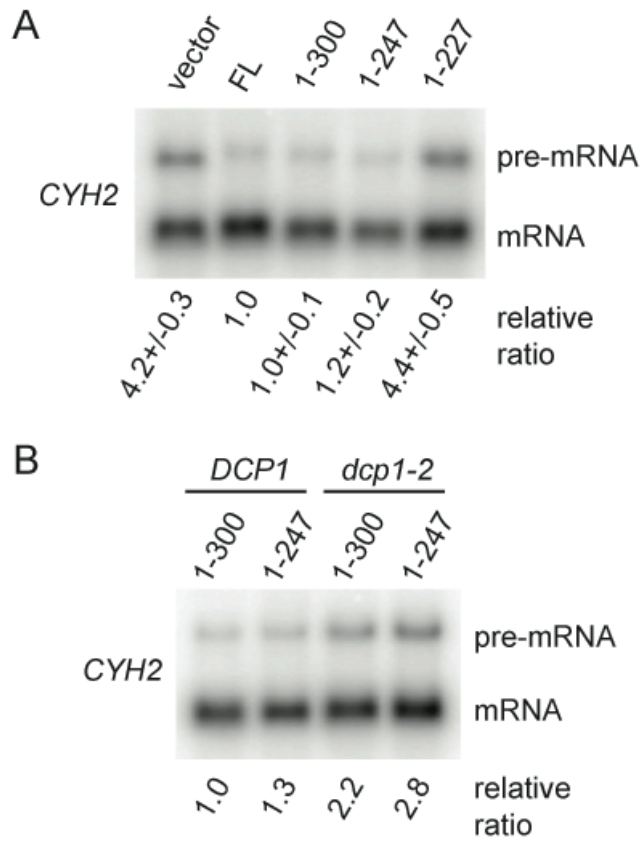**FIGURE 2**: The region 248-300 of Dcp2 is required for Edc3 binding *in vitro*

(A)

(B)
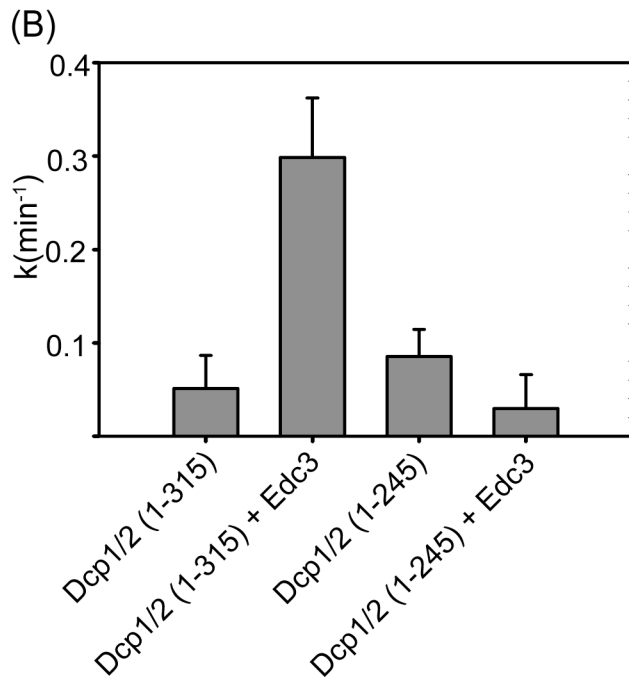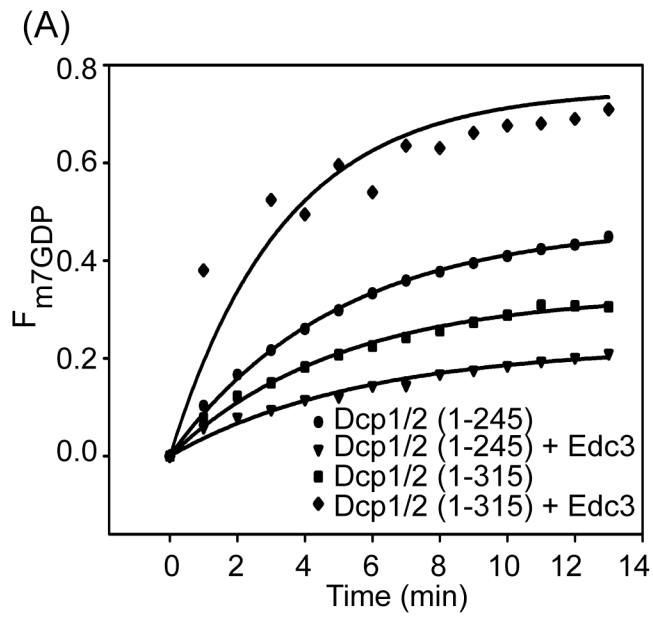
FIGURE 3: The region 245-315 of Dcp2 is required for stimulation of decapping by
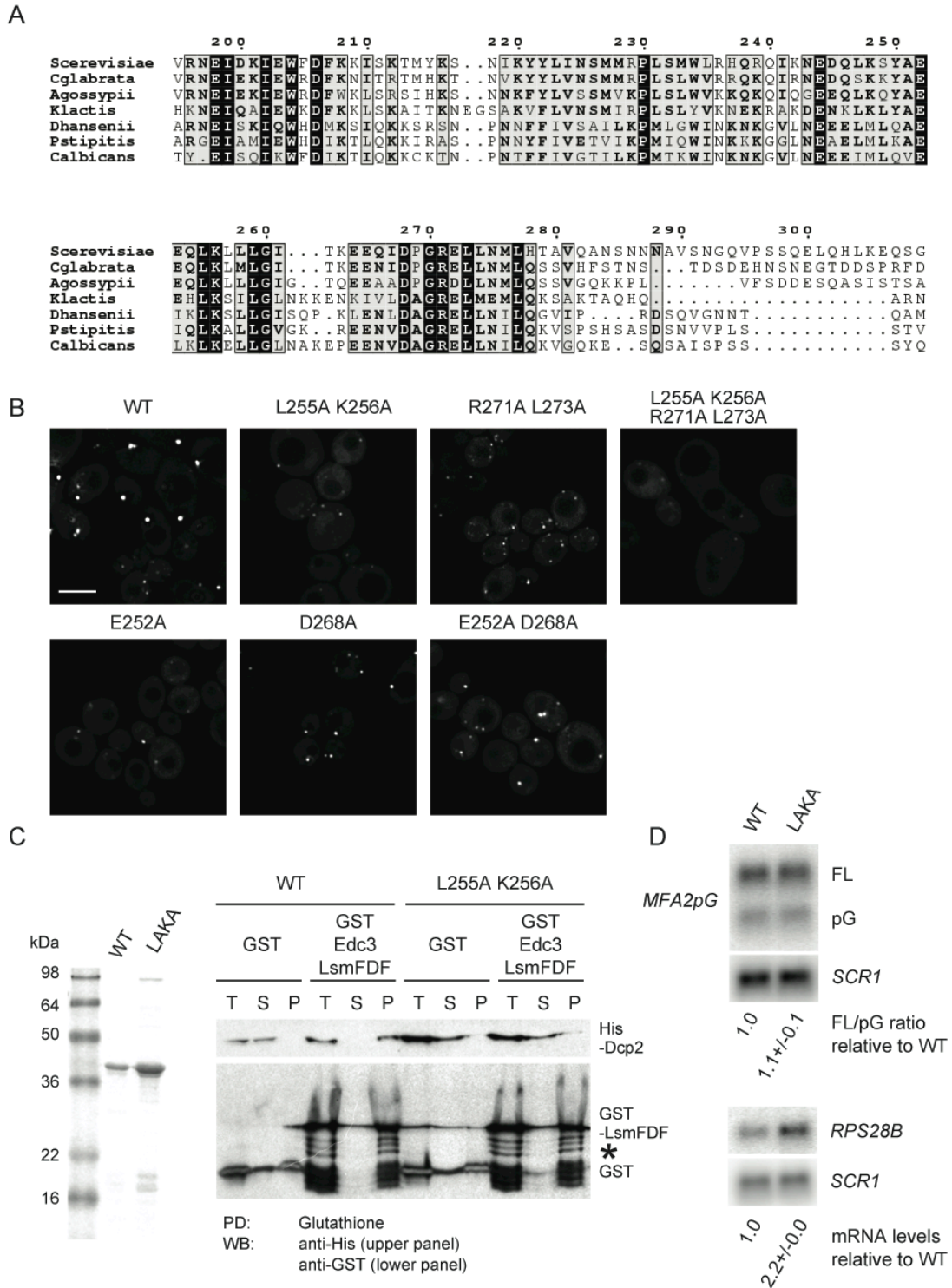
Edc3 *in vitro*

FIGURE 4: The region 248-300 of Dcp2 promote the function of Dcp2

FIGURE 5: The region 2480300 of Dcp2 is required for efficient degradation of

RPS28B mRNA but not for degradation of YRA1 pre-mRNA.

FIGURE 6: The region 248-300 of Dcp2 is dispensable for NMD

FIGURE 7: Mutations in the region 248-300 of Dcp2 impairs interaction between Dcp2 and Edc3.

SUPPLEMENTAL MATERIAL

SUPPLEMENTAL REFERENCES:

Caponigro, G., and R. Parker. 1995. Multiple functions for the poly(A)-binding protein in mRNA decapping and deadenylation in yeast. *Genes Dev*. **9**:2421-2432

Caponigro, G., D. Muhlrad, and R. Parker. 1993. A small segment of the MAT alpha 1 transcript promotes mRNA decay in *Saccharomyces cerevisiae*: a stimulatory role for rare codons. *Mol. Cell Biol*. **13**: 5141-5148

SUPPLEMENTAL FIGURE LEGENDS

Figure S1: (A) Coomassie blue-stained SDS-PAGE of recombinant purified proteins used in *in vitro* decapping assays. Representative decapping time courses for (B) 50 nM GB1-Dcp1:Dcp2 (1-245), (C) 50 nM GB1-Dcp1:Dcp2 (1-245) with 500nM Edc3, (D) 50 nM GB1-Dcp1:Dcp2 (1-315), and (E) 50 nM GB1-Dcp1:Dcp2 (1-315) with 500nM Edc3.

Figure S2: (A) Growth phenotype of strains lacking C-terminal regions of the chromosomal *DCP2* gene (yRP2706, yRP2702, yRP2703, yRP2708, yRP2709 and yRP2710) was analyzed by serial dilution spotting. Cells were incubated on YP media containing 2% glucose for 2 days at 25˚C. (B) The *MFA2pG* mRNA was analyzed in the same strains as described in (A). Cells were grown in YP media containing 2% galactose to mid-log phase at 24˚C. The ratio of the full-length mRNA (FL) to the decay intermediate (pG) relative to the ratio in yRP2706 (full-length Dcp2 without tag) was indicated below each lane. The average and standard deviation of values obtained with three independent strains of each genotype. (C) The protein levels of Dcp2 (1-300)-3HA and Dcp2 (1-247)-3HA. Cells of the strains yRP2702, yRP2703, yRP2709 and yRP2710 were grown in YP media containing 2% galactose to mid-log phase at 24˚C.   Anti-HA antibody and anti-Pgk1 antibody were used in Western blot to detect HA-tagged proteins and the endogenous Pgk1 proteins as a loading control.

TABLE S1. Oligonucleotides used in this study

| Number	Sequences	Description	Sources
oRP1440	CGGGAGCTCTCGTCGTAAGGCTGACACTGCA	To create pRP1891, pRP1892, pR1893, pRP1896, pRP1903, pRP1904, pRP1905, pRP1906, pRP1907, pRP1908, pRP1909 and pRP1910	This study
oRP1458	CAGTCGCGATGTCTAATGCGAAGGTACTTTTATTTTTTTCAGAT	To create pRP1903	This study
oRP1441	GGGGATCCGCTTCCTATGCAAAATGCTTAATAATTCATTAGACC	To create pRP1891	This study
oRP1442	GGGGATCCGCTCTTGGCTCGAGGGTACCTGT	To create pRP1892, pRP1896, pRP1904, pRP1906, pRP1907, pRP1908, pRP1909 and pRP1910	This study
oRP1443	GGGGATCCGCAATTGATCTTCATTTTTTATTTGCCTCTGATGCCT	To create pRP1893 and pRP1905	This study
oRP1459	ACATCGCGAATGAATGAAGATCAATTGAAATCCTATGCGGAA	To create pRP1894	This study
oRP1460	ACATCGCGAATGCCTTCAATATTTCCATCTCTTTCTGAACCG	To create pRP1895	This study
oRP1444	CAGTCGCGACATATGTCACTGCCGCTACGACA	To create pRP1897 and pRP1898	This study
oRP1445	CAGACGGGATCCTCATCACTCTTGGCTCGAGGGTACCTGT	To create pRP1897	This study
oRP1446	CAGACGGGATCCTCATCACAATTGATCTTCATTTTTTATTTGCCTCTGATGCCT	To create pRP1898	This study
oRP1447	AATCCTATGCGGAAGAACAAGCGGCATTGTTGTTGGGTATCACTAA	To create pRP1896	This study
oRP1448	TTAGTGATACCCAACAACAATGCCGCTTGTTCTTCCGCATAGGATT	To create pRP1896	This study
oRP1465	ATCAATTGAAATCCTATGCGGCAGAACAATTGAAATTGTTGTT	To create pRP1908	This study
oRP1466	AACAACAATTTCAATTGTTCTGCCGCATAGGATTTCAATTGAT	To create pRP1908	This study
oRP1467	TCACTAAGGAGGAGCAGATTGCTCCCGGTAGAGAGTTGCTGAA	To create pRP1909	This study
oRP1468	TTCAGCAACTCTCTACCGGGAGCAATCTGCTCCTCCTTAGTGA	To create pRP1909	This study
oRP1469	AGGAGCAGATTGATCCCGGTGCAGAGGCGCTGAATATGTTACATACTGC	To create pRP1906	This study

179

oRP1470	GCAGTATGTAACATATTCAGCGCCTCTGCACCGGGATCAATCTGCTCCT	To create pRP1906	This study
oRP1471	GGAATTCGAGCTCCAAGATCTAGTGTTATACGTTTTATAGACACACTGTAAATG	To create pRP1454	This study
oRP1472	TGATATCGAATTCCTGCAGCCCGGGGGATCCACTAGTCCGCAGATAAATTGACGCACC	To create pRP1454	This study
oRP1473	CGAATTGGAGCTCCACCGCGGTGGCGGCCGCTCTAGACGTCGTAAGGCTGACACTGCAGAAG	To create pRP1449, pRP1450 and pRP1453	This study
oRP1474	CGGGATCCAGATCTTTCACTCTTGGCTCGAGGGTACCTGTCCGTTGGA	To create pRP1453	This study
oRP1475	CGGGATCCAGATCTTTCACAATTGATCTTCATTTTTTATTTGCCTCTG	To create pRP1450	This study
oRP1476	CGGGATCCAGATCTTTCACATGGAATTAATCAGATAATACTTGATATT	To create pRP1449	This study
oRP1449	GTTAAGGCATCAGAGGCAAATAAAAAATGAAGATCAATTGTGAGGCGCGCCACTTCTAAA	To create yRP2703 and yRP2705	This study
oRP1450	TAATGCGGTCTCCAACGGACAGGTACCCTCGAGCCAAGAGTGAGGCGCGCCACTTCTAAA	To create yRP2702 and yRP2704	This study
oRP1451	CATTTACAGTGTGTCTATAAAACGTATAACACTTATTCTTGAATTCGAGCTCGTTTAAAC	To create yRP2702, yRP2703, yRP2704, yRP2705, yRP2706, yRP2708, yRP2709 and yRP2710	This study
oRP1461	TTCAGGGTCTAATGAATTATTAAGCATTTTGCATAGGAAGTGAGGCGCGCCACTTCTAAA	To create yRP2706	This study
oRP1462	GTTAAGGCATCAGAGGCAAATAAAAAATGAAGATCAATTGCGGATCCCCGGGTTAATTAA	To create yRP2710	This study
oRP1463	TTCAGGGTCTAATGAATTATTAAGCATTTTGCATAGGAAGCGGATCCCCGGGTTAATTAA	To create yRP2708	This study
oRP1464	TAATGCGGTCTCCAACGGACAGGTACCCTCGAGCCAAGAGCGGATCCCCGGGTTAATTAA	To create yRP2709	This study
oRP1452	GCCCAAGCCTCTTAATGATGG	To verify integration in the *DCP2* locus	This study
oRP1453	CGGTGATGTCAAATTGTGTTATGG	To verify integration in the *DCP2* locus	This study
oRP1454	ATGGGCTCGCGATAATGTCG	To verify integration with the kanMX casette	This study
oRP1455	GCGATTCCGACTCGTCCAAC	To verify integration with the kanMX casette	This study
oRP140	ATATTGATTAGATCAGGAATTCC	Probe for *MFA2pG* mRNA	Caponigro and Parker, 1995
oRP100	GTCTAGCCGCGAGGAAGG	Probe for *SCR1* RNA	Caponigro *et al.*, 1993

180

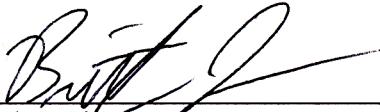| oRP1300	GCTTTCTGTGCTTACCGATACGACCTTTACCGG	Probe for *CYH2* mRNA	This study
oRP1456	TTAGCAGGCTTTTCTCTCTTTGGTT	Probe for *YRA1* mRNA	This study
oRP1439	CATCATTGAGTATTTCTACGCATTTG	Probe for *RPS28B* mRNA	This study
oRP831	ACTTAGAGCTCACTAGTGCGGCCGCGTCGTAAGGCTGACACTGC	To verify the sequence of *DCP2*	T. Dunckley
oRP842	GAGATTAATTCCGATGGGG	To verify the sequence of *DCP2*	T. Dunckley
oRP843	CATCATTAAGAGGCTTGGGC	To verify the sequence of *DCP2*	T. Dunckley
oRP844	TTGTTGTTGATGATAACCCG	To verify the sequence of *DCP2*	T. Dunckley
oRP845	CCACATTGATAAGGGTCTC	To verify the sequence of *DCP2*	T. Dunckley
oRP846	CGATAAATCTTCATTCGGAC	To verify the sequence of *DCP2*	T. Dunckley
oRP864	CCTTCTGTTGGTTGTGTTCTCC	To verify the sequence of *DCP2*	T. Dunckley
oRP865	CGGACAGGTACCCTCGAGCCAAGAGC	To verify the sequence of *DCP2*	T. Dunckley
oRP1457	CCATGATGAGACCCTTATCAATG	To verify the sequence of *DCP2*	T. Dunckley
oRP1477	GAAGGATTCCACAGTTGTTTAATCCTCC	To verify the sequence of *DCP2*	This study
oRP1478	CCTTCACCCTCTCCACTGACAG	To verify sequence uptream of the GFP gene	This study
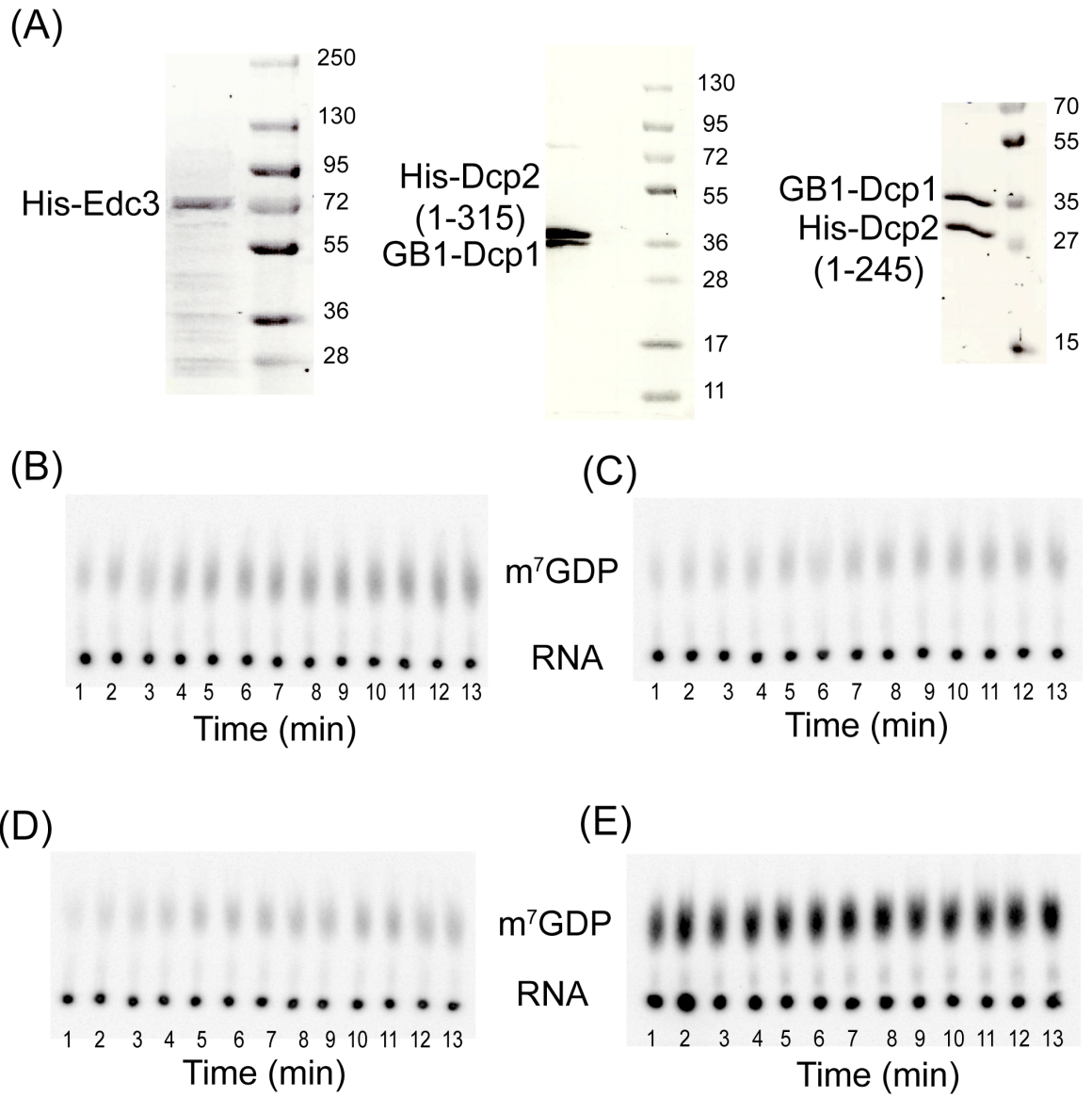
FIGURE S1
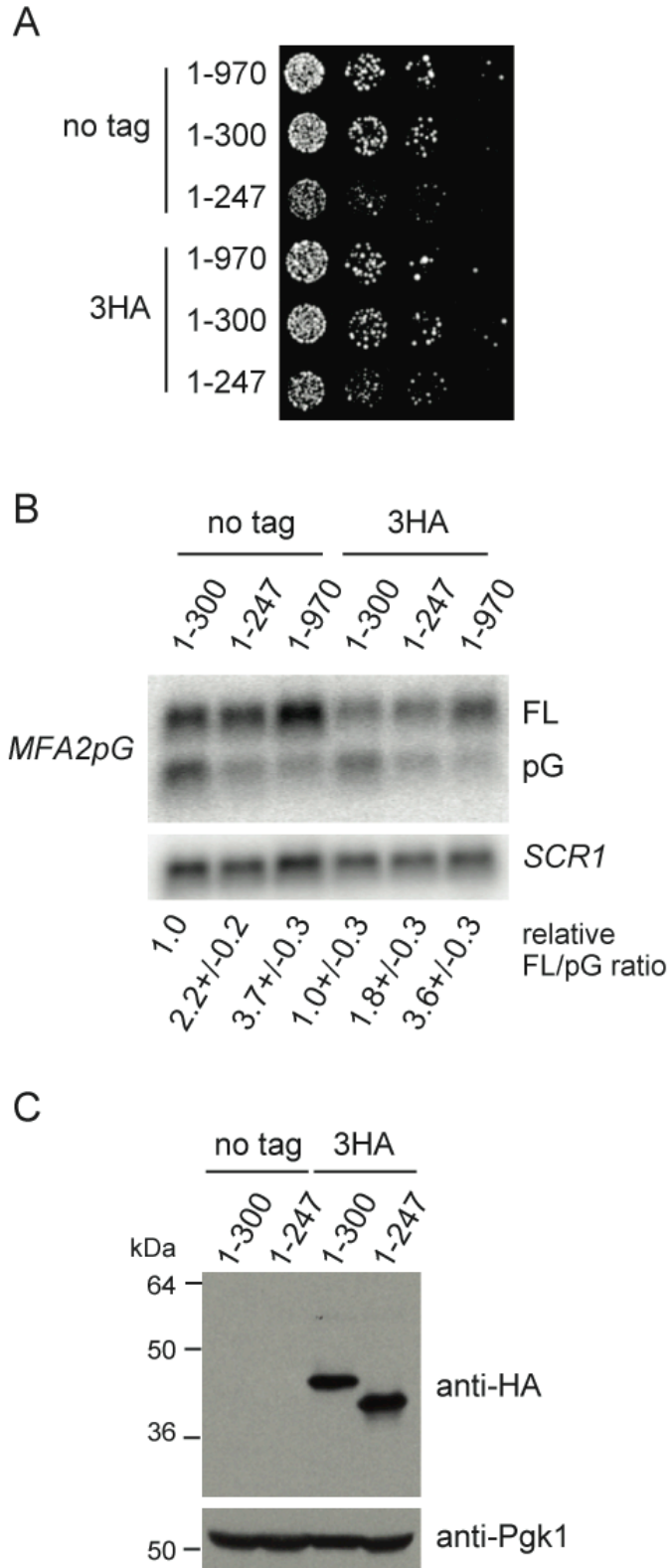
FIGURE S2

UCSF Library Release Form

Publishing Agreement

It is the policy of the University to encourage the distribution of all theses, dissertations, and manuscripts. Copies of all UCSF theses, dissertations, and manuscripts will be routed to the library via the Graduate Division. The library will make all theses, dissertations, and manuscripts accessible to the public and will preserve these to the best of their abilities, in perpetuity.

Please sign the following statement:

I hereby grant permission to the Graduate Division of the University of California, San Francisco to release copies of my thesis, dissertation, or manuscript to the Campus Library to provide access and preservation, in whole or in part, in perpetuity.

_____   12/31/09
Author Signature   Date